

INFORMATION TO USERS

While the most advanced technology has been used to photograph and reproduce this manuscript, the quality of the reproduction is heavily dependent upon the quality of the material submitted. For example:

- Manuscript pages may have indistinct print. In such cases, the best available copy has been filmed.
- Manuscripts may not always be complete. In such cases, a note will indicate that it is not possible to obtain missing pages.
- Copyrighted material may have been removed from the manuscript. In such cases, a note will indicate the deletion.

Oversize materials (e.g., maps, drawings, and charts) are photographed by sectioning the original, beginning at the upper left-hand corner and continuing from left to right in equal sections with small overlaps. Each oversize page is also filmed as one exposure and is available, for an additional charge, as a standard 35mm slide or as a 17"x 23" black and white photographic print.

Most photographs reproduce acceptably on positive microfilm or microfiche but lack the clarity on xerographic copies made from the microfilm. For an additional charge, 35mm slides of 6"x 9" black and white photographic prints are available for any photographs or illustrations that cannot be reproduced satisfactorily by xerography.

Order Number 8717742

**Wake dynamics behind a single gas bubble in a liquid and
liquid-solid fluidized media**

Tsuchiya, Katsumi, Ph.D.
The Ohio State University, 1987

Copyright ©1987 by Tsuchiya, Katsumi. All rights reserved.

U·M·I
300 N. Zeeb Rd.
Ann Arbor, MI 48106

PLEASE NOTE:

In all cases this material has been filmed in the best possible way from the available copy. Problems encountered with this document have been identified here with a check mark ✓.

1. Glossy photographs or pages _____
2. Colored illustrations, paper or print _____
3. Photographs with dark background _____
4. Illustrations are poor copy _____
5. Pages with black marks, not original copy _____
6. Print shows through as there is text on both sides of page _____
7. Indistinct, broken or small print on several pages ✓
8. Print exceeds margin requirements _____
9. Tightly bound copy with print lost in spine _____
10. Computer printout pages with indistinct print _____
11. Page(s) _____ lacking when material received, and not available from school or author.
12. Page(s) _____ seem to be missing in numbering only as text follows.
13. Two pages numbered _____. Text follows.
14. Curling and wrinkled pages ✓
15. Dissertation contains pages with print at a slant, filmed as received _____
16. Other _____

University
Microfilms
International

**WAKE DYNAMICS BEHIND A SINGLE GAS BUBBLE IN A
LIQUID AND LIQUID-SOLID FLUIDIZED MEDIA**

DISSERTATION

Presented in Partial Fulfillment of the Requirements for
the Degree Doctor of Philosophy in the Graduate
School of The Ohio State University

By

Katsumi Tsuchiya, B.S., M.S.

The Ohio State University

1987

Reading Committee:


Dr. Liang-Shih Fan

Dr. James F. Davis

Dr. Kent S. Knaebel

Dr. L. James Lee

Approved By


Adviser
Department of Chemical Engineering

Copyright by
Katsumi Tauchiya
1987

ACKNOWLEDGMENTS

The author wishes to express his most sincere thanks and gratitude to his adviser, Professor Liang-Shih Fan, for his encouragement, guidance, patience and financial support during the course of this research. The assistance of Dr. Kunihiro Kitano in the construction of the experimental apparatus is also greatly acknowledged.

This work was supported by National Science Foundation Grant CBT-8516874. The support is highly appreciated.

The author, finally, would like to express his warmest thanks to his parents and to his wife, Junko, for their support and encouragement in order for him to complete this work.

VITA

August 5, 1958 Born - Shizuoka, Japan

March 1981 B.S.Ch.E., Shizuoka University,
Hamamatsu, Japan

April 1981 - June 1981 Research Student, Department of
Chemical Engineering, Shizuoka
University, Hamamatsu, Japan

Summer 1981 Student Technician, Department
of Chemical Engineering, West
Virginia University, Morgantown,
West Virginia

September 1981 - August 1983 Research Associate, Department
of Chemical Engineering, West
Virginia University, Morgantown,
West Virginia

August 1983 M.S.Ch.E., West Virginia
University, Morgantown, West
Virginia

September 1983 - August 1984 Teaching Associate, Department
of Chemical Engineering, The Ohio
State University, Columbus, Ohio

September 1984 - June 1987 Research Associate, Department
of Chemical Engineering, The Ohio
State University, Columbus, Ohio

PUBLICATIONS

Co-authored the following publications:

1. "Simulation of Spray Drying Absorber for Removal of HCl in Flue Gas from Incinerators," *Ind. Eng. Chem. Process Des. Dev.*, 23, 300 (1984).

2. "Catalytic Cracking of Benzene on Iron Oxide-Silica: Catalyst Activity and Reaction Mechanism," *Applied Catalysis*, 16, 103 (1985).
3. "Dynamic Structure of the Wake Behind a Circular-Cap Bubble in a Liquid-Solid Fluidized Bed," presented in the Workshop at the Fifth International Conference on Fluidization, Denmark, May 18-23, 1986; Paper (BB6) presented at the 39th APS Annual Meeting, Division of Fluid Dynamics, Columbus, Ohio, November 23-25, 1986.
4. "Wake Structures of a Single Bubble in a Liquid-Solid Fluidized Bed," Paper (10b) presented at the AIChE Annual Meeting, Miami Beach, Florida, November 2-7, 1986.
5. "Advances in Gas-Liquid-Solid Fluidization: Fundamentals and Applications," Paper (28g) presented at the AIChE Annual Meeting, Miami Beach, Florida, November 2-7, 1986; to appear in "Transport Processes in Fluidized Particles," L.K. Doraiswamy and A.S. Mujumdar, Eds., Elsevier Science Publisher (1987).
6. "Near-Wake Structure of a Single Gas Bubble in a Two-Dimensional Liquid-Solid Fluidized Bed: Vortex Shedding and Wake Size Variation," *Chem. Eng. Sci.* (in review, 1987).
7. "Vortex Motion in the Near Wake Behind a Single Gas Bubble in a Two-Dimensional Liquid and Liquid-Solid Media," *J. Fluid Mech.* (in review, 1987).
8. "Bubble-Wake Pendulum Model for Wake Size Prediction in Liquid and Liquid-Solid Media," *Chem. Eng. Sci.* (in review, 1987).
9. "Structural Wake Model in Gas-Liquid-Solid Fluidization," to be submitted to *Chem. Eng. Sci.* (in preparation).
10. "Wake Structures and Bubble Coalescence Mechanisms in a Stream of Bubbles in a Two-Dimensional Liquid-Solid Fluidized Bed," to be submitted to *Chem. Eng. Sci.* (in preparation).

FIELDS OF STUDY

Major Field: Chemical Engineering

Studies in Fluidization
Fluid Mechanics

TABLE OF CONTENTS

	Page
ACKNOWLEDGMENTS	ii
VITA	iii
LIST OF TABLES	vii
LIST OF FIGURES	viii
NOMENCLATURE	xi
ABSTRACT	xv
CHAPTER 1. <i>INTRODUCTION</i>	1
SYNOPSIS	1
FLUID DYNAMICS OF WAKE FLOW	4
CHAPTER 2. <i>NEAR-WAKE STRUCTURE: VORTEX SHEDDING AND WAKE SIZE</i> ...	11
ABSTRACT	11
INTRODUCTION	12
EXPERIMENTAL	15
RESULTS AND DISCUSSION	20
A. Bubble Shape and Rise Velocity	20
B. Wake Nature and Geometry	25
C. Wake Formation-Shedding Mechanisms	26
D. Vortex Shedding Frequency	33
E. Wake Boundaries and Sizes	37
CONCLUDING REMARKS	52
CHAPTER 3. <i>VORTEX MOTION IN THE NEAR WAKE</i>	54
ABSTRACT	54

	Page
INTRODUCTION	55
EXPERIMENTAL	58
RESULTS AND DISCUSSION	60
A. Vortex Center Trajectories and Velocities	60
B. Vortex Size and Shape Variations	68
C. Liquid and Solid Particle Trajectories	76
D. Particle Velocity Profiles	86
CONCLUDING REMARKS	89
CHAPTER 4. <i>WAKE SIZE PREDICTION</i>	91
ABSTRACT	91
INTRODUCTION	92
PHYSICAL DESCRIPTION AND MODELING	96
A. Motion of Single Bubble	96
B. Rigid Body Vibration of a Bubble and Bubble-Wake	97
1. Physical description	97
2. Bubble-wake pendulum model	99
RESULTS AND DISCUSSION	106
A. Simulation Parameters	106
B. Effect of Wake Size on Vortex Shedding Frequency	110
C. Prediction of Wake Size from Vortex Shedding Frequency	113
CONCLUDING REMARKS	117
CHAPTER 5. <i>CONCLUSIONS AND RECOMMENDATIONS</i>	118
BIBLIOGRAPHY	123
APPENDIX A. Raw Data - Average Bubble Properties	129
APPENDIX B. Raw Data and Correlations for Bubble Shape Parameters and Bubble Rise Velocity	131

LIST OF TABLES

Table		Page
2.1	Physical Properties of Spherical Particles	19
4.1	Relationships for Parameters Necessary to Evaluate Effective Wake Size (unit: cgs)	107
A.1	Average Bubble Properties	130

LIST OF FIGURES

Figure	Page
1.1 Postulated liquid flow fields and solid particle trajectories around a single bubble and parametric interrelationship in three phase systems	9
2.1 Schematic diagram of the experimental system	17
2.2 Aspect ratio of single bubbles rising in liquid and liquid-solid media	21
2.3 Rise velocity of single bubbles relative to liquid phase	23
2.4 (a) Photograph of a circular-cap nitrogen bubble rising in stationary water and its wake visualized through hydrogen bubble tracers. (b) Schematic interpretation of the wake flow	27
2.5 (a) Photograph of a circular-cap nitrogen bubble and its wake rising through a water-774 μm glass bead fluidized bed. (b) Schematic interpretation of the wake flow	28
2.6a Mechanistic description of vortex formation and shedding - alternate shedding	30
2.6b Mechanistic description of vortex formation and shedding - parallel shedding	34
2.7 Relationship between Strouhal number and Reynolds number for vortex shedding from single two-dimensional bubbles ..	35
2.8 Schematic definition of primary wake boundary	38
2.9 Dynamic variations in primary wake area (k_{pw}) and angle of attack (α) in stationary water	41
2.10 Dynamic variations in primary wake area (k_{pw}), liquid wake area (k_{lw}) and angle of attack (α) during (a) steady growth period and (b) steady shedding period in a water-1.5 mm acetate particle fluidized bed	42
2.11 Dynamic variations in primary wake area (k_{pw}), liquid wake area (k_{lw}) and angle of attack (α) during steady shedding period in a water-774 μm glass bead fluidized bed	43

Figure	Page
2.12 Normalized variation of primary wake size as expressed by the form of a saw-tooth wave function	48
2.13 Mean primary wake size marked with minimum and maximum values	49
3.1 Schematic diagram of the experimental system	59
3.2a Vortex center trajectories behind a circular-cap bubble in stationary water	62
3.2b Vortex center trajectories behind a circular-cap bubble in a water-1.5 mm acetate particle fluidized medium	64
3.3a Time variation of vertical downward distance traveled by vortices in stationary water	66
3.3b Time variation of vertical downward distance traveled by vortices in a water-1.5 mm acetate particle fluidized medium	67
3.4a Time variation of equivalent circular diameter of vortices in stationary water	70
3.4b Time variation of equivalent circular diameter of vortices in a water-1.5 mm acetate particle fluidized medium	71
3.5a Positional variation of vortex eccentricity in stationary water	74
3.5b Positional variation of vortex eccentricity in a water-1.5 mm acetate particle fluidized medium	75
3.6 Liquid element trajectories viewed from bubble base center	77
3.7 Time variation of vertical downward displacement of liquid elements	79
3.8 Time variation of lateral displacement of liquid elements	80
3.9a Solid particle trajectories: observer moving with bubble base center	82
3.9b Solid particle trajectories: observer moving with vortex center	83
3.10 Sequential development of particle-free region	85

Figure	Page
3.11 Instantaneous solids flow field expressed by particle streaks	87
3.12 Instantaneous particle velocity profiles in the regions across the wake in terms of (a) vertical velocity component and (b) direction of velocity vector	88
4.1 Schematic representation of vibrating bubble-wake	101
4.2 Radius of rotation of bubble-wake rocking correlated in terms of bubble size	109
4.3a Effect of wake size on alternate vortex shedding frequency in two-dimensional water-solid fluidized media..	111
4.3b Effect of wake size on alternate vortex shedding frequency in three-dimensional water and water-solid media	112
4.4 Prediction of wake size under various conditions	114
4.5 Effect of moment of inertia of the primary wake on wake size	116
A.1 Aspect ratio of single bubbles correlated in terms of bubble size	132
A.2 Upper semi-height-to-breadth ratio of single bubbles correlated in terms of bubble size	133
A.3 Equivalent bubble diameter of single bubbles correlated in terms of bubble size	134
A.4 Rise velocity of single bubbles correlated in terms of bubble size	135
A.5 Variation of maximum inclined angle of bubble-wake with respect to bubble size	136

NOMENCLATURE

- A amplitude of sinusoidal wave form, cm
- a distance between consecutive vortices on the same side of body, cm
- b bubble breadth, cm
- b_c critical bubble diameter for bubble to be spherical, cm
- C_A added mass coefficient, dimensionless
- C_b coefficient for gyration radius of bubble, dimensionless
- C_{pw} coefficient for gyration radius of primary wake, dimensionless
- d cylinder diameter, cm
- d_e equivalent spherical bubble diameter in three dimensions (3D) or equivalent circular bubble diameter in two dimensions (2D), cm
- d_p particle diameter, cm
- d_v equivalent circular vortex diameter, cm
- d_{v1} length of vortex major axis, cm
- d_{v2} length of vortex minor axis, cm
- d_w wake width, cm
- E bubble aspect ratio = h/b
- Fr_b bubble Froude number based on bubble breadth = U_b^2/gb
- f_{BW} natural frequency of bubble-wake, s^{-1}
- f_{pw} frequency in primary wake size variation, s^{-1}
- f_v individual vortex shedding frequency, s^{-1}
- f_v' shedding frequency of vortex pairs = $f_v/2$, s^{-1}
- G body force per unit mass, cm/s^2
- g gravitational acceleration, cm/s^2
- H effective height of bed expansion, cm

H_0 static bed height, cm
 h bubble height, cm
 h_c upper semi-height of bubble from its center of gravity, cm
 h_{pw} primary wake height, cm
 h_w average length of wavering portion of wake, cm
 h_1 upper semi-height of bubble, cm
 I total mass moment of inertia of bubble-wake, $g\text{ cm}^2$
 I_b mass moment of inertia of bubble, $g\text{ cm}^2$
 I_{pw} mass moment of inertia of primary wake, $g\text{ cm}^2$
 K_{pw} coefficient for k_{pw} defined by eq. (4.15), dimensionless
 k ratio of wake size to bubble size (size: volume in 3D or area in 2D)
 k_{lw} ratio of liquid wake size to bubble size
 k_{pw} ratio of primary wake size to bubble size
 \bar{k}_{pw} mean ratio of primary wake size to bubble size
 k_{STW} ratio of stable turbulent wake size to bubble size
 L distance between pivot and center of gravity of bubble, cm
 l distance between pivot and center of gravity of primary wake, cm
 ndS surface element, cm^2
 p pressure, dyn/cm^2
 R radius of rotation of bubble-wake rocking or average frontal radius of curvature of bubble, cm
 Re_b bubble Reynolds number based on bubble breadth = $b U_b/\nu$
 Re_e bubble Reynolds number based on equivalent bubble diameter = $d_e U_b/\nu$
 r position vector, cm
 r radial distance from vortex center, cm
 \bar{r}_b gyration radius of bubble, cm

\bar{r}_{pw} gyration radius of primary wake, cm
 r_v order of magnitude of vortex core radius, cm
 Sr' Strouhal number for vortex pair shedding based on cylinder diameter = $f_v'd/U_o$
 Sr_b Strouhal number for individual vortex shedding based on bubble breadth = $f_v'b/U_b$
 Sr_b' Strouhal number for vortex pair shedding based on bubble breadth = $f_v'b/U_b$
 T restoring torque, dyn cm
 t time, s
 t_{vo} moment of vortex generation, s
 t_o initial time of each cycle in primary wake size variation, s
 U_b bubble rise velocity relative to liquid phase, cm/s
 U_l superficial liquid velocity, cm/s
 U_v vortex velocity relative to liquid phase, cm/s
 U_o mean stream velocity, cm/s
 u velocity vector, cm/s
 u_{in} velocity along inner boundary of a free shear layer, cm/s
 u_{out} velocity along outer boundary of a free shear layer, cm/s
 u_{px} particle downward velocity relative to bubble, cm/s
 u_θ tangential velocity around vortex center, cm/s
 V_b bubble volume, cm³
 V_{pw} primary wake volume, cm³
 x flow direction; vertical downward distance from bubble base, cm
 y horizontal right-hand distance from the center of bubble base, cm

Greek Letters

α angle of attack, deg

α_{BW} inclined angle of bubble-wake, deg or rad
 $\bar{\alpha}_{BW}$ average inclined angle of bubble-wake, deg or rad
 Γ circulation, cm^2/s
 γ_{pw} density ratio = ρ_{pw}/ρ_l
 Δk_{pw} average difference between maximum and minimum ratios of primary wake size to bubble size
 ϵ bed voidage
 η sinusoidal wave form of interface, cm
 k measure of strength of a free shear layer, cm/s
 λ wavelength, cm
 ν liquid kinematic viscosity, cm^2/s
 ρ_g gas density, g/cm^3
 ρ_l liquid density, g/cm^3
 ρ_{pw} primary wake density, g/cm^3
 ρ_s solid density, g/cm^3
 τ time elapsed from the moment of vortex generation, s
 ω vorticity vector, s^{-1}
 ω vorticity, s^{-1}

ABSTRACT

Dynamic characteristics of the wake behind a single gas bubble have been investigated in a liquid and liquid-solid suspensions. A visual study was conducted in a two-dimensional system via a video camera moving at the same speed as the bubble. Through the visualization the wake structure and the vortex behavior within the wake were examined. Wake dynamics was also studied theoretically based on an analogy between the bubble-wake rocking and a mechanical vibration.

The bubble wake was observed to consist of two fluid mechanically distinct regions: primary wake (near-wake) and secondary wake. Vortices formed in the primary wake are shed periodically either from alternating sides or from both sides simultaneously, depending on the bubble size. The shedding frequency (the Strouhal number) was shown to be a function of the bubble Reynolds number but independent of particle properties. The primary wake size periodically varies in the form of a saw-tooth wave function.

The vortex properties, such as center trajectory, descent velocity with respect to the bubble, size variation, and shape deformation during the course of descent, were determined visually. Vortex behavior was found to be similar in both the liquid and liquid-solid media except the vortex life: shorter life in the liquid-solid suspensions than in the liquid. The trajectories of liquid elements and

solid particles around the near-wake were strongly influenced by the presence of vortices. The deviation of solid particles from liquid flow path created particle concentration gradients in the near wake.

A mechanistic model which interrelates the frequency of vortex shedding and the size of the bubble wake has been developed based on secondary motion of a single bubble. In the model, the bubble and its primary wake are regarded as a single semi-rigid body steadily rocking at the vortex shedding frequency. The model was utilized to predict the wake size. Agreement between the predicted and the experimental values was favorable over a wide range of the bubble Reynolds number.

In this study the primary wake is identified, from a fluid mechanic point of view, as a localized region inherent to an individual bubble and partially isolated from the surrounding medium. The results presented in this dissertation thus can be effectively used in the design of multiphase (multibubble) contacting systems.

CHAPTER 1

INTRODUCTION

SYNOPSIS

There are a variety of physical and chemical processes which involve multiphase contacting devices such as bubble column reactors (gas-liquid), gas-solid fluidized beds, gas-slurry bubble columns, and gas-liquid-solid (three phase) fluidized beds. The hydrodynamics of these systems, upon which mass and heat transfer and solids mixing behavior are strongly dependent, is extremely complex and poorly understood.

The wake, which resides immediately behind a rising bubble and contains a certain proportion of fluid and solid, if any, plays an important role in the hydrodynamics of multiphase systems. In gas-liquid contacting systems the flow, or more specifically, velocity distribution in the wake region has been noted to control the diffusion/dispersion of gas molecules from bubbles into liquid media (Levich, 1962; Brignell, 1974; Yabe and Kunii, 1978). In addition, the bubbles induce liquid agitation through the entrainment and expelling of liquid wakes. The larger the wake, the more enhanced this liquid mixing (thus, the axial liquid dispersion) becomes.

Similarly, the wake has been recognized as one of the key factors responsible for solids mixing in gas-solid fluidized beds. Two out of the three mechanisms proposed for this phenomenon are due to the presence of the wake (Rowe et al., 1965; Gibilaro and Rowe, 1974; Naimer et al., 1982): solids are entrained in the bubble wakes from the bottom of the bed, carried to the top, dumped on the surface, and eventually circulating downward - solids circulation (Woollard and Potter, 1968); some solids are exchanged between the bubble wake and the surrounding emulsion phases during the rise of the bubbles - solids exchange (Sutherland, 1961; Rowe and Partridge, 1962; Chiba and Kobayashi, 1977). The role of the wake in solids mixing in other systems is also obvious; axial dispersion of solid particles in gas-slurry bubble columns (Dayan and Zalmanovich, 1982) and particle entrainment from gas-liquid-solid fluidized beds into the freeboard region (Page and Harrison, 1974).

In three phase fluidized beds the wake has been identified as the primary factor in explaining bed contraction upon the introduction of gas bubbles into liquid-solid fluidized beds (Stewart and Davidson, 1964; Ostergaard, 1965; Rigby and Capes, 1970). The wake concept (e.g., Bhatia and Epstein, 1974) has provided an essential framework for a global treatment of the bed behavior; however, there is a general lack of fluid dynamic understanding of bubble flow and wake structure.

The ultimate design of practical multiphase contacting devices cannot be realized unless one can account quantitatively for the above-mentioned hydrodynamic phenomena. In such systems bubbles rise

in swarms; nevertheless, the author believes that these complex phenomena can be systematically studied based on the behavior of a single bubble and its wake together with the bubble-bubble and/or bubble-wake interactions.

This study focuses on a fundamental description of wake structure of, or flow field behind, a single gas bubble in multiphase systems including gas-liquid systems and gas-liquid-solid fluidized systems. The main body of this dissertation consists of four chapters. All the chapters are presented in such a manner that each chapter is essentially self-contained: the reader should refer to the Introduction in individual chapters for more specific definitions of the problems and literature reviews.

Chapter 2 deals with the dynamic structures of the wake of a single gas bubble in liquid-solid fluidized media using a "two-dimensional" apparatus. The two-dimensional system was employed due to its convenience for flow visualization study, especially in the presence of high concentration of non-transparent solid particles, and as a "diagnostic tool" for the characterization of fundamental phenomena to be extended to a real, three-dimensional system. The primary objective is to understand and, possibly, to unify the physical description of the structure of the near wake over a wide range of the bubble Reynolds number through varying the bubble size. Two specific topics are discussed: wake instability and wake size variation.

Chapter 3 is devoted to the motion of individual vortices in the near wake of a single bubble in a two-dimensional liquid and liquid-solid fluidized media. The flow field around the near wake is characterized by the trajectories of the vortex center, liquid elements and solid particles.

After studying the near-wake properties experimentally in Chapters 2 and 3, the bubble wake dynamics is treated theoretically in Chapter 4. A phenomenological model is proposed which accounts for a bubble-wake motion caused by vortex shedding from the primary wake. Time variations of size and shape of the primary wake are not incorporated into the model; however, the periodicity of the wake phenomena (vortex shedding frequency) is utilized to predict the primary wake size, which is one of the most important parameters necessary for the quantitative treatment of three-phase fluidized bed behavior. Chapter 6 lists the conclusions and some recommendations for future study.

Before turning to the main discussions, the rest of this chapter is spared for the basic theories involved in the wake flow.

FLUID DYNAMICS OF WAKE FLOW

It goes without saying that all wake flow phenomena, however complex, cannot violate fundamental fluid dynamic laws. In the following relevant fluid mechanic laws/theories and plausible flow models are discussed for mainly single phase (liquid) systems with or without boundaries of different phase(s).

As indicated in the forthcoming chapters, a circulating flow pattern in the near wake behind a bubble is an inherent characteristic prevailing in the wake flow, whether steady or unsteady. This circulatory flow, or vortical motion, has its foundation on either of the following well-known theorems: Helmholtz's theorem of vortex motion or Kelvin's (Thomson's) circulation theorem. The contents of both the theorems of Helmholtz and Kelvin are identical, coming from the dynamical equation of motion, although the former is derived for only ideal fluids and the latter includes compressible fluids. The theorems state in an extended sense that the rate of change of circulation Γ associated with a closed curve always made up of the identical fluid elements is governed by the torques produced by all the forces acting in the fluid in the way:

$$\frac{D\Gamma}{Dt} = - \int \frac{dp}{\rho} + \int G \cdot dr + \int \nu \nabla^2 u \cdot dr \quad (1.1)$$

The first term on the right-hand side represents pressure torques. In most situations fluids are barotropic, i.e., of a single-valued pressure-density relation, leading to no circulation caused by pressure. The second term gives body-force torques, which are zero if the body force G is irrotational, or conservative. The centrally-directed forces like gravity fall into this category, while Coriolis forces and Lorentz forces are two important rotational body forces in oceanographic and magneto-hydrodynamic flows, respectively. The third term is the torques produced by viscous forces acting on the fluid elements.

Knowing that the circulation around any infinitesimal surface element dS moving with the fluid is equal to the flux of vorticity ω through that surface (Karamcheti, 1966), i.e.,

$$d\Gamma = \omega \cdot dS \quad (1.2)$$

and applying the following formula for the rate of change of outflow of ω through any surface element moving with the fluid (see e.g., Sommerfeld (1950) for a proof)

$$\frac{D}{Dt}(\omega \cdot dS) = \left[\frac{\partial \omega}{\partial t} - \nabla \times (u \times \omega) \right] \cdot dS \quad (1.3)$$

Equation (1.1) can be expressed in terms of ω as

$$\frac{D\omega}{Dt} = \omega \cdot \nabla u + \nu \nabla^2 \omega \quad (1.4)$$

for an incompressible fluid moving in an irrotational body force field. Equation (1.4) is known as the vorticity equation and can also be obtained directly by taking the curl of both sides of the equation of motion (Batchelor, 1967). In two-dimensional and axisymmetric flows, ω is everywhere normal to the flow plane and orthogonal to ∇u , respectively, leading to the term $\omega \cdot \nabla u$ being identically zero.

Now that we apply the above theorems to the wake flow behind bluff bodies. It is reasonable to assume that the fluids (continuous phase) in our systems are incompressible and only body force acting on the systems is gravity (irrotational). The bodies we are dealing with are basically axisymmetric or two-dimensional. Therefore, our starting point in the following discussion is summarized in the mathematical form:

$$\frac{D\omega}{Dt} = \nu \nabla^2 \omega \quad (1.5)$$

That is, the flux of vorticity across a material surface element varies solely as a consequence of local diffusion of vorticity, by the action of viscosity.

We now describe the generation of vorticity/circulation from the boundary between the body and the fluid. When the fluid is set in a motion at $t = 0$ relative to the body, vorticity will be generated along the boundary. This fluid motion at $t = 0$ is inevitably irrotational in the interior of the fluid, since there was no vorticity at $t < 0$. Note that vorticity is neither created nor destroyed in the interior of a homogeneous fluid. Due to the no-slip condition, however small the viscosity may be, vorticity is concentrated at the boundary at the initial stage, forming a boundary layer along the boundary. This boundary layer separates from the bluff body at sharp edges if any, for example, at the rim of a spherical cap. Vorticity is spread from this separated sheet of vorticity, so-called free shear layer, into the irrotational fluid by the action of viscosity as stated by eq. (1.5).

At high Reynolds numbers, either convection is strong (through the speed of the body being high) or diffusion is weak (through the fluid viscosity being small). Thus, there is a region, ahead of and to the side of the body, where the flow is approximately irrotational all the time. In the region behind the body, however, the thickness of the free shear layer, which is proportional to $(\nu t)^{1/2}$, is no longer small compared with the breadth of the body. If there is an

ultimate steady state attained, the diffusion of vorticity due to viscosity will result in a uniform distribution of vorticity within this region. At this limit, paradoxically, viscous forces have vanished altogether, leaving nothing to cause further changes in circulation (see eq. (1.1)). In addition, the difference in magnitude of the velocities outside and inside the region behind the body, or wake, - inner velocity being smaller than outer velocity - causes an eventual circulating flow pattern inside the wake.

The above fluid mechanic description leads to a simplification of the flow field around a bluff body, such as an ellipsoid or spherical cap, immersed in a uniform flow. Figure 1.1 gives such an idealized flow model for a steady state flow around a spherical-cap bubble. The flow model may be postulated to consist of: (1) irrotational flow of an ideal fluid (potential flow) outside the body and its wake, (2) inviscid rotational flow inside the closed wake (a doublet of vortex cores in two-dimensional flow; a vortex core ring in three-dimensional axisymmetric flow), (3) thin boundary layer around the surface enclosing the body and its closed wake, and (4) "external and internal wakes" along the axis of symmetry. Within the internal wake there is no vorticity diffusion. Here the external and internal wakes result from the boundary layer, or free shear layer. Fluid elements discharged around the rear stagnation point of the closed wake from the interior boundary layer will move upwards in the internal wake to reenter the boundary layer along the base of the body. Fluid from the exterior boundary layer will move downwards and leave the closed wake region for the far wake. A similar flow model was proposed by Harper

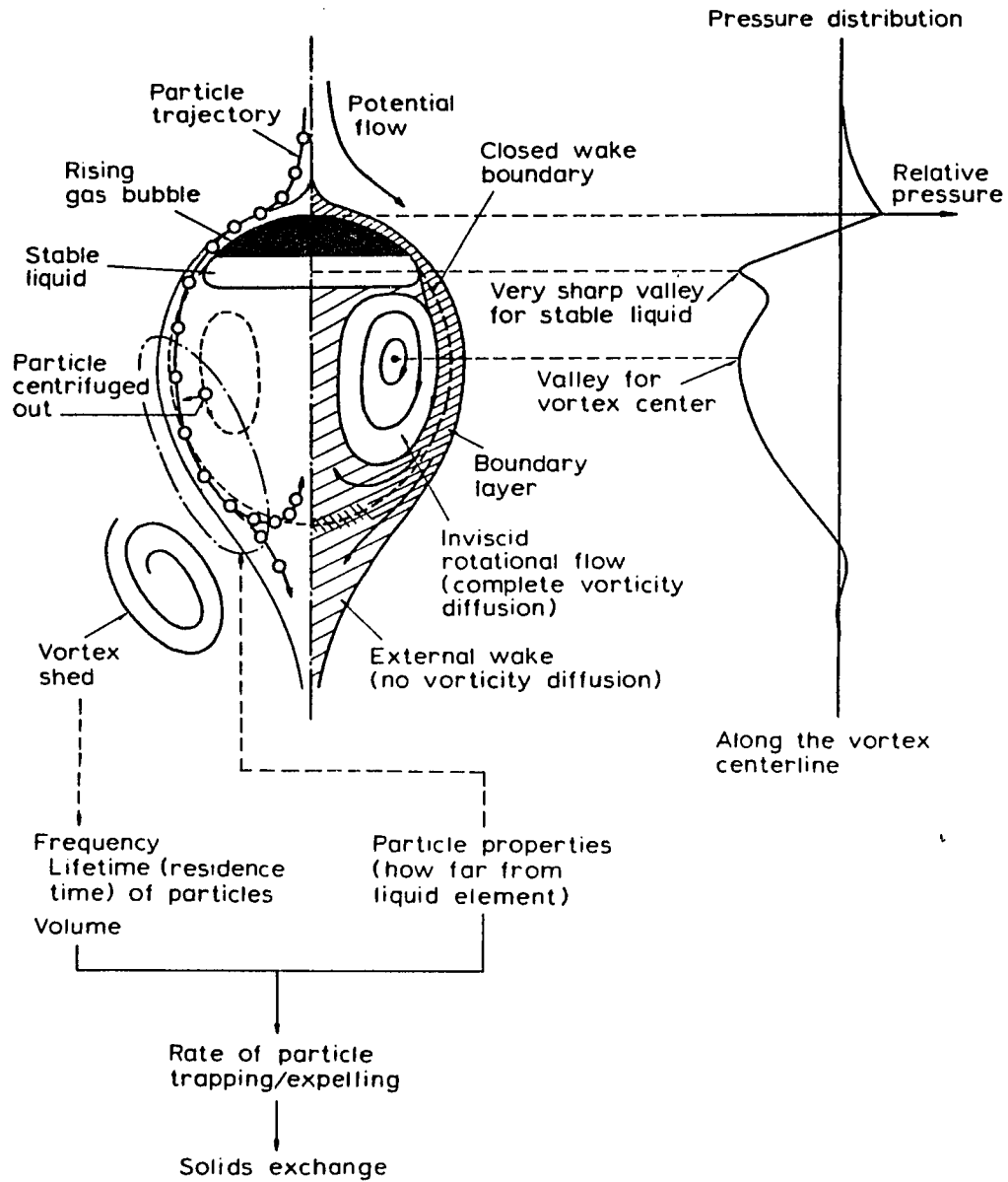


Figure 1.1 Postulated liquid flow fields and solid particle trajectories around a single bubble and parametric interrelationship in three phase systems.

and Moore (1968) for a spherical liquid drop moving at high Reynolds number in another liquid of comparable density and viscosity. Some other details shown in the figure is explained in the coming chapters.

The unsteady wake flow, accompanied by vortex shedding, is discussed in the next chapter.

CHAPTER 2

NEAR-WAKE STRUCTURE: VORTEX SHEDDING AND WAKE SIZE

ABSTRACT

The fluid mechanic behavior of a single gas bubble and its wake in a two-dimensional liquid-solid fluidized bed was examined visually via a video camera moving at the same speed as the bubble. The bubble wake was observed to consist of two regions: primary wake (near-wake) and secondary wake. Wake formation-shedding mechanisms were illustrated for both symmetric and asymmetric shedding modes. The shedding frequency, expressed in terms of the Strouhal number, was shown to be a function of the Reynolds number but independent of particle properties. The boundaries between the primary and secondary wakes were qualitatively identified for several wake structures. The primary wake size periodically varies in the form of a saw-tooth wave function, while the liquid wake exhibits no appreciable cyclic variation in size.

INTRODUCTION

Gas-liquid-solid fluidization has been utilized in chemical, petrochemical and biochemical processing due, in part, to its inherent particle mixing characteristics. Among the mechanisms responsible for solids mixing is solids exchange between the bubble wake and the liquid-solid fluidized region. This mechanism predominates when the bubble size is large, which can be realized at low liquid flow rate, or in the coalesced bubble regime (Muroyama and Fan, 1985).

The role of the bubble wake has been recognized as the key factor in explaining various phenomena occurring in three-phase fluidized beds such as solids mixing, particle entrainment into the freeboard (Page and Harrison, 1974) and bed contraction upon the introduction of gas bubbles into liquid-solid fluidized beds (Stewart and Davidson, 1964; Ostergaard, 1965; Rigby and Capes, 1970). The wake concept (e.g., Bhatia and Epstein, 1974) has provided an essential framework for a global treatment of the bed behavior; however, there is a general lack of fluid dynamic understanding of bubble wake structure in liquid-solid suspensions. Information on bubble wake structure is mostly limited to two-phase systems, i.e., gas-liquid systems.

For gas-liquid systems, the nature and geometry of the wake have been extensively studied for large spherical-cap bubbles or circular-cap bubbles in two-dimensional systems. The wake geometry in these systems, however, has long been disputed and historically grouped into three types: (1) closed laminar/toroidal wake, (2) closed turbulent wake, and (3) open turbulent wake (Coppus et al., 1977). Closed

laminar/toroidal wakes have been observed behind large spherical-cap bubbles rising in viscous liquids or behind circular-cap bubbles (see Fig. 1.1). The closed laminar wake is hydrodynamically stable, consists of a well-defined boundary and a toroidal vortex ring inside, and exchanges no liquid with the external flow (Coppus et al., 1977; Bhaga and Weber, 1981). Stability is due to high liquid viscosity or wall effects. Keeping the bubble volume constant and decreasing viscosity, or increasing the bubble Reynolds number, Bhaga and Weber (1981) demonstrated that the flow in the wake becomes less stable and starts shedding vortices (transition to the open wake). For circular-cap bubbles rising between two flat plates, the wake appears to be more stable than that behind the three-dimensional bubbles. Using a 6.4 mm thick apparatus, Collins (1965b) showed the wake to be closed and to consist of a large stable vortex pair. The Reynolds number based on the bubble radius of curvature was as high as 2.5×10^4 . At the same Reynolds number range, on the other hand, Crabtree and Bridgwater (1967) found considerable wake shedding. In their experiment they used a vessel of thicker gap (12.7 mm). Accordingly, the thinner the gap between the plates of a two-dimensional apparatus is, the more stabilized the wake flow becomes.

Turbulent wakes have been observed behind large bubbles rising in less viscous liquids. There have been controversial arguments among the researchers (e.g., Maxworthy, 1967; Wegener and Parlange, 1973; Hills, 1975; Coppus et al., 1977) regarding the geometry of the turbulent wakes; i.e., whether they are closed or open. A closed turbulent wake was first visualized by Davies and Taylor (1950)

applying flash shadow photography to a large spherical-cap bubble rising in nitrobenzene. The optical anisotropy of the liquid under shear allowed a closed region of high shear, thus high turbulence, to be clearly shown immediately behind the bubble. The wake boundary approximately completed a sphere but no detailed flow pattern inside the wake was visible. Care should be exercised, however, when interpreting this result. As pointed out by Maxworthy (1967) and supported by Wegener and Parlange (1973), a turbulent wake cannot be confined to a completely closed region due to the momentum defect in the liquid following the passage of the bubble: the bubble must experience a finite drag.

Accordingly, an open geometry appears to be more reasonable for describing turbulent wakes. Employing schlieren photography, Wegener and Parlange (1973) showed that the wakes extended far downstream from the bubbles at the Reynolds number based on equivalent spherical bubble diameter (Re_e) greater than 3000. In their photographs the flow inside the wake appears to be chaotic and no circulatory flow patterns are recognized. However, they indicated that there should exist a vortical motion within the near wake, based on the motion of small satellite bubbles. In addition, it is possible for the fine detail of the schlieren technique to obscure the large scale flow patterns, as pointed out by Hills (1975).

The word "turbulent" thus may be misleading as an expression of the wake nature at higher Reynolds numbers, if it indicates totally "chaotic" motion inside the wake. Increasing the Re_e up to 1.5×10^4 , Coppus et al. (1977) still found an enclosed region immediately behind

the bubble, in which a broad circulatory flow pattern was identified, although less stable and rather irregular. This near-wake region was followed by a vortex street extending far behind the bubble. Even at a lower Reynolds number ($Re_e = 56$), Slaughter and Wraith (1968) observed a streaming tail extending along the bubble rise path below a toroidal vortex travelling with the bubble. This structure was revealed by intensifying the optical effect with a shadow-graph technique in an 87% wt/wt aqueous glycerol solution.

Bubble behavior in gas-liquid-solid fluidized beds of small, light particles resembles that observed in viscous liquids (Stewart and Davidson, 1964; Ostergaard, 1973). However, no systematic studies on the wake structure in three-phase fluidization have appeared in the literature since Rigby and Capes' (1970) first introduction of the dynamic nature of the wake, or vortex shedding, in explaining the bed contraction phenomenon.

The present chapter focuses on a fundamental description of wake structure of, or flow field behind, a single bubble in gas-liquid-solid fluidized systems. The dynamic nature of the bubble wake, which was visualized through a two-dimensional fluidized bed and a video camera moving upward at the same speed as the bubble, is presented.

EXPERIMENTAL

Visualization of the dynamic structure of the bubble wake was achieved by monitoring a rising bubble with a video camera which moved vertically at the same speed as the bubble. Using this technique the bubble remained in the center of the screen throughout its rise. A

schematic diagram of the experimental system is depicted in Fig. 2.1. The two-dimensional Plexiglas column is of 104 cm height, 40.6 cm width and 0.8 cm nominal gap thickness. The hydrostatic deflection of the column plates is minimized by clamping with three sets of lateral, U-shape Plexiglas channels with square bottoms and 6.4 cm height. Liquid distribution is achieved through four inlet valves and four compartments of 12.7 cm high, 1.9 cm thick packed beds of three layers; 3 mm lead shot, 2.3 mm alumina particles and 774 μm glass beads. The fluidized particles are supported on a 200-mesh wire cloth. Single gas bubbles are injected through a 0.64 mm o.d. nozzle, which is flush-mounted on the rear wall 10 cm above the liquid distributor. The bubble size is readily controlled by altering the gas delivery pressure and/or the opening time of a solenoid valve, which can be preset at desirable values. With this method single bubbles are quickly injected without any satellites.

A variable speed vertical bubble tracking system was constructed. The set-up consists of four parallel vertical stainless ground shafts (2.54 cm o.d.) with two ball bushing bearings on each shaft (Thomson Industries, Inc.), a DC motor (90 V, 1/2 HP maximum) with an SCR speed controller (Dayton Electric Manufacturing Co.), and sprockets and a chain which transform the rotational motion to the vertical. The bearing system ensures smooth linear motion, which carries the video camera (Panasonic WV-1800). Since the bubble rises at an almost constant velocity, the bubble can be roughly tracked by setting the DC motor input voltage at the predetermined value for each bubble. A fine adjustment is made manually during the bubble rise in order to

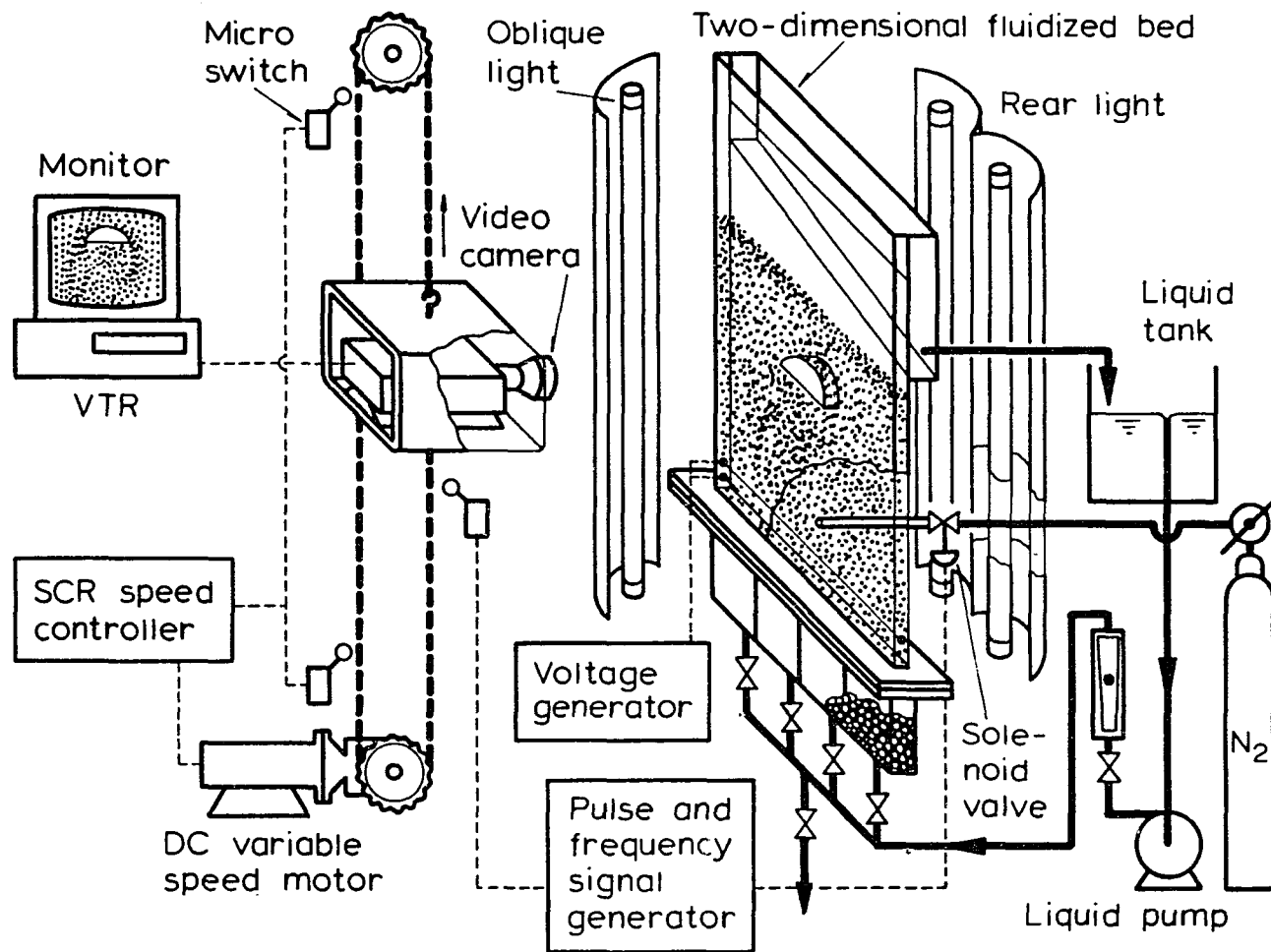


Figure 2.1 Schematic diagram of the experimental system.

keep the bubble at the fixed position on the screen. Micro-switches are used to synchronize the bubble injection timing with the camera location during its initial rise and to terminate the camera rise as it reaches the top of the column. The signal from the camera is monitored via a video recorder (Sony VO-5800 U-matic). Recorded data are either directly photographed or traced field by field from the screen and are analyzed using a digitizer (Houston Instrument TG-1017) for the measurements of relevant coordinates, lengths, and areas.

Nitrogen, tap water and four different types of spherical particles were used in the experiments. The physical properties of the particles are listed in Table 2.1. The bed expansion ratio was kept constant for each bed material in the range between 1.4 and 2.0. Some runs were performed in the absence of particles where the liquid flow around a bubble was visualized by hydrogen bubble tracers. A thin (nominally about 0.05 cm) wire of tungsten was used as the cathode, which extended horizontally across the long axis of the column just above the liquid distributor, to generate fine hydrogen bubbles. Since the measured rise velocities of hydrogen bubbles were much smaller than the subject bubble rise velocity, usually by three orders of magnitude, hydrogen bubbles were assumed to reasonably represent the liquid flow. Those runs serve as a basis for elucidating the effects of the presence of solid particles on the bubble wake structure.

Table 2.1. Physical Properties of Spherical Particles

Type of Particle	Notation	Average Diameter [mm]	Density [g/cm ³]	Terminal Velocity [cm/s]
Glass Bead	GB460	0.460	2.50	6.73
Glass Bead	GB774	0.774	2.50	11.9
Activated Carbon	AC778	0.778	1.509*	5.69
Acetate Ball	AT1500	1.50	1.252	6.99
Sand**	SD775	0.775	2.45	11.6

* Wet density: Dry density is 0.91 g/cm³.

** Rigby and Capes (1970).

RESULTS AND DISCUSSION

A. Bubble Shape and Rise Velocity

Bubbles in motion are generally classified by shape as spherical, oblate ellipsoidal and spherical-cap (in three dimensions) with the actual shape depending upon the relative magnitudes of the dominant forces acting on the bubble, such as surface tension or inertial forces. Although the bubbles in the size range covered in the present study underwent marked shape oscillations, the bubble shape was represented by an average shape over several cycles of oscillations. Figure 2.2 shows the aspect ratio (maximum height/maximum breadth) of single bubbles as a function of the bubble breadth. Hereafter the bubble breadth will be used as a characteristic length based on the following discussion.

The wake size is not controlled by the equivalent circular bubble diameter but by the distance between the separation points at both sides of the bubble. At higher Reynolds numbers, bubbles are of oblate shape such as elliptical and/or circular-cap. The separation points are rather fixed at both edges - the portions of the bubble surface with the sharpest curvature. Thus, the characteristic length governing the wake phenomena should be the actual distance from edge to edge, i.e., the bubble breadth.

The aspect ratio decreased with increasing bubble size and approached an asymptotic value of about 0.32 in the circular-cap regime. The corresponding value for three-dimensional spherical-cap bubbles is known to be around 0.24. No systematic effects of particle

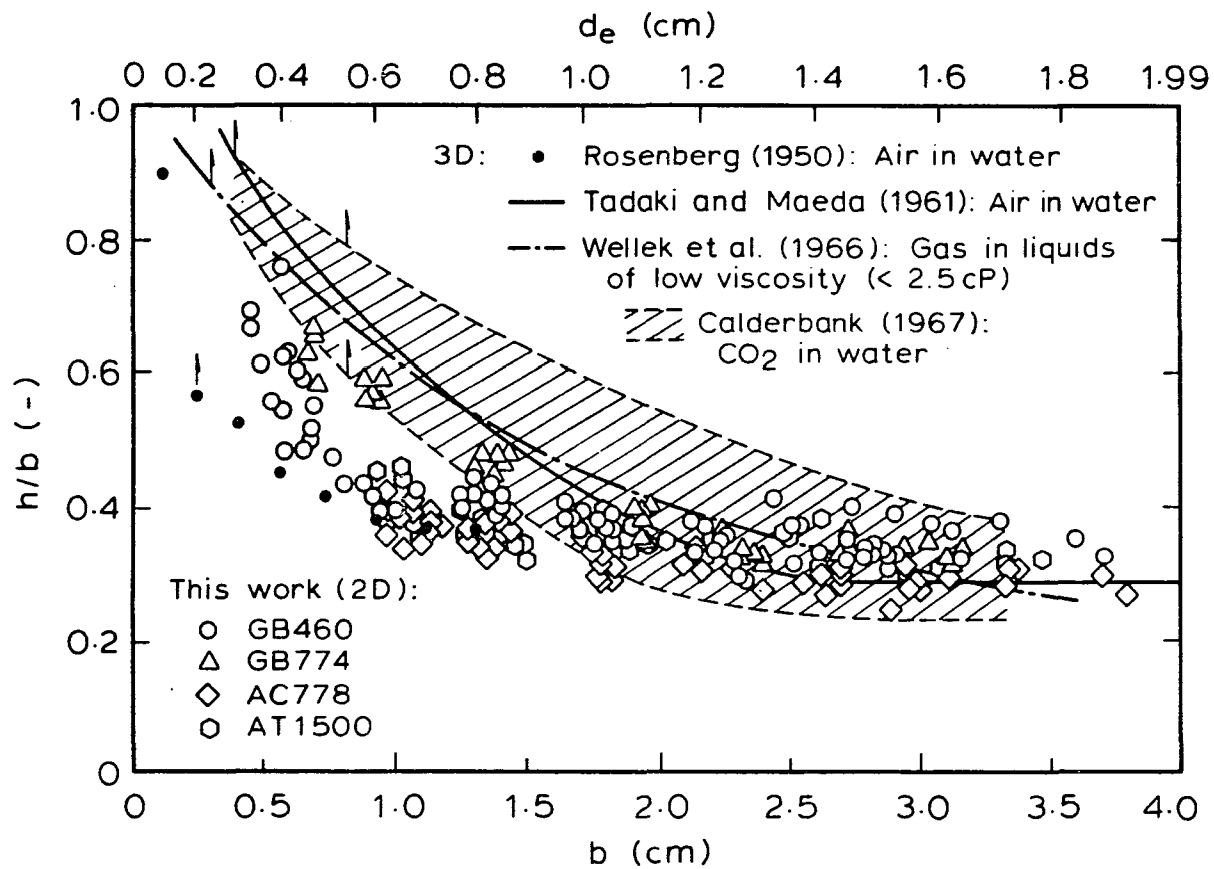


Figure 2.2 Aspect ratio of single bubbles rising in liquid and liquid-solid media.

properties were observed on the bubble shape over the particle size and density ranges investigated in the present study (see Table 2.1).

In order to compare the two-dimensional data obtained in the present work with the existing three-dimensional results from the literature, the bubble breadth was related, based on the present data, to the equivalent bubble diameter, which has been conventionally used as a characteristic length in almost all the literature (e.g., Tadaki and Maeda, 1961; Wellek et al., 1966; Calderbank, 1967; Clift et al., 1978). The relation is given by

$$b = 1.72 d_e^{1.23} \quad (\text{two-dimensional, } 0.35 < d_e < 2.0 \text{ cm}) \quad (2.1)$$

with a $\pm 8.9\%$ average error. This simple correlation was employed since only water was used in the present study and the bubble rise velocity was later found to be a function of the bubble size. A similar relation was proposed by Uno and Kintner (1956) for three-dimensional bubbles rising in liquids of viscosity less than 10 cP. From their graphical correlation the corresponding parameters can be read as 1.56 and 1.18 respectively for $0.08 < d_e < 1.6$ cm. The existing three-dimensional data or correlations are thus plotted in Fig. 2.2 against the upper abscissa (d_e). Notice that both two- and three-dimensional aspect ratios fall in the same range, especially for $d_e > 1.0$ cm.

The bubble rise velocity is plotted against the bubble breadth in Fig. 2.3. Although the rise velocity was primarily a function of the bubble size, there were noticeable influences of particle properties. To correlate the results the Mendelson equation (Mendelson, 1967),

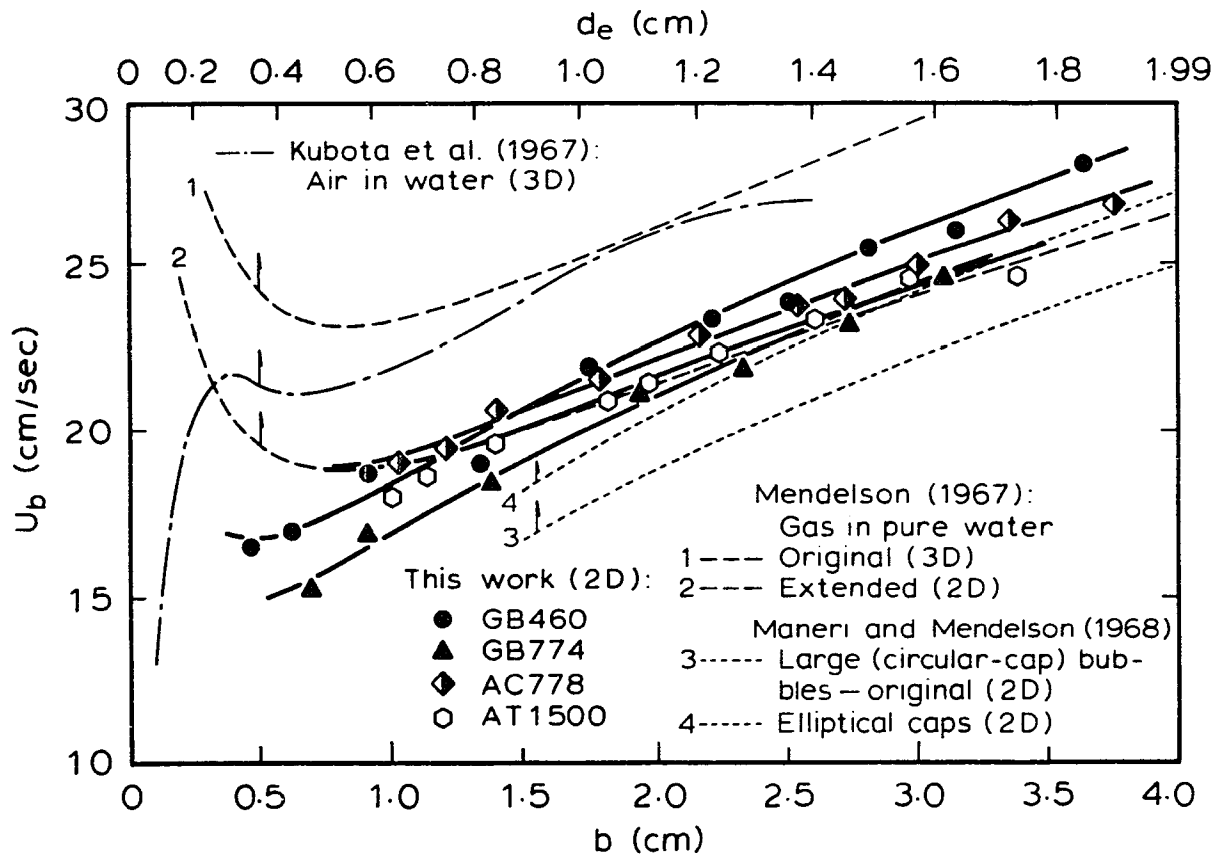


Figure 2.3 Rise velocity of single bubbles relative to liquid phase.

which was derived based on a wave analogy, was chosen as the starting point, for it has been proved to be applicable to three-dimensional bubbles of intermediate ($d_e > 1.3$ mm in pure water) to large size (Calderbank et al., 1970; Clift et al., 1978). The equation has two competing terms, surface tension and inertial force terms, and was assumed to have the same proportionality in two dimensions. The equation derived for two-dimensional bubbles by Maneri and Mendelson (1968), although having the same formula, overestimated the surface tension term and thus was not employed in the present study. The final correlation is given in terms of d_e by

$$U_b = f(d_p) \sqrt{g(d_p, \rho_s) / d_e + d_e} \quad (2.2)$$

where

$$f(d_p) = 18.1 + 0.0258 d_p^{-1.43} \quad (2.2a)$$

$$g(d_p, \rho_s) = 0.294 - 0.291 d_p^{0.319} [(\rho_s - \rho_l) / \rho_l]^{1.17} \quad (2.2b)$$

with a $\pm 2.5\%$ average error. The range of applicability is: $0.046 < d_p < 0.15$ cm; $1.25 < \rho_s < 2.50$ g/cm³; and $1.4 < H/H_0 < 2.0$ ($0.57 < \epsilon < 0.70$). Here H/H_0 gives the bed expansion ratio. Note that both coefficients are reduced to those for pure water as d_p and ρ_s approach zero and ρ_l , respectively. The value of proportional constant for pure water, 18.1, was selected based on the ratio of two-dimensional rise velocity to three-dimensional velocity for large bubbles. It was also taken into account that the bubbles in the present study were more closely approximated by elliptical caps than circular caps, especially around the edge region and that the elliptical cap rises 9%

faster than the circular cap of the identical size (Hills, 1975). The 9% discrepancy was observed by Collins (1965a) and Grace and Harrison (1967) and demonstrated in Fig. 2.3 employing the Maneri-Mendelson equation (Maneri and Mendelson, 1968) for large bubbles where the surface tension effect is negligible. As shown in the figure, the relative bubble rise velocities in the two-dimensional water-solid fluidized beds have the same order of magnitude as those in two-dimensional pure water except for smaller bubble size.

B. Wake Nature and Geometry

As indicated in the Introduction in this chapter, the bubble wake may not be completely turbulent except at extremely high Reynolds numbers (greater than 10^5 based on liquid viscosity). In gas-liquid-solid fluidized beds, the Reynolds number is moderately high and some disturbances in the flow field exist due to the solid particles and bulk flow; consequently, the wake structure falls between the two extremes of closed laminar and open turbulent. The wake structure can be considered to consist of a primary wake which moves in close association with the bubble and a secondary wake which includes a free shear layer and vortices shed from the primary wake. The primary wake is an enclosed region immediately behind and travelling with the bubble in which broad although irregular circulatory flow patterns can be identified. The secondary wake, on the other hand, has an open structure and can be a streaming tail extending along the bubble rise path below the primary wake at lower Reynolds numbers or a vortex street extending far behind the bubble at higher Reynolds numbers. In

addition, the secondary wake may include the drift effect induced by a passing bubble.

Figures 2.4(a) and 2.4(b) show a photograph of a relatively large two-dimensional nitrogen bubble rising in stagnant water at $Re_b = 8150$ and its wake visualized through hydrogen bubble tracers and a schematic interpretation of the wake flow, respectively. It can be seen that the bubble wake consists of two regions. The primary wake, or near-wake region, includes two vortices, one of which is represented by a well-established circulation (left-hand side) and the other being formed. The slightly deformed vortex seen below is isolated by streams of the external flow across the wake from left to right. This vortex is considered outside the primary wake. A similar wake structure was observed for a two-dimensional nitrogen bubble of the same size rising through a water-774 μm glass bead fluidized bed as shown in Figs 2.5(a) and 2.5(b). Again, the distinctive dual-wake structure can be clearly seen. Also seen in this case is the concentration gradient of solid particles in the wake: lower solids concentration regions were observed immediately beneath the bubble base and around the vortex center; higher concentration regions around the vortices, especially in the regions where two vortices interact.

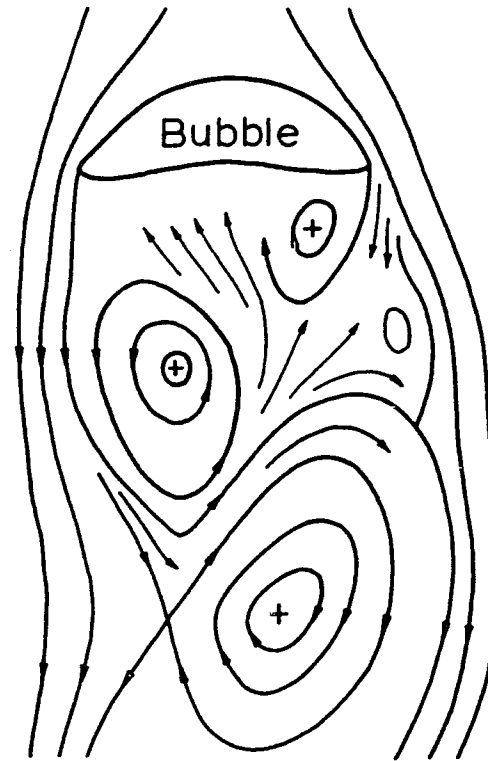
C. Wake Formation-Shedding Mechanisms

The most important fluid dynamic characteristic of the wake is probably its instability. Initially, the wake consists of a closed laminar region of a toroidal vortex ring (main portion) and a narrow tail following it. As the bubble accelerates and the wake grows in

N₂-Water



(a)



+ Vortex center
— Liquid flow

(b)

Figure 2.4 (a) Photograph of a circular-cap nitrogen bubble rising in stationary water and its wake visualized through hydrogen bubble tracers. (b) Schematic interpretation of the wake flow.

N₂-Water - GB774

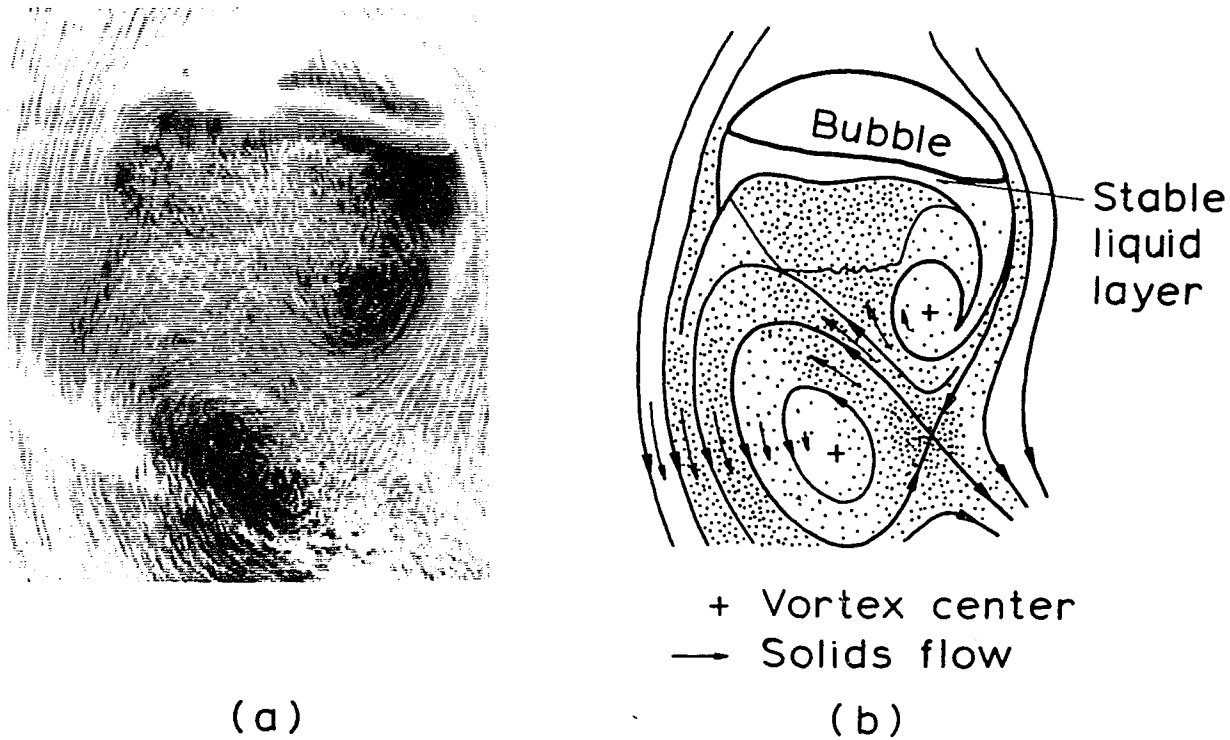


Figure 2.5 (a) Photograph of a circular-cap nitrogen bubble and its wake rising through a water-774 μm glass bead fluidized bed.
(b) Schematic interpretation of the wake flow.

size by continuously accumulating material from outside the wake, the symmetry of this flow will be perturbed and eventually some wake material will be discharged.

Wake shedding phenomena have been observed over a wide range of bubble flow. Any bubble which experiences secondary motion is suspected to shed its wake. The bubble shape may vary from an ellipsoid to a spherical-cap. The critical Re_e for the onset of wake shedding is reported as low as 100-110 for gas-liquid systems (Wegener and Parlange, 1973; Bhaga and Weber, 1981).

The nature of wake shedding is closely interrelated to the type of path followed by the bubbles. For instance, the periodic nature of asymmetric wake shedding is no doubt the cause of a zig-zag path in bubble motion or bubble rocking. Asymmetric shedding of a vortex from one side takes place as the inherently symmetric nature of the flow around small bubbles or bubbles in viscous media is disturbed when the Reynolds number increases. Subsequently, vortices are shed periodically from alternating sides. Although different in the degree of wake instability, two-dimensional wakes are considered to represent or at least approximate the projection, or cross section, of three-dimensional wake configurations.

Mechanisms of wake formation and shedding can be described based on localized fluid dynamic properties of the flow field around a rising bubble. As shown in Fig. 2.6(a) where the sketches represent the observations made in the present study, the formation of vortices in the near wake region originates from the separation of the external potential flow at the bubble edge. The separation of the flow induces

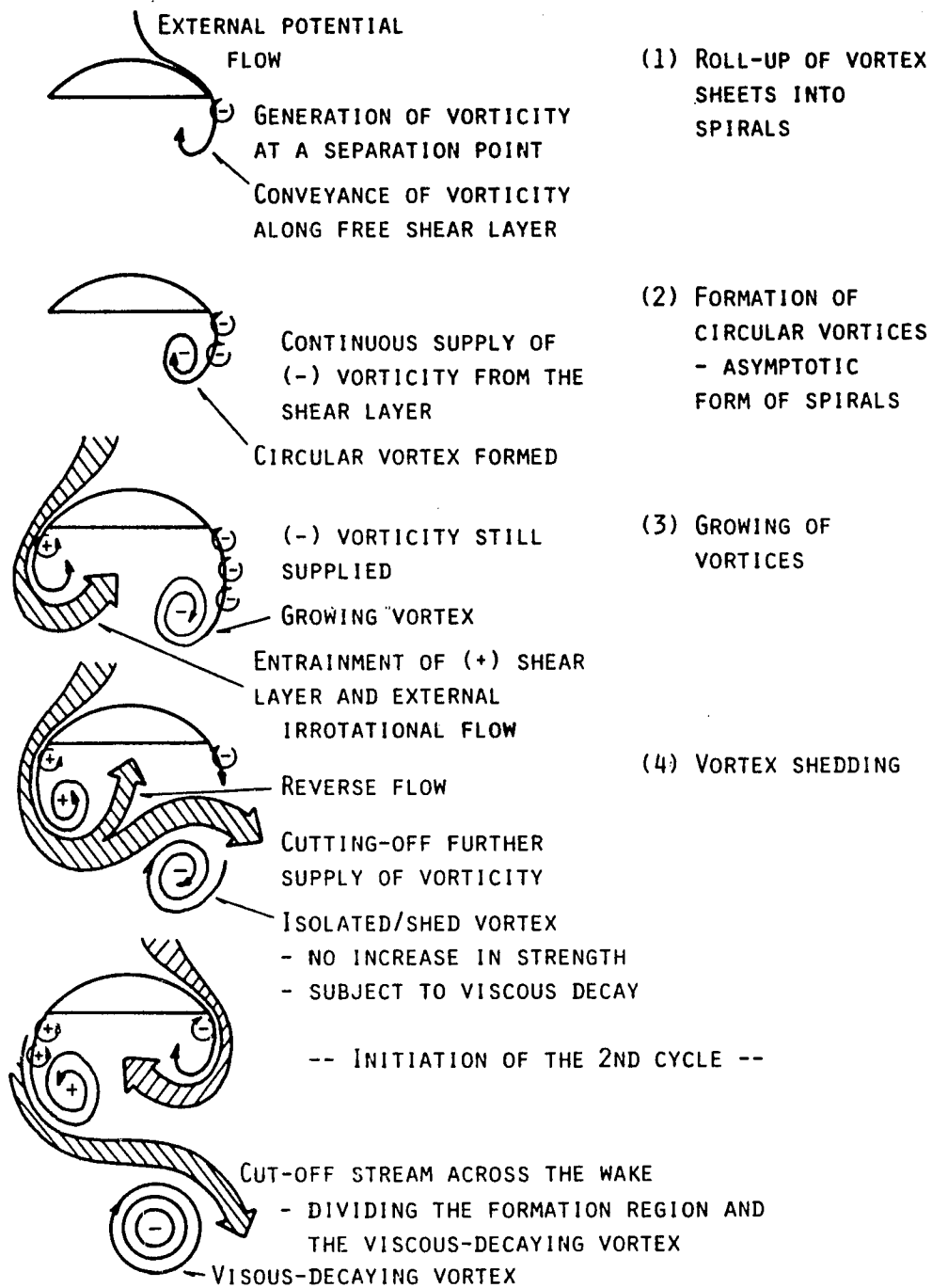


Figure 2.6a Mechanistic description of vortex formation and shedding - alternate shedding.

the generation of vorticity at the separation points, which is followed by the conveyance of vorticity along the free shear layer. This free shear layer, or vortex sheet, tends to roll up into a spiral form due to differences in the characteristic velocities between the outer and inner boundaries of the shear layer. Thus the rate of increase in the strength of the vorticity shed from the bubble edge can be approximated (Fage and Johansen, 1927; Sarpkaya, 1975; Kiya and Arie, 1977) by

$$\frac{\partial \Gamma}{\partial t} = \frac{1}{2} (u_{\text{out}}^2 - u_{\text{in}}^2) \approx \frac{1}{2} u_{\text{out}}^2 \quad (2.3)$$

The rolled up vortex sheet will eventually form a circular-cross-sectioned vortex. At this stage, the vortex is still attached to the bubble edge via the shear layer and grows as vorticity is continuously supplied through the shear layer. The vortex continues to grow until it becomes strong enough to draw the external flow and opposite shear layer across the wake. When this happens, oppositely-signed vorticity of sufficient concentration cuts off further supply of vorticity to the vortex and the vortex ceases to increase in strength and starts detaching from the bubble. At this moment the vortex is said to be shed. A very similar description was given by Gerrard (1966) on the basic mechanism controlling the frequency of vortex shedding from bluff bodies. The cut-off stream divides the near wake, or what Gerrard (1966) called the formation region, from the shed viscous-decaying vortex. The roll-up of the vortex sheet through the cut-off of the vorticity supply constitutes one cycle of the vortex formation-shedding process.

Parallel shedding may take place if the above process proceeds almost simultaneously from both edges. Most likely, however, parallel shedding occurs when the vortex sheets become unstable before forming well-established spiral/circulation flow patterns or even before rolling up. This is the case for large circular-cap bubbles.

The form of instability induced along a shear layer, or velocity discontinuity in a homogeneous fluid, is known as Helmholtz or Rayleigh instability. Employing a simple sinusoidal wave form at the interface along the shear layer $y = \eta(x,t)$:

$$\eta(x,t) = A \exp\left[\frac{2\pi i}{\lambda}(x - \kappa t)\right] \quad (2.4)$$

and knowing (Currie, 1974, p. 213)

$$\kappa = \frac{u_{\text{out}} + u_{\text{in}}}{2} \pm i \frac{u_{\text{out}} - u_{\text{in}}}{2} \quad (2.5)$$

we can easily deduce that the shear layer is unstable; the interfacial wave will exponentially grow with time. Here A is the amplitude, λ is the wavelength, x is the flow direction, t is the time, and κ is a measure of the sheet strength. As argued by Saffman and Baker (1979), the vortex sheet in an unsteady flow stretches/shrinks in length resulting in its strength being decreased/increased according to Kelvin's theorem (the conservation of circulation). In addition, this local variation in length corresponds to the same rate of increase/decrease in the wavelength of a disturbance. Now, based on eqs (2.4) and (2.5), the more compressed the sheet (i.e., the stronger the sheet and the shorter the wave), the more destabilized it tends to

be. The instability is also promoted by external disturbances due to the turbulence in the bulk flow.

The local stretching/shrinking of the vortex sheet as well as diffusion and dissipation of vorticity by the action of viscosity eventually breaks up the deforming sheet, leading to blobs of vorticity being shed from the bubble edge. A formation-shedding process of this kind is depicted schematically in Fig. 2.6(b). The occurrence of this vorticity-blob discharge on one side should affect neither the other side discharge nor the bubble motion appreciably because the shed vorticity blob is weak in "hydrodynamic" forces, or of small momentum, and does not invade into the interior of the near wake. Vorticity-blob discharge only causes the dilations of the bubble edge and not systematic alternative shedding. The discharged vorticity blobs from both edges may later organize themselves into a large-scale vortical motion since each of them possesses a unique sign of vorticity. The "organized" vorticity blobs at both sides now draw the external flows into the wake: some fluid elements are spouted towards the bubble base while others from each side collide around the wake centerline leaving a chaotic turbulent region.

D. Vortex Shedding Frequency

Shedding frequency of an individual vortex, represented by the Strouhal number, Sr_b , is plotted against Re_b (based on water viscosity) in Fig. 2.7 for the particles listed in Table 2.1. Each data point represents the average for bubbles of identical size range (see Appendix A for the summary of the bubble properties averaged over

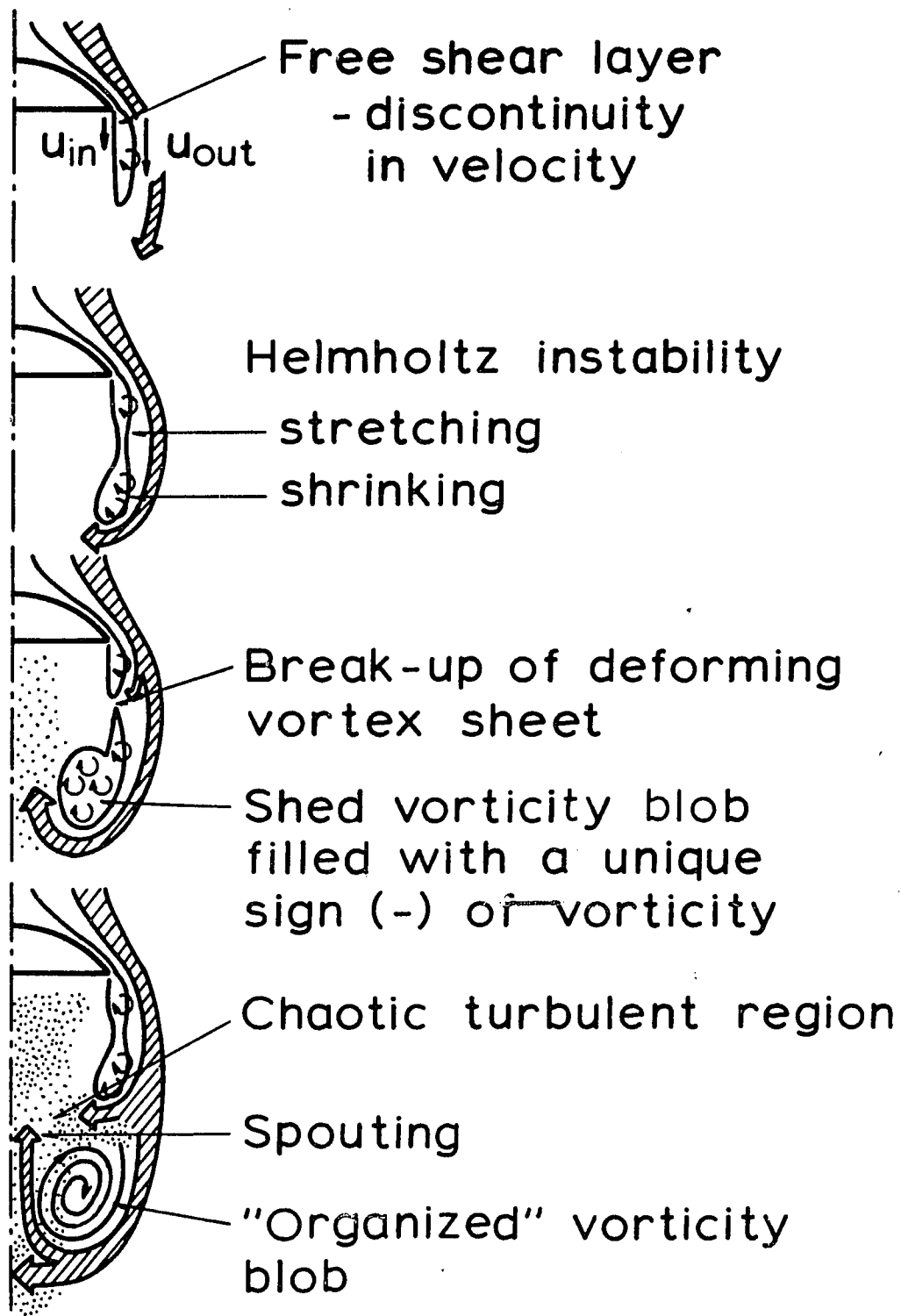


Figure 2.6b Mechanistic description of vortex formation and shedding - parallel shedding.

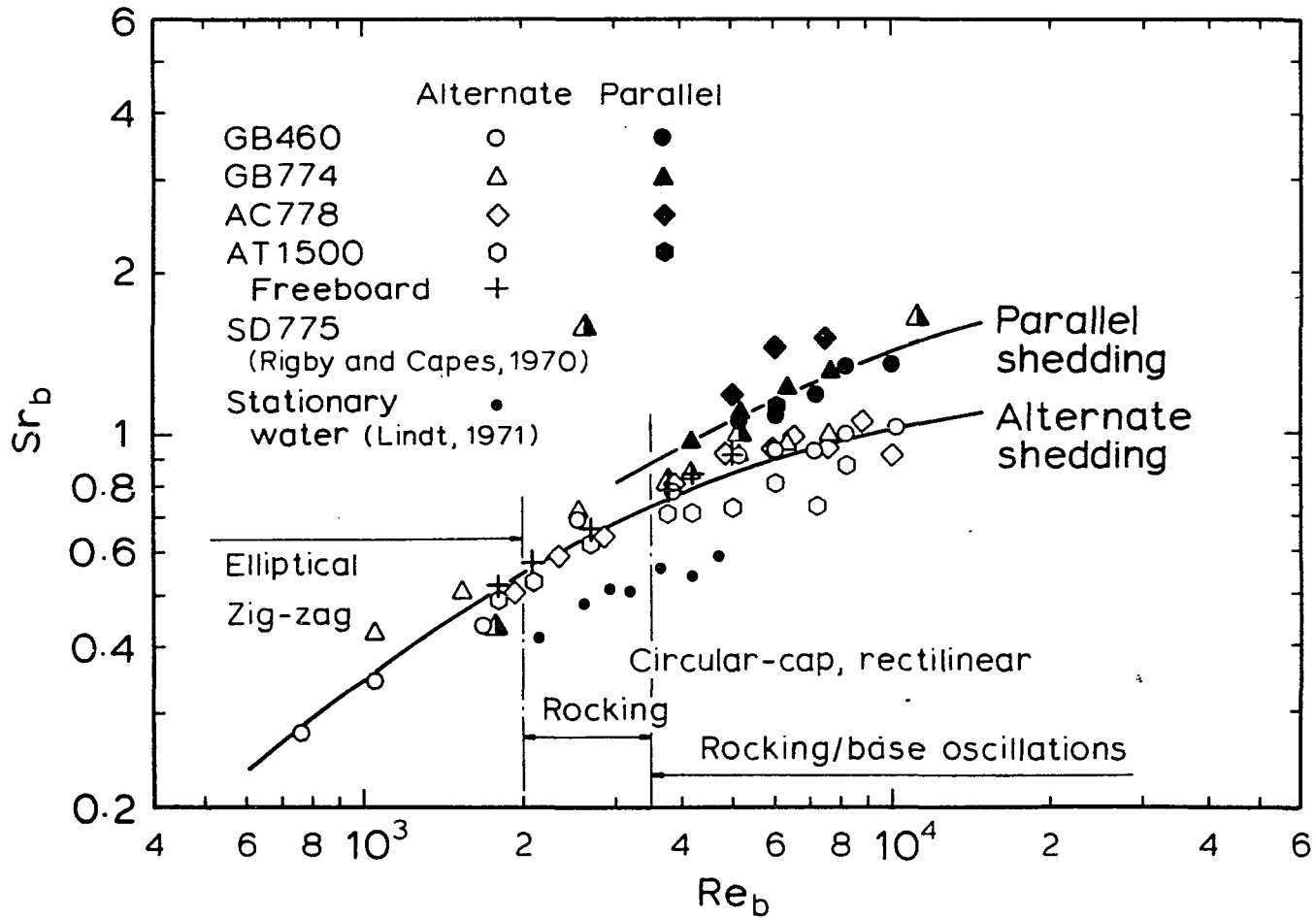


Figure 2.7 Relationship between Strouhal number and Reynolds number for vortex shedding from single two-dimensional bubbles.

each bubble size range). Also included in the figure are the results of Rigby and Capes (1970) and Lindt (1971). The range of data includes elliptical bubbles with a zig-zag motion to circular-caps in a rectilinear path with rocking as well as base oscillations. Periodic, alternate shedding of vortices was observed at low Re_b (< 3500) and the Sr_b was uniquely defined and monotonically (linearly in log-log scale) increased for each particle. At higher Re_b , shedding occurred rather irregularly. Careful observations, however, revealed co-existence of alternate and parallel shedding modes. The parallel shedding mode gives higher shedding frequencies. Accordingly, bubble motion could not be clearly defined; both rocking and base oscillations occurred for a single bubble during its rise.

Essentially no appreciable effects of particles on the Sr_b were observed; however, the largest particles (1.5 mm acetate) gave slightly smaller values at high Re_b . Furthermore, Sr_b evaluated indirectly from the bubble rocking frequency in the freeboard region over a water-acetate particle fluidized bed equaled those evaluated in the bed. Since the freeboard can be considered as a gas-liquid system, this suggests that, in this case, the presence of particles does not significantly alter the shedding frequency. Sr_b evaluated by Lindt (1971) for single bubbles rising in stationary water were, however, a little smaller, by a factor of approximately 1/3, although with the same trend. This could be attributed to the nature of the surroundings: all the systems besides Lindt's (1971) were disturbed by the liquid flow, which may have destabilized the wake flow appreciably.

The Sr_b was thus uniquely correlated with Re_b for each shedding mode as

$$Sr_b = \begin{cases} 1/(2420Re_b^{-1.02} + 0.776) & \text{(alternate)} & (2.6a) \\ 1/(981Re_b^{-0.888} + 0.425) & \text{(parallel)} & (2.6b) \end{cases}$$

where the empirical parameters were evaluated employing a nonlinear regression (Powell method, Powell, 1964; also see Beveridge and Schechter, 1970). Note that the correlated values of Sr_b were not sensitive to the values of these parameters. The applicable Re_b is between 800 and 10^4 . Other conditions are the same as for eq. (2.2).

E. Wake Boundaries and Sizes

The size of the primary wake can be estimated due to its periodic nature; however, defining the boundary between the primary and the secondary wake, which extends far downstream, is difficult and somewhat arbitrary. The complicated hydrodynamic flow fields surrounding the bubble often lack a clear boundary between the primary and secondary wakes. The following represents qualitatively identified boundaries between the primary and secondary wakes (two-dimensional projection) for several important representative wake structures.

For steady flows, the primary wake observed for large bubbles in a viscous medium or at low Reynolds numbers ($Re_e < 110$) is laminar and closed as shown in Figs 2.8(a) and 2.8(b). This type of primary wake, as shown enclosed by dotted lines and shaded inside, consists mostly of a well-developed toroidal vortex ring (three-dimensional) and a

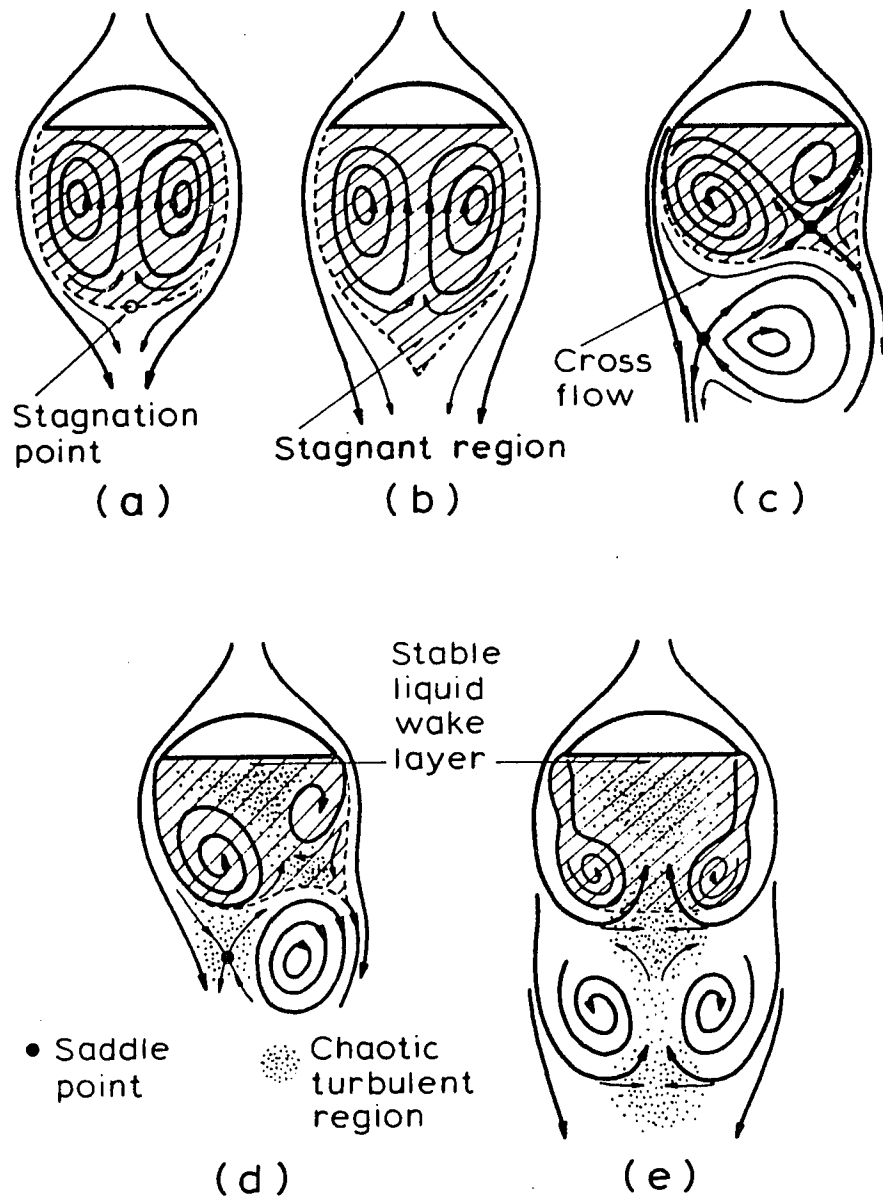


Figure 2.8 Schematic definition of primary wake boundary.

stagnation region near the rear stagnation point. Depending upon the Reynolds number and/or wake stability, this stagnant region may have negligible volume (Fig. 2.8(a)) as reported by Collins (1965b) or a non-negligible volume in a cusp shape (Fig. 2.8(b)) as claimed by Batchelor (1956) and Bessler (1984). The shape and size of the boundary is invariant with time. Note that in both gas-liquid and gas-liquid-solid systems such a primary wake has also been observed during the initial stable growth period of the wake before the symmetry of the wake flow is disturbed; consequently, this type of structure precedes the non-steady structures which develop after the initial stable growth period.

At higher Reynolds numbers for intermediate to large bubbles in liquids and/or liquid suspensions with low inertia solid particles, the wake flow is unsteady but has steady (cyclic) vortex shedding; Fig. 2.8(c) depicts a representative primary wake boundary for this case. The vortices generated in the near wake region are well developed before leaving the primary wake. The shedding scheme is the asymmetric alternate mode discussed previously. Thus, the primary wake boundary is marked by the cut-off stream which crosses the wake center axis from one side of the free shear layer to the other. The shape and size of the boundary vary periodically due to vortex shedding; the minimum size occurs at the moment of vortex shedding from one side, the maximum size occurs just before shedding.

Over this same Reynolds number range, but for larger inertia particles, the wake flow is still asymmetric shedding and the shed material has large-scale vortical motion. However, there is a region

of chaotic turbulence about the wake center axis in addition to the stagnant turbulent layer directly behind the bubble as shown in Fig. 2.8(d). This region may result from either the high inertia solid particles deviating from the liquid flow pattern and being expelled from the vortex region to the central wake region or the turbulent shear layers being dragged into the interior. Consequently, the primary wake is said to be "open" since it cannot be distinguished from the adjacent secondary wake region due to this turbulent region. Nevertheless, the boundary can be defined, as shown in the figure, by connecting the outermost streamlines of the vortices at each side (dotted line).

For very large bubbles rising at high Reynolds numbers the wake flow is unsteady and has parallel wake shedding; Fig. 2.8(e) shows a phase (or time) averaged primary wake boundary for this case. As explained previously, the shedding possibly takes place due to the instability induced along the free shear layer. Thus, the primary wake boundary can be defined by connecting the end point of two vortex sheets hanging from the bubble edges. The primary wake contains the vortex sheets or blobs, which may not have established a well-defined vortical motion, and rather a wide region of chaotic turbulence around the wake center axis.

After defining proper boundaries based on the flow field the primary wake size can be determined. Examples of the dynamic variations in the primary wake area, normalized with respect to the bubble area at each instant, (k_{pw}) and the angle of attack (α) for three different systems are given in Figs 2.9, 2.10 and 2.11. A

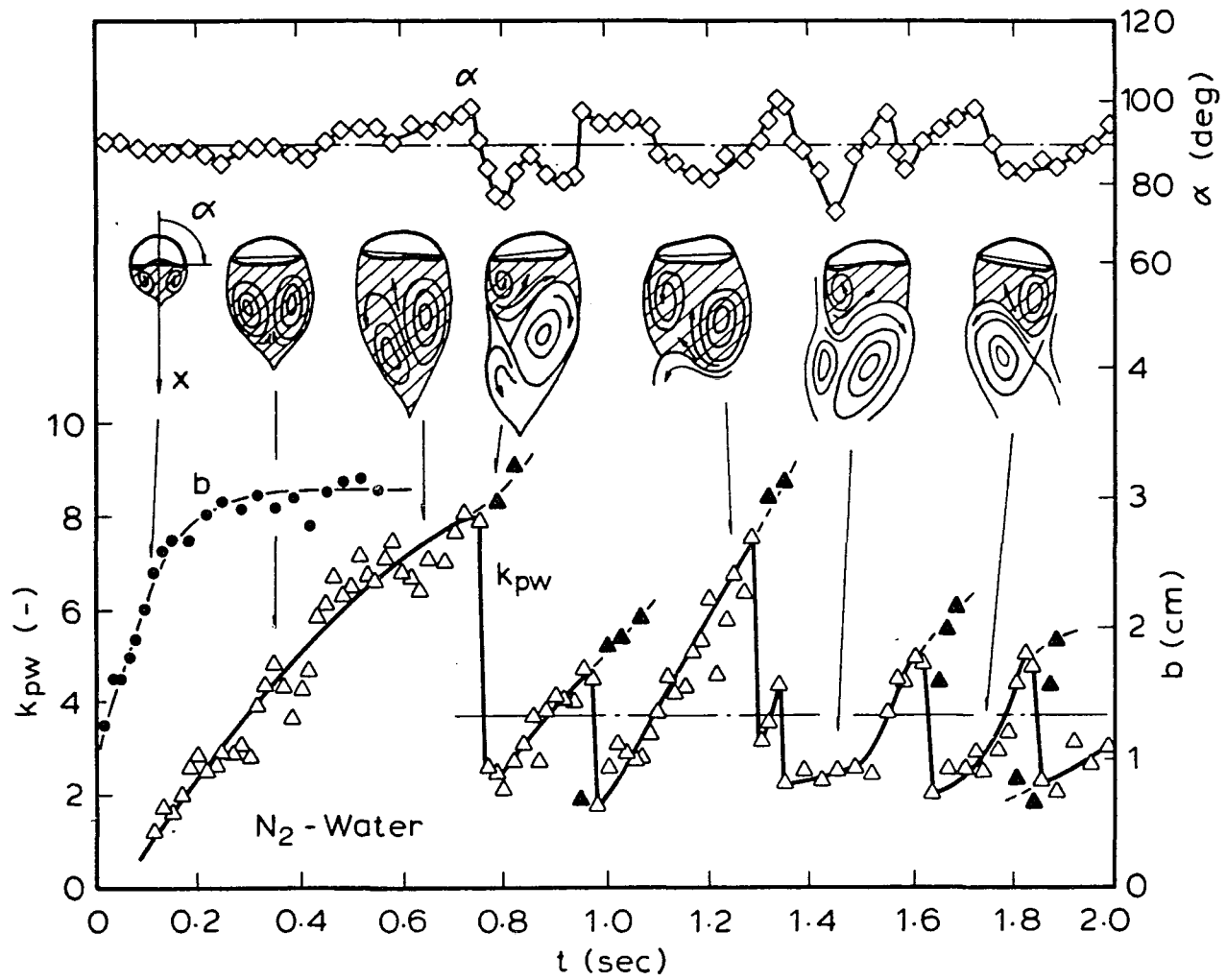


Figure 2.9 Dynamic variations in primary wake area (k_{pw}) and angle of attack (α) in stationary water.

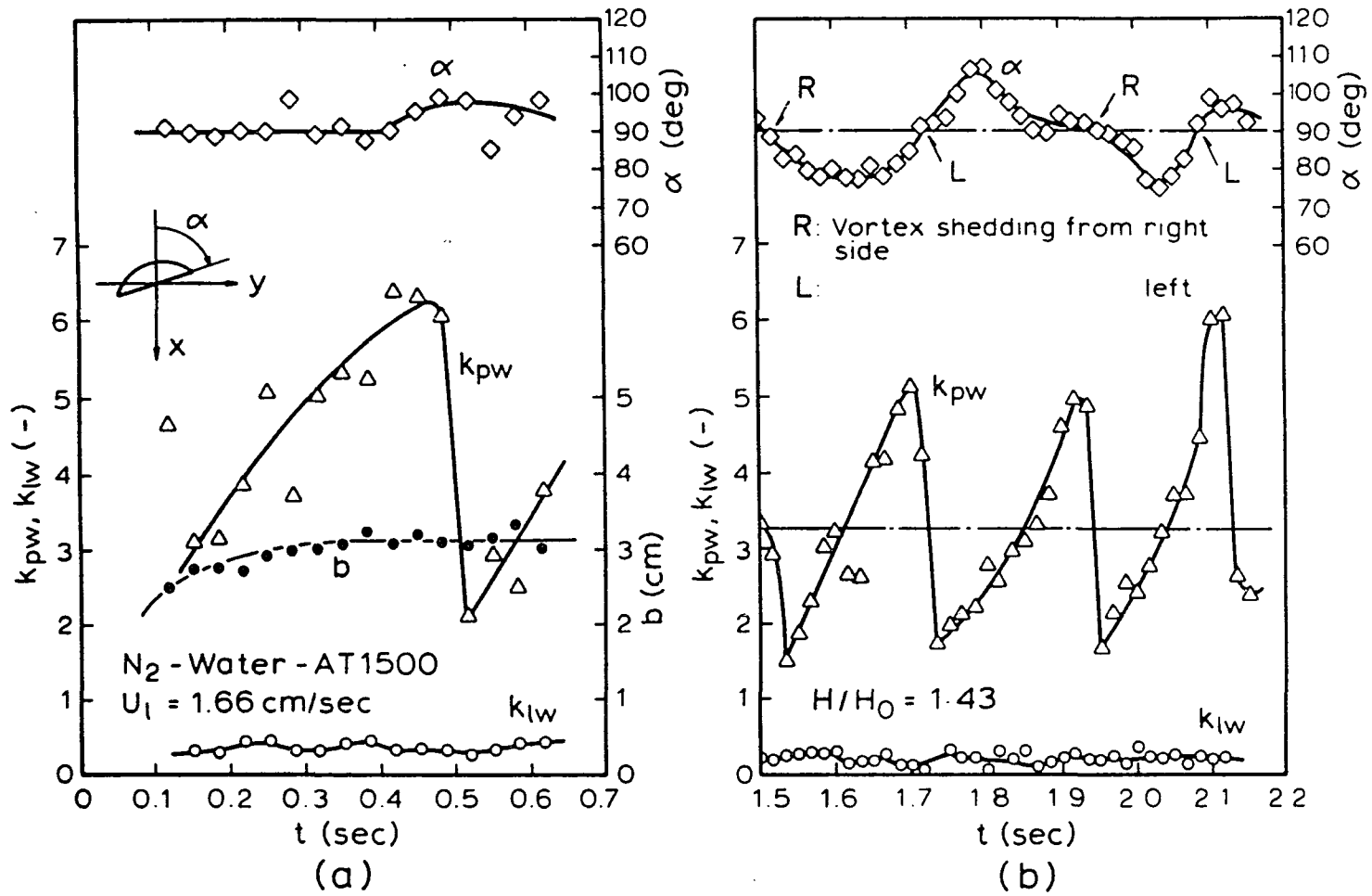


Figure 2.10 Dynamic variations in primary wake area (k_{pw}), liquid wake area (k_{lw}) and angle of attack (α) during (a) steady growth period and (b) steady shedding period in a water-1.5 mm acetate particle fluidized bed.

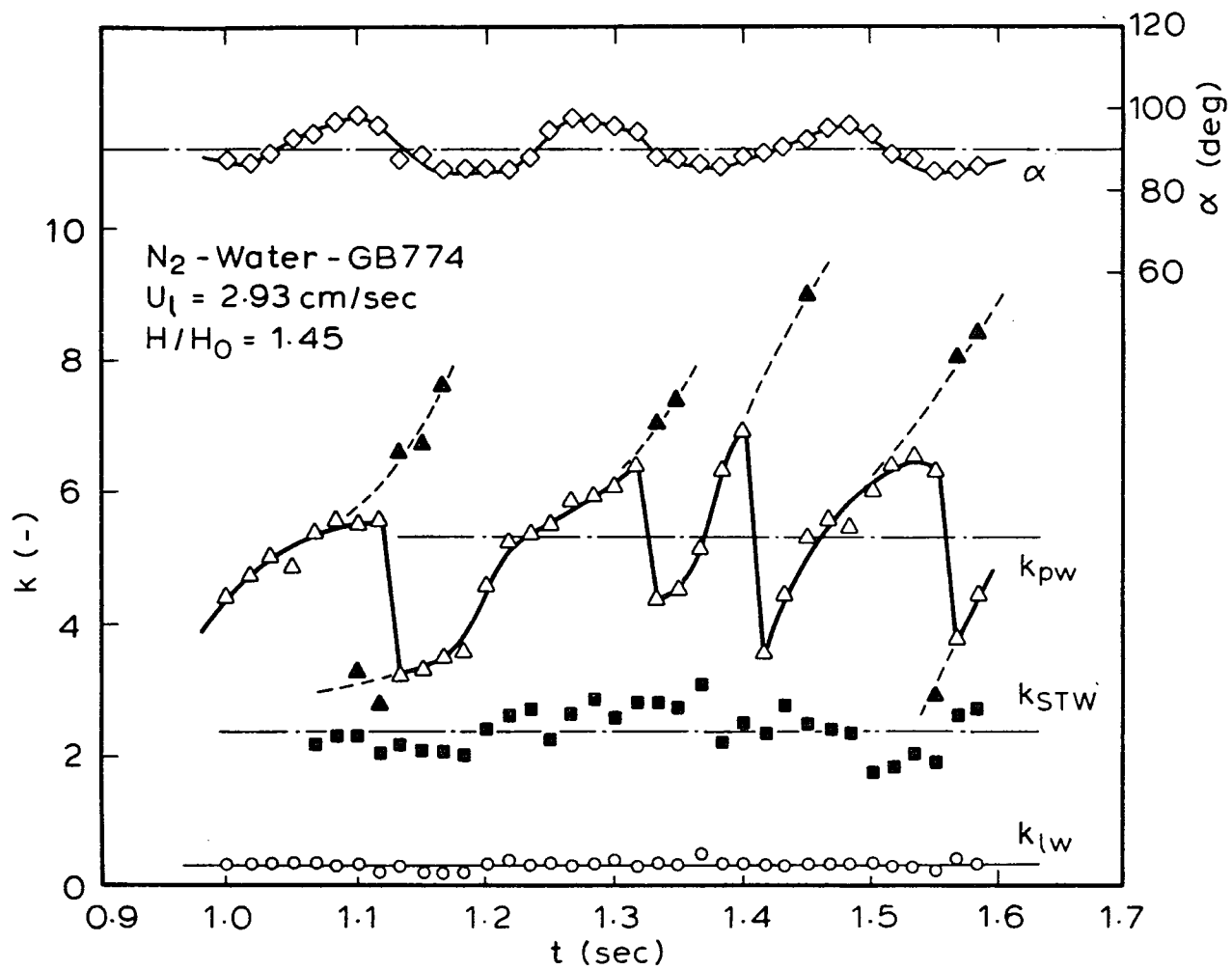


Figure 2.11 Dynamic variations in primary wake area (k_{pw}), liquid wake area (k_{Lw}) and angle of attack (α) during steady shedding period in a water-774 μ m glass bead fluidized bed.

circular-cap bubble of size $b \approx 3$ cm was injected into each system. Figure 2.9 depicts the variations over the 2.0 s period right after the injection of the bubble into stationary water. Although the bubble reached its steady-state geometry quickly (less than 0.3 s), the bubble wake steadily grew in size (to about 8 times the bubble area) until about 0.75 s had elapsed before it shed any wake material - the steady growth period. Note that during this period the angle of attack remained almost constant around 90° , which characterizes the symmetry of the wake flow. When α starts deviating from 90° and drastically varies its value around 90° , the wake is considered shed. Once this asymmetry sets off, periodic vortex shedding, thus the periodic variation of the primary wake size, follows - the steady shedding period. The figure includes 5 cycles of such a variation. The size and duration of each peak were not uniform in this case since shedding did not occur purely alternately; however, the cycle can be characterized by the so-called saw-tooth wave function. The primary wake size varied from about 2.3 to 5.4 times the bubble size with the mean value around 3.7 at an average frequency of 6.2 s^{-1} . The angle of attack varied correspondingly, although the frequencies in both variations did not match exactly. The solid triangles connected with the dotted lines given in the figure indicate the uncertainty in the determination of the moment of vortex shedding and thus, the maximum/minimum primary wake size.

Figure 2.10(a) shows the increase in primary wake area in the steady growth period for a bubble rising in a water-1.5 mm acetate particle fluidized bed. Results similar to those in the previous case

were obtained: the primary wake grew to about 6 times the bubble area then dropped in size to about twice the bubble size. Dynamic variations in the steady shedding period are shown in Fig. 2.10(b). The figure includes three cycles of purely asymmetric vortex shedding with a frequency of about 5 s^{-1} . The primary wake size again periodically varied in the form of a saw-tooth wave function from about 1.5 to 5.5 times the bubble size. Also clearly demonstrated in this example is that the shedding frequency can be estimated by the corresponding bubble rocking frequency if vortex shedding takes place purely alternately. Notice a one-to-one correspondence between the frequency in the primary wake size variation and that in the angle of attack variation as shown in the figure: a decrease in α from 90° corresponds to vortex shedding from the right side of the bubble and an increase in α indicates shedding from the left side.

Figure 2.11 shows the variations in the steady shedding period for the bubble rising in a water-774 μm glass bead fluidized bed. In this case shedding occurred rather symmetrically; however, since the bubble size was not large enough to have purely symmetric shedding, there remained some asymmetry. Although the bubble rocking was not clearly seen, the bubble edge wobbled alternately on each side leading to a sinusoidal fluctuation in α as shown in the figure. The primary wake size variation did not correspond to this one to one because two vortices/vortical blobs were often shed almost simultaneously. The primary wake size fluctuated between 3.7 and 6.6 times the bubble area over three cycles of its variation. Also observed within the primary wake in this case was a turbulent but stable

region, or stable turbulent wake (STW), immediately beneath the bubble whose size was rather constant around 2.4 times the bubble size. This region did not include the main portion of the vortical motion and was highly concentrated with solid particles.

The primary wake includes a stable liquid layer with negligible solids concentration located immediately beneath the bubble base. Its existence, from a hydrodynamic point of view, has been indirectly shown by Lazarek and Littman (1974) by measuring the pressure field around a rising bubble: refer to a very sharp valley (a local minimum) immediately beneath the bubble base in the pressure distribution shown in Fig. 1.1 (Chapter 1). The size of the stable liquid layer has been extensively investigated due to its critical role in the wake model (Efremov and Vakhrushev, 1970; Rigby and Capes, 1970; Bhatia and Epstein, 1974; Darton and Harrison, 1975, 1976; Baker et al., 1977). The wake volume normalized with respect to the bubble volume, or k , usually refers to the volume of this liquid wake region. As shown in Figs 2.10 and 2.11 the liquid wake area did not exhibit cyclic variation under the given conditions. No correspondence to the vortex shedding frequency was detected, although the average size was slightly smaller in the steady shedding period than in the steady growth period. This verifies the approach taken by Darton and Harrison (1976) to theoretically determine the height of the liquid-wake layer based on steady wake configurations.

Despite the fact that the amplitude and frequency of the primary wake size fluctuation in the steady shedding period are different from condition to condition as shown above, its periodic nature can be

universally expressed by the form of a saw-tooth wave function. Thus, when all the results are normalized with respect to the duration of and the difference between the maximum and minimum sizes in each cycle, they tend to fall into the same curve as shown in Fig. 2.12. The shape of the fluctuation for one cycle can be approximated by a simple form

$$\frac{k_{pw} - \bar{k}_{pw}}{\Delta k_{pw}} = f_{pw}(t - t_0) - \frac{1}{2} \quad (2.7)$$

where t_0 , the initial time of each cycle, is relative so that it can be set arbitrarily. f_{pw} is the average frequency in the primary wake size variation and equals the shedding frequency of an individual vortex for the alternate shedding mode or one half of f_v for the parallel shedding mode, which has been given by eq. (2.6a) or (2.6b), respectively. The parameters \bar{k}_{pw} , the mean primary wake size, and Δk_{pw} , the average difference between the maximum and minimum sizes, are discussed in the following.

Figure 2.13 shows the mean primary wake size versus the Reynolds number Re_b . The mean values were obtained over at least three cycles of primary wake size variation and marked with possible minimum and maximum values. The primary wake size was expressed in terms of the area ratio ($k_{pw}^{(2D)}$: left-hand side ordinate) and volume ratio ($k_{pw}^{(3D)}$: right-hand side ordinate). Here the area ratio was based on actual measurement while the volume ratio was based on a geometrical assumption on the bubble and primary wake shapes. A 3D bubble was assumed an axisymmetric ellipsoid with length of major axis b and

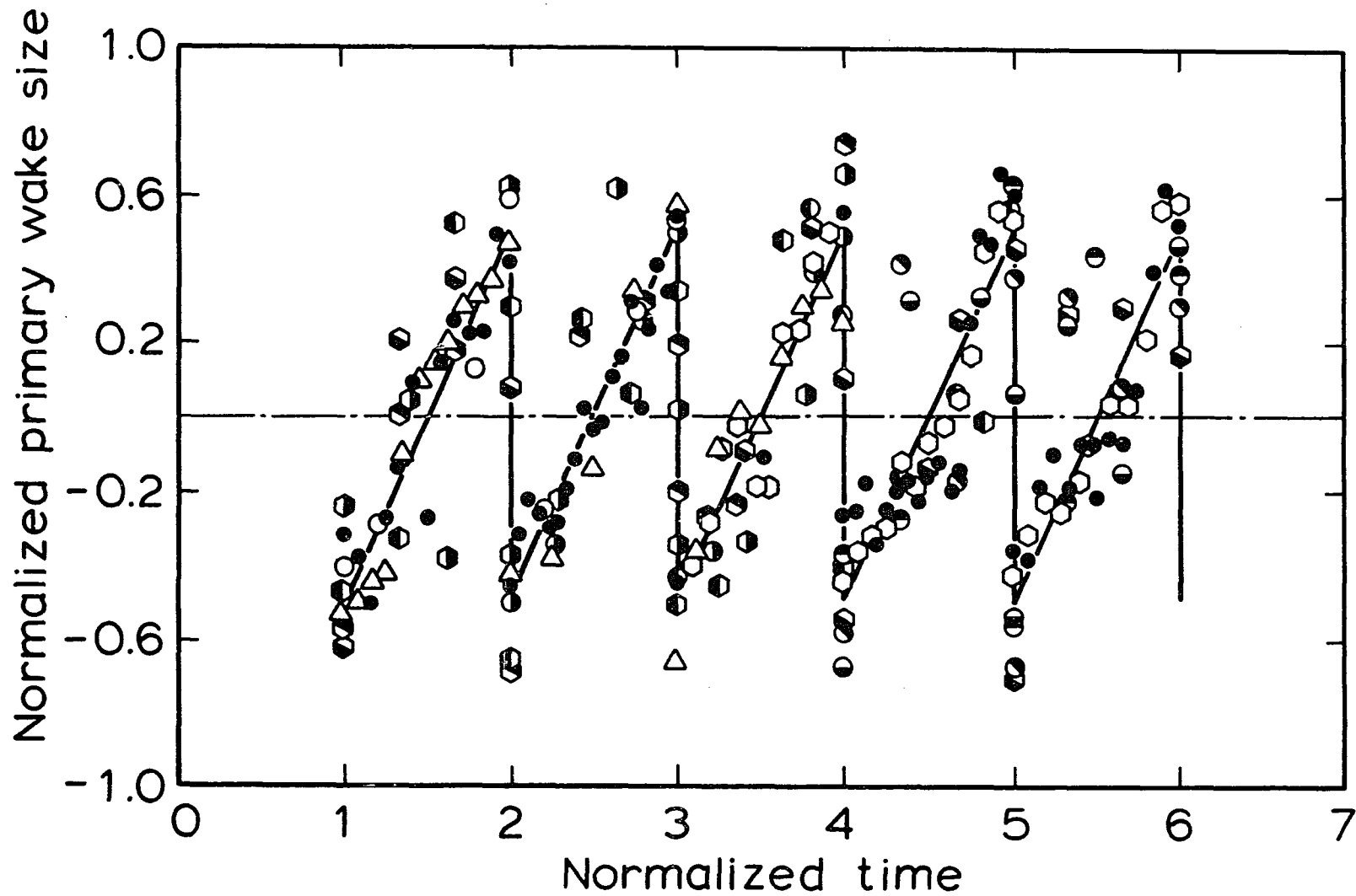


Figure 2.12 Normalized variation of primary wake size as expressed by the form of a saw-tooth wave function.

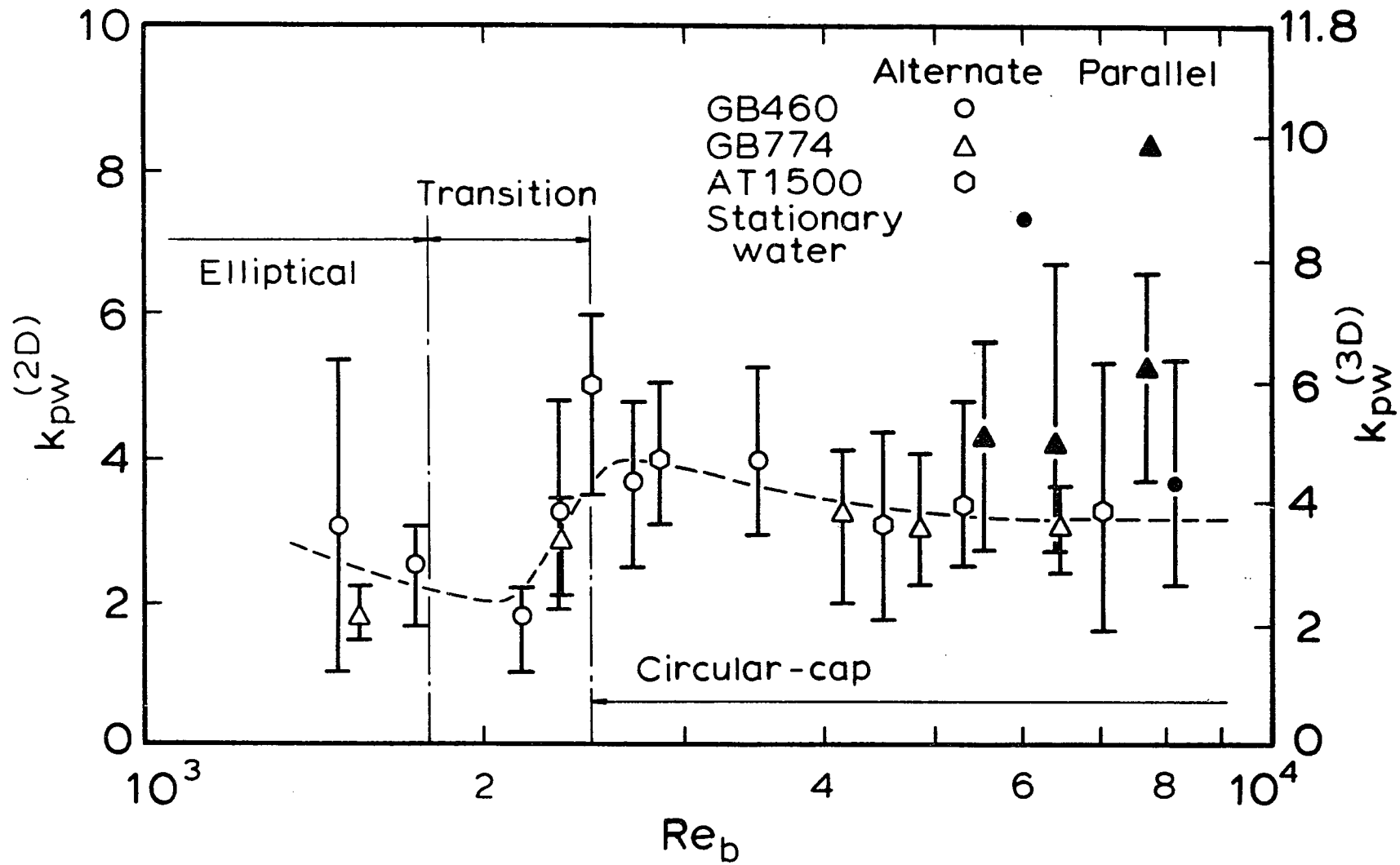


Figure 2.13 Mean primary wake size marked with minimum and maximum values.

minor axis h and the wake was assumed a cylinder of diameter b whose projected area was the same as the one actually measured. Assuming a spherical-cap shape overestimated its projected area even for a relatively large bubble due to the round edges of the actual bubble.

Although the data were somewhat scattered, partly because of the intrinsic unsteadiness of the wake geometry and partly because of the difficulty in measurement, the primary wake size was found to be a weak function of Re_b . Consideration of the bubble-shape and motion regime, however, revealed that \bar{k}_{pw} slightly decreased with increasing Re_b in each regime. For instance, the \bar{k}_{pw} shifted from one value to another when the transition from the elliptical to circular-cap regime took place at $Re_b \approx 2000$; however, the \bar{k}_{pw} before and after the transition were almost constant. The lower average value in the elliptical regime can be explained by the two facts: (1) the wake size is mainly controlled by the bubble breadth and the relative velocity of the bubble with respect to the surroundings, which is proportional to b^n where $0 < n < 1/2$, and (2) the bubble area sharply decreases as its shape changes from an ellipse to circular cap for the bubble of identical breadth. The same trend can be seen in the results presented by Kojima et al. (1975) for an air-10% NaCl aqueous solution system. Their experimental range was $2000 < Re_e < 5000$ ($0.4 < d_e < 2.0$ cm). In this range the averaged mean value of the $k_{pw}^{(3D)}$ in the present work was around 4.2, which indeed was close to that reported by Kojima et al. (1975) of 4.7. Coppus et al. (1977) found the volume ratio to be constant over the Reynolds number range $Re_e = 70-2 \times 10^4$ (1-130 cP) for large spherical-cap bubbles and reported an average value

of 22. This, however, appears to be too large; the primary wake region was elongated profoundly due to the wall effects. The size of the water tunnel Coppus et al. (1977) used was 25 x 25 cm cross-section; the breadth of spherical-cap bubbles was as large as 8 cm.

The size of a sphere-completing wake, which is often employed to approximate the geometry of bubble wakes in various systems (gas-liquid: Davies and Taylor, 1950; Parlange, 1969; gas-slurry: Dayan and Zalmanovich, 1982; gas-liquid-solid: Darton and Harrison, 1976; Kl-Temtamy and Epstein, 1978), is 10.9 ($= k_{pw}^{(3D)}$) for a spherical-cap bubble with an included angle of 100° . A corresponding two-dimensional circle-completing wake has $k_{pw}^{(2D)} = 7.27$. The sphere-completing wake may be a reasonable representation of a closed laminar wake whose internal flow can be modeled by Hill's spherical vortex (Hill, 1894). Based on the data obtained in this study, however, the assumption of sphere-completing wake overestimates the primary wake size under moderate/high Reynolds number conditions by more than 200%. The overestimation is due to the vortex sheet bounding the primary wake follows a path which is much closer to the vertical downward line from the bubble edge than the sphere-completing wake circumference and wake instability/vortex shedding occurs at high Reynolds numbers.

The average difference between the maximum and minimum sizes of the primary wake was as large as the mean primary wake size itself. The overall average value for $\Delta k_{pw}^{(2D)}$ was estimated to be around 2.4. The ratio of the primary wake area to the bubble area is thus fairly constant at 3.3 ± 1.2 over a wide range of Reynolds numbers investigated in the present study, i.e., $Re_D = 1500-8150$.

CONCLUDING REMARKS

The wakes of a relatively large gas bubble, including elliptical and circular-cap shapes, injected into a liquid-solid fluidized bed investigated in the present study consist of two regions: the primary and secondary wakes. The primary wake, or near-wake, region is characterized by large-scale vortical motion and is responsible for various hydrodynamic phenomena.

The most critical fluid dynamic characteristic of the wake is its instability. Periodic wake shedding can take place either asymmetrically or symmetrically. The dynamics of vortical motion is the key to vortex formation and shedding. The asymmetric vortex formation-shedding mechanism consists of the roll-up of a vortex sheet, growth of a circular vortex, and entrainment of external flow by the growing vortex on one side and the cut-off stream from the other side which intercepts the vorticity supply and isolates the vortex. The vortex sheet instability occurring independently on each side of a large bubble is responsible for the symmetric shedding. Vortex shedding frequency, expressed in terms of the Strouhal number, is a function of the Reynolds number for each shedding mode and appears independent of particle properties.

The primary wake size varies periodically in the form of a saw-tooth wave function, while the liquid wake exhibits no appreciable cyclic variation in size. The mean primary wake size is a weak function of the Reynolds number and may depend on the bubble-shape and motion regime. The mean value for the ratio of the primary wake area to the bubble area was estimated to be 3.3 ± 1.2 for the range $1500 <$

$Re_b < 8150$, which is less than one half of the value for a circle-completing wake, i.e., 7.27.

CHAPTER 3

VORTEX MOTION IN THE NEAR WAKE

ABSTRACT

The properties of vortices generated at the edges of two-dimensional single gas bubbles rising in water and/or water-solid fluidized media were experimentally investigated. The locus of the center, descent velocity with respect to the bubble, size variation, and shape deformation of each vortex during the course of descent were determined visually via a video camera system with an aid of hydrogen bubble tracers for liquid flow and solid particle tracers for solids flow. Vortex behavior was found to be, in general, very similar in both the liquid and liquid-solid media except the vortex life: shorter life in the liquid-solid suspensions than in the liquid. The trajectories of liquid elements and solid particles obtained in the near-wake region were strongly influenced by the presence of vortices. The deviation of solid particles from liquid flow path created particle concentration gradients in the near wake. Particle velocity profiles, obtained from an instantaneous flow field around the bubble, exhibited the disturbances caused by the passage of the bubble, which may be characterized by the vortical motion and the cross flow.

INTRODUCTION

It has been observed that, unless at very low Reynolds numbers, vortices generated behind a two-dimensional bluff body are eventually discharged downstream forming a so-called Karman vortex street (e.g., Birkhoff, 1953; Roshko, 1955; Perry et al., 1982). Although the properties of vortex streets in the far wake have been studied extensively, little attention has been placed on the flow immediately behind the body, or in the near wake.

The near wake plays an important role in characterizing the vortex properties since it is the region where the vortex formation-shedding process takes place. Gerrard (1966) gave a physical argument that the formation region size, the vortex strength, and the vortex shedding frequency closely interrelated with each other. In the previous chapter, Gerrard's argument was extended to explain the instability of the bubble wake in a two-dimensional liquid-solid fluidized bed. Another physical interpretation of the vortex shedding process was given by Perry et al. (1982). They claimed that "a deep insight into the mechanism of vortex shedding can be obtained by studying the instantaneous streamline patterns at various phases of the vortex-shedding cycle." Their flow concept, the so-called critical point theory, provides a phenomenological interpretation of the wake flow characteristics: based on this theory one can unify at least qualitatively the description of the dynamic nature of the wake, both non-turbulent and phase-averaged turbulent, in terms of large-scale vortical motion.

For intermediate-to-large-size ($d_e > 1 \text{ mm}$) gas bubbles rising freely in low viscous liquids, the bubble takes a variety of shapes depending on the surrounding force field and exhibits complicated behavior, e.g., zig-zag or helical trajectories, rocking, and oscillations of bubble base or even whole body. In the presence of such "secondary" motion of the bubble, it is extremely difficult to study the wake flow at microscopic levels. Note that the vortex described in the present study refers to a broad circulatory flow pattern, which is essentially an assemblage composed of a number of small eddies of an identical sign.

The motion of an isolated line vortex (two-dimensional vortex) in liquids has been studied for many years. Ting and Tung (1965) studied the motion of a vortex, which was subject to viscous decay, through solving the Navier-Stokes equations in a two-dimensional incompressible stream. They showed that, as a first-order approximation, the vortex motion can be represented by the classical inviscid solution superimposed with the solution of a decaying circular vortex. The matched solution thus removes the singularity at the vortex center associated with the classical inviscid theory by confining the viscous effects to a finite area about the vortex center. In the investigation of the trajectories and decay rates of line vortex pairs at moderately high Reynolds numbers under the influence of a ground plane, Barker and Crow (1977) found that the vortex trajectory is influenced by the size of a finite vortex core, which is determined by the vortex strength.

In the wake of a bluff object, vortices are no longer isolated but interact with each other in the confined area. This mutual interaction of nearby vortices (non-viscous effect) causes the deformation of each vortex (Christiansen and Zabusky, 1973), making the mathematical description far more complex. The interactions of vortices, especially free vortices with finite cores, have received profound attention in the past two decades owing to recent improvements in computational efficiency in the numerical simulation of incompressible fluid flows. Comprehensive reviews are available in the literature on this subject (Saffman and Baker, 1979; Leonard, 1980). Experimental exploration, however, is still needed to obtain more insights into the wake vortex phenomena.

The large-scale vortical motion in the near wake has a great impact on the trajectories of liquid or solid particles around a rising bubble since it engulfs some particles into the vortex area and at the same time creates centrifugal force fields. Tracing the particle trajectories around rising bubbles can provide an estimate of the average residence time of liquid or solids in the primary wake, which is essentially identical to the near wake or the formation region (see Chapter 2 for the specific definition of the primary wake). In designing multiphase contacting devices such as gas-liquid-solid fluidized bed reactors, the knowledge of the average residence time is crucial, for it determines the contact time of the liquid and/or solid phase with the gas molecules diffused from the bubble into the wake region. It also plays a key role in solids entrainment into the freeboard.

In Chapter 2, the dynamic/periodic nature of the near wake of a single bubble rising through a two-dimensional liquid-solid medium, especially vortex shedding and the primary wake boundary variation was studied. This chapter is intended to continue the investigation of the bubble wake dynamics by focusing on the motion of individual vortices and the trajectories of liquid elements and/or solid particles around the wake vortices in a two-dimensional liquid and/or liquid-solid media. A liquid element (or liquid particle) in the present context is defined as a very small volume of liquid behaving like a single particle and its motion is assumed to be reasonably represented by that of a hydrogen bubble.

EXPERIMENTAL

A schematic diagram of the experimental system is given in Fig. 3.1. A two-dimensional Plexiglas of 104 cm height, 40.6 cm width and 0.8 cm nominal gap thickness was used to visually observe the motion of the vortices behind a rising bubble. A video camera moving at the same speed as the bubble was employed to fix the frame of reference at the bubble center. Liquid distribution was achieved through four inlet valves and four compartments of 12.7 cm high, 1.9 cm thick packed beds of three layers; 3 mm lead shot, 2.3 mm alumina particles and 774 μm glass beads. Single gas bubbles were injected through a 0.64 mm o.d. nozzle flush-mounted on the rear wall 10 cm above the liquid distributor. A micro-switch was used to synchronize the bubble injection timing with the camera location during its initial rise. The signal from the camera was monitored via a Sony VO-5800 video

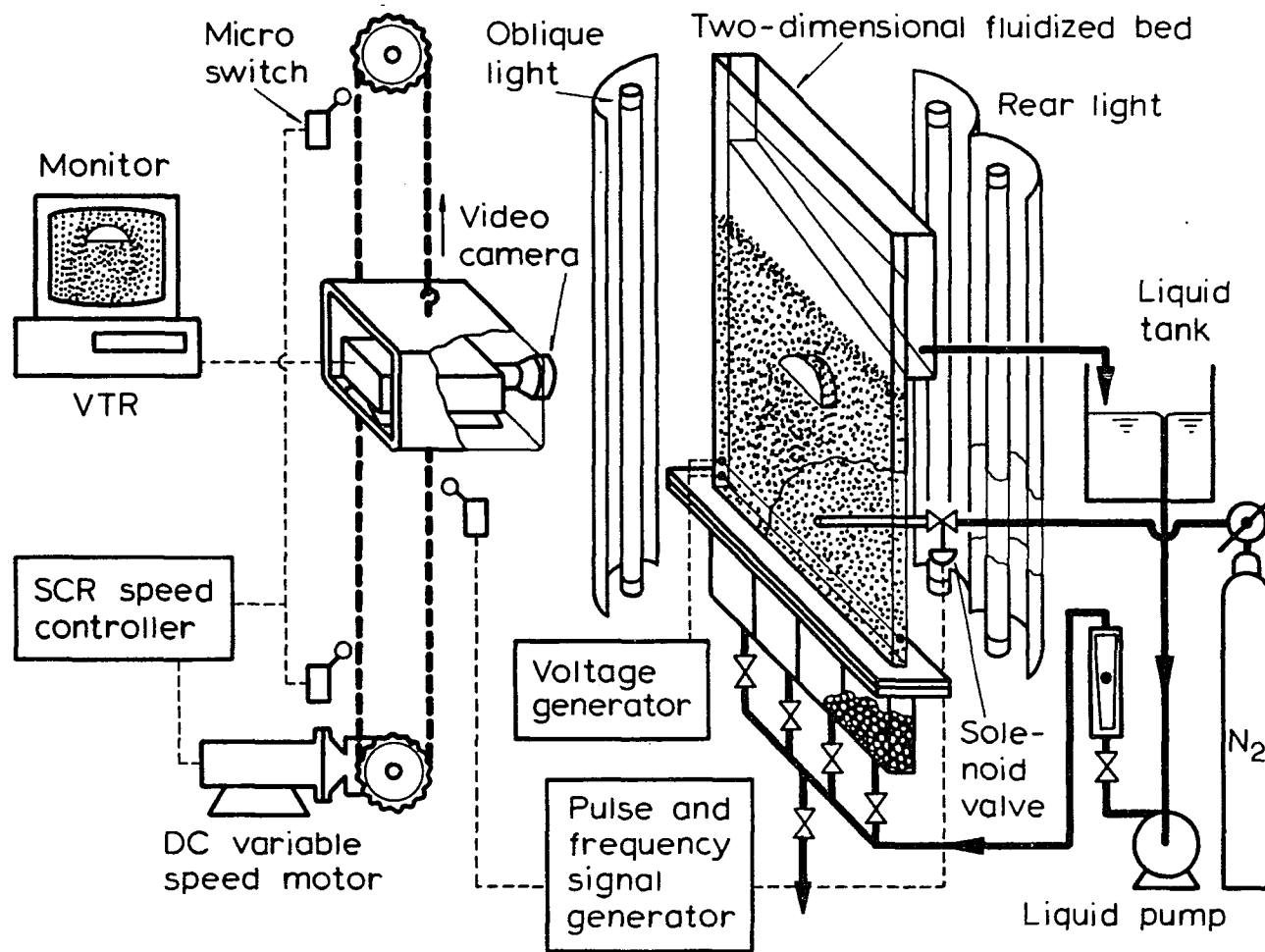


Figure 3.1 Schematic diagram of the experimental system.

recorder. Recorded data were either photographed or traced field by field, which in turn were analyzed using a Houston Instrument TG-1017 digitizer. Further details of the experimental apparatus have been given in Chapter 2.

Nitrogen bubbles were injected into either tap water with hydrogen bubble tracers or water-solid particle suspension systems. To generate fine hydrogen bubbles, a thin (nominally about 0.05 cm) wire of tungsten was used as the cathode, which extended horizontally across the long axis of the column just above the liquid distributor. The rise velocities of hydrogen bubbles are much smaller than the subject bubble rise velocity, usually by three orders of magnitude. The particles used were all spherical whose size and density ranged from 0.46 to 1.5 mm and from 1.25 to 2.50 g/cm³, respectively (see Table 2.1 for details). In some experiments colored particle tracers were employed to follow individual particle motion. Different lighting was employed for each specific observation: for example, illumination from the rear with a light-diffusing sheet enabled one to observe the wake boundary and the individual vortex trajectory in the water-solid mixtures, while lighting from the oblique direction with a black background was scattered by hydrogen bubbles and/or the tracer particles giving the particle trajectories and thus velocities.

RESULTS AND DISCUSSION

A. Vortex Center Trajectories and Velocities

A vortex formed in the near wake of a rising bubble, which is a resultant of a free shear layer separated from an edge of the bubble

and rolled up into a spiral form, descends relative to the bubble and eventually leaves the near wake. In the following the descending trajectory and the descent velocity of the center of each vortex as well as the size and shape variations of an "apparent" vortex core are described.

Figure 3.2(a) depicts the trajectories of vortex centers being shed from a bubble rising in stationary water. The bubble whose size was 3.10 cm in breadth, b , rose rectilinearly with rocking and some shape dilations. In the figure the bubble is approximated by a circular cap which has the same size (breadth) and aspect ratio ($= h/b$) as those of the bubble of mean properties in two extreme orientations - the maximum and minimum angles of attack determined over the observed period. The angle of attack (α) is defined schematically in the figure. The vertical and horizontal distances from the bubble base center, x and y , are normalized with respect to b . As can be seen in the figure, some vortices followed the same type of trajectory, i.e., from a bubble edge to the wake central axis and then descending downward (shown in the figure through solid lines). This kind of vortex trajectory in the near wake thus may be characterized by an inverted isosceles triangle shape - asymmetric/alternate descent.

Some vortices, however, took different paths, i.e., two vortices, from the opposite sides, descended simultaneously rather than alternately (Vortex pairs 1-2 and 4-5 in Fig. 3.2(a)) - symmetric/parallel descent. This happened during the initial stable growth period and occasionally during the steady shedding period for

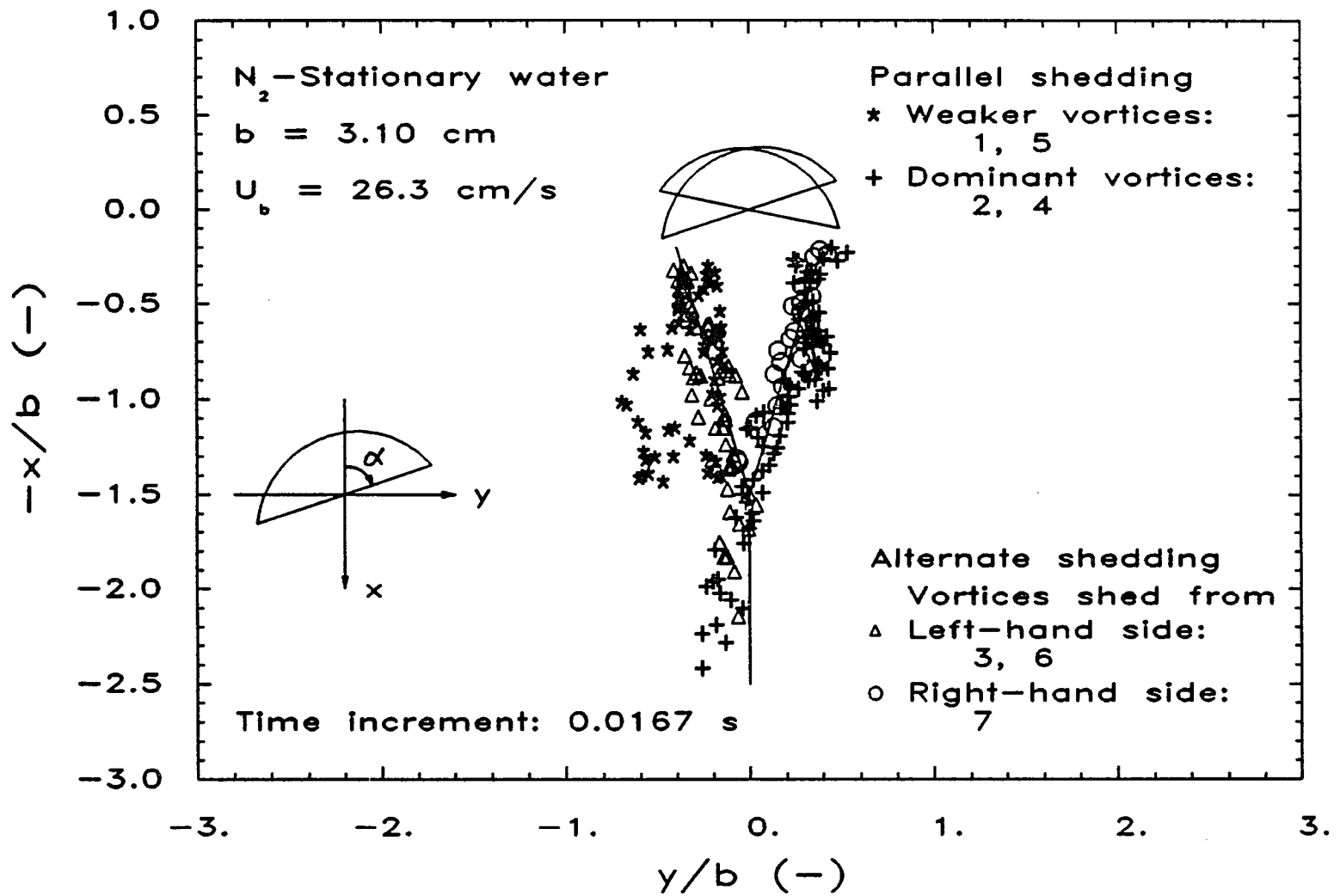


Figure 3.2a Vortex center trajectories behind a circular-cap bubble in stationary water.

the present size of (relatively large) bubble. Two vortices continued to descend in parallel until the symmetry of the wake flow was disturbed. When this happened, one vortex (Vortex 2 or 4) grew in size (thus in strength) faster than the other and had a strong impact on the trajectory of the weaker vortex. In contrast to the dominant vortex taking the same path as that in the alternate case, the weaker one was pushed away from the wake central axis. The interaction between these two vortices will be discussed later in terms of vortex size and shape.

Figure 3.2(b) gives the vortex center trajectories under a bubble of about the same size ($b = 2.89$ cm) in a water-1.5 mm acetate particle (AT1500, $\rho_s = 1.25$ g/cm³) fluidized medium. Note, since the flow field in liquid-solid systems is visualized using solid particles in the present study, the wake in the liquid-solid system, strictly speaking, refers to the wake of solid particles (solids wake). As shown in the figure, the locus of the vortex centers, or more specifically the centers of the circulating flow pattern of the solid particles, exhibited the same trends as that in stationary water. Vortex pair 1-2 during the steady growth period took the parallel path with Vortex 2 being the dominant vortex: during the steady shedding period the vortices were formed alternately and thus, they took the paths characterized by an inverted isosceles triangle shape. The height of the triangle was slightly shorter indicating the primary wake size in the liquid-solid system (solids wake) was a little smaller than that in the liquid system (liquid wake).

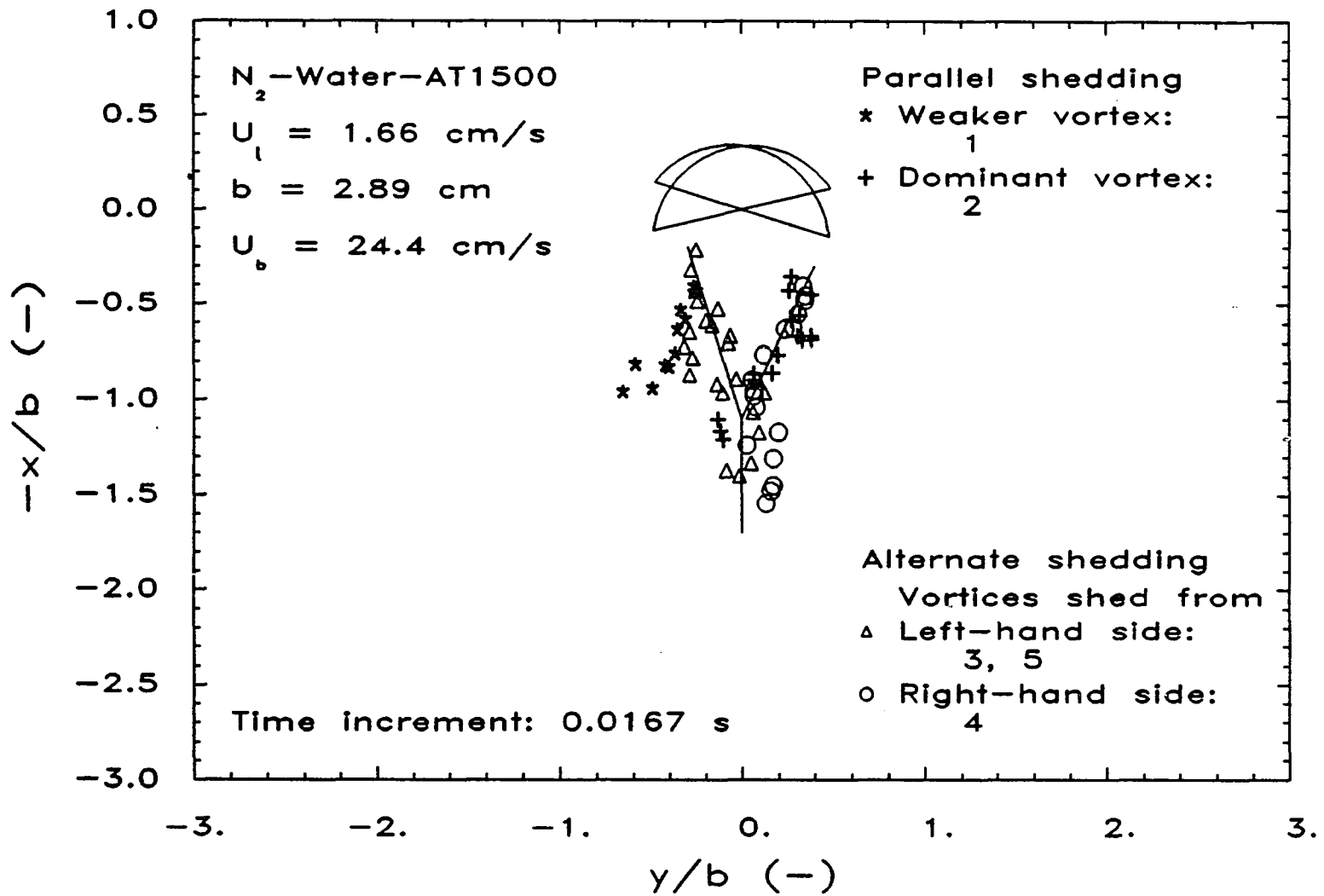


Figure 3.2b Vortex center trajectories behind a circular-cap bubble in a water-1.5 mm acetate particle fluidized medium.

Most vortices in the water-solid medium, however, lost their identity of having solids circulatory flow faster than the vortices in stationary water, once they were out of the primary wake. In other words, the vortices in the liquid-solid fluidized media have shorter "life" than those in the stationary liquid due to the more extensive external disturbances and/or the larger inertia of solid particles than that of liquid elements.

The descent velocity of the vortex center can be estimated from the relationship between the vertical downward distance travelled by the vortex (x/b) and time (t). Figures 3.3(a) and 3.3(b) show such a relationship for every vortex in the liquid and liquid-solid systems, respectively. The slope of each curve represents the descent velocity of each vortex center. As can be seen in the figures, before a vortex interacts with the external flow, the vortex descends at almost a constant velocity: the vortex within the primary wake is "protected" from the external disturbances. Note that the average height of the primary wake, h_{pw} , for each system is indicated in each figure. h_{pw} , defined schematically in Fig. 3.3(a), was obtained from the actual measurement of time-varying primary wake area and a certain geometrical assumption on the primary wake shape (see Chapter 2). Once the vortex goes out of the primary wake, however, it accelerates and eventually reaches the surrounding velocity, U_b . This happened, in the liquid system (Fig. 3.3(a)), when the normalized distance x/b was above 2. The descending velocity in the near wake is different from vortex to vortex. Nevertheless, it appears to have two specific values; large descending rate for the alternate descending mode and

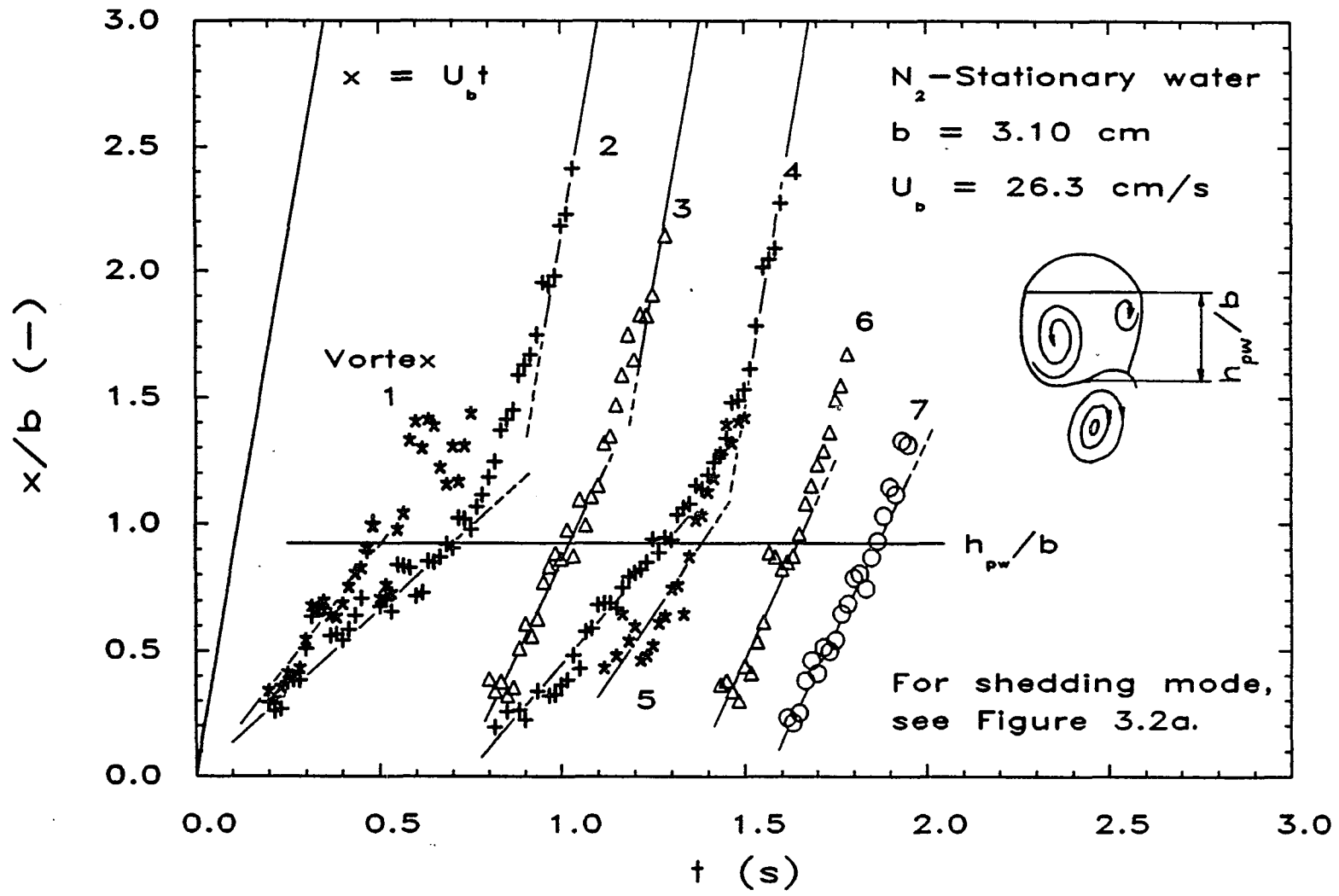


Figure 3.3a Time variation of vertical downward distance traveled by vortices in stationary water.

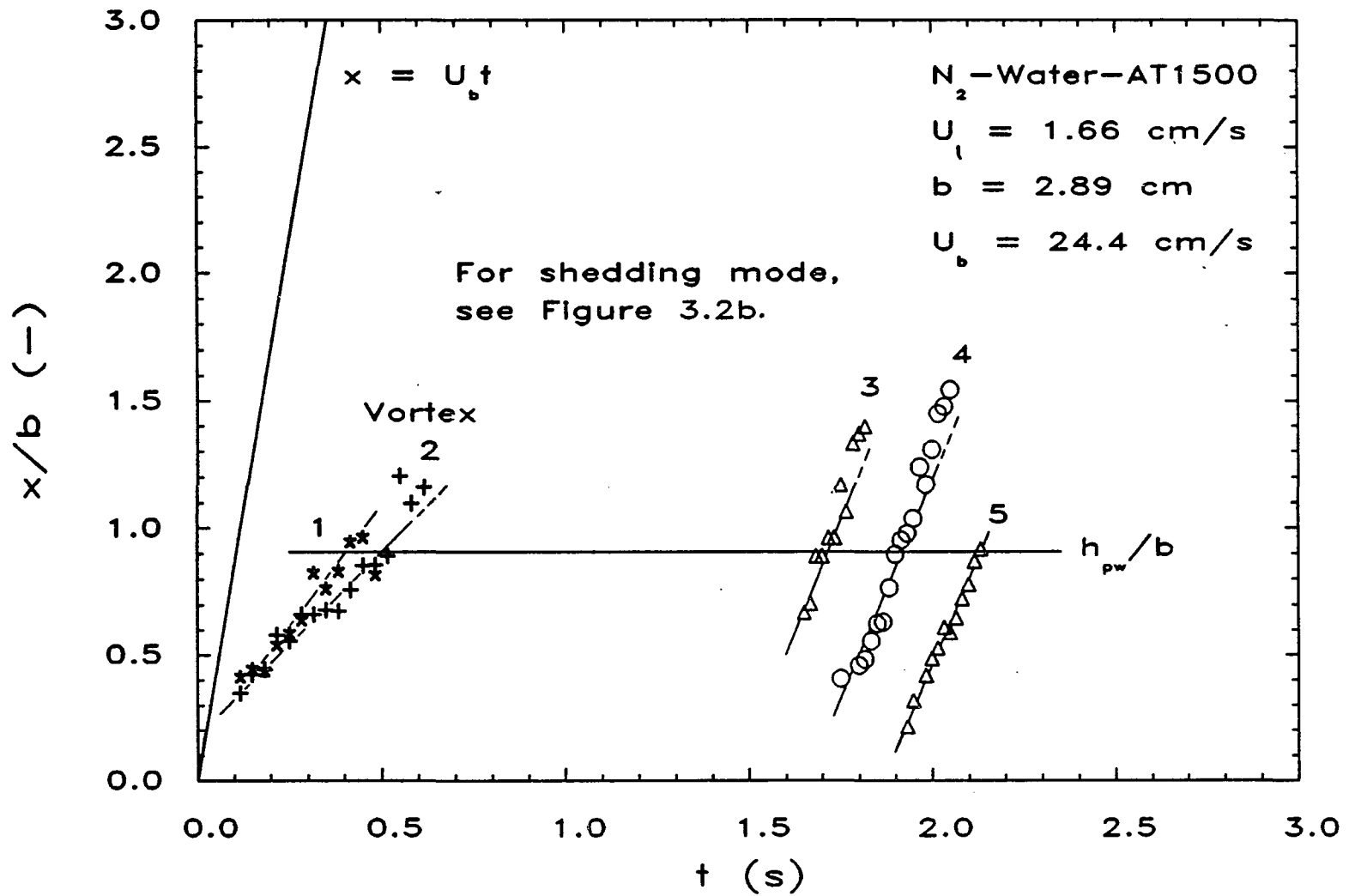


Figure 3.3b Time variation of vertical downward distance traveled by vortices in a water-1.5 mm acetate particle fluidized medium.

smaller rate for the parallel descending mode.

The vortex descending rate, estimated from the slope, in the primary wake was compared between the liquid and liquid-solid systems. For the asymmetric descending mode, each system gave almost the identical rate, $U_b - U_v = 8.6$ cm/s (Vortices 3, 6 and 7 in the liquid system; Vortices 3, 4 and 5 in the liquid-solid system). This indicates that large-scale vortex dynamics are similar between both systems and there is no appreciable particle effect on the vortex descending velocity.

B. Vortex Size and Shape Variations

In real fluids, a two-dimensional vortex has a finite-size core in which vorticity is concentrated and if the Reynolds number is sufficiently high, then it has almost uniform vorticity distribution inside. This vortex core varies its size with time due to viscous action and deforms under the non-viscous influence of the external flow field, or more specifically the presence of nearby vortices.

When a vortex resides in a uniform stream of infinite extent and is isolated from any other rotational flow fields, its rotational field can be represented by the Gaussian vorticity distribution:

$$\omega(r, \tau) = \frac{\Gamma}{4\pi\nu\tau} \exp\left(-\frac{r^2}{4\nu\tau}\right) \quad (3.1)$$

which is the exact solution for the viscous part of the vorticity transport equation:

$$\frac{D\omega}{D\tau} = \nu\nabla^2\omega \quad (3.2)$$

subject to the viscous decay of an axially symmetric vortex (Oseen, 1911; Ting and Tung, 1965). The corresponding velocity distribution around the vortex center is given by

$$u_{\theta}(r, \tau) = \frac{\Gamma}{2\pi r} \left[1 - \exp\left(-\frac{r^2}{4\nu\tau}\right) \right] \quad (3.3)$$

A graphical representation of this velocity distribution (e.g., see Schlichting, 1960) suggests that there is a circular region of finite area outside of which vorticity plays no significant role since $\omega \rightarrow 0$ (irrotational vortex flow) as r increases. The boundary between this circular region, or vortex core, and the surrounding irrotational region can only be defined vaguely because of continuous vorticity distribution given by eq. (3.1); however, noting that u_{θ} takes a maximum value at $r = r_v$, which gives the order of magnitude of the vortex core radius, we can obtain

$$r_v = 2.24\sqrt{\nu\tau} \quad (3.4)$$

Equation (3.4) is obtained by taking the derivative of eq. (3.3) with respect to r and setting it equal to zero. That is, the vortex diameter increases by viscous action in proportion to the square root of the time elapsed from its generation (τ).

Figures 3.4(a) and 3.4(b) give the variation of the normalized equivalent circular diameter of the vortex (d_v/b) with respect to the net time elapsed from the moment of generation of each vortex ($t - t_{v0}$) in the liquid and liquid-solid systems, respectively. The moment of vortex generation (t_{v0}) was estimated by extrapolating the time at

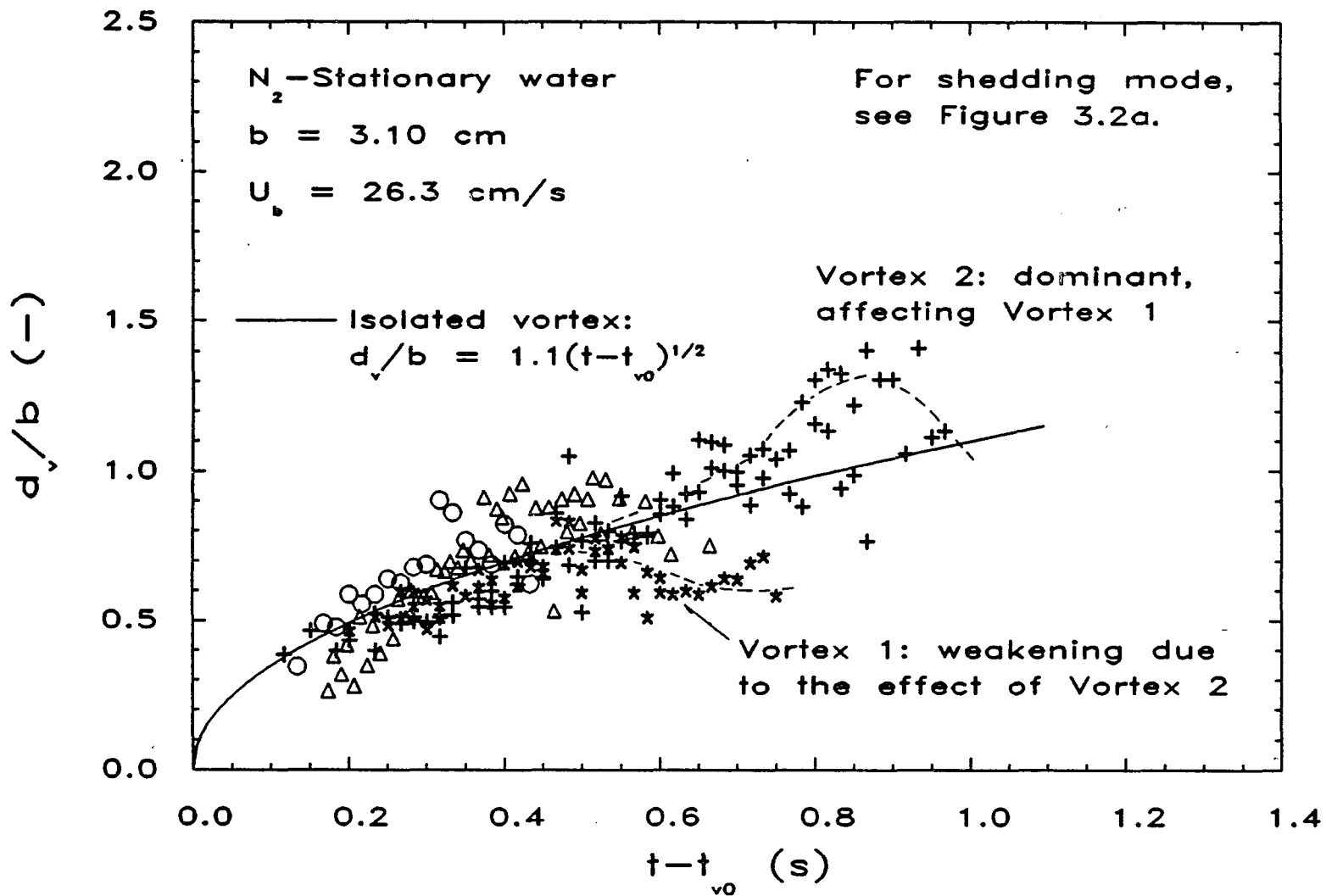


Figure 3.4a Time variation of equivalent circular diameter of vortices in stationary water.

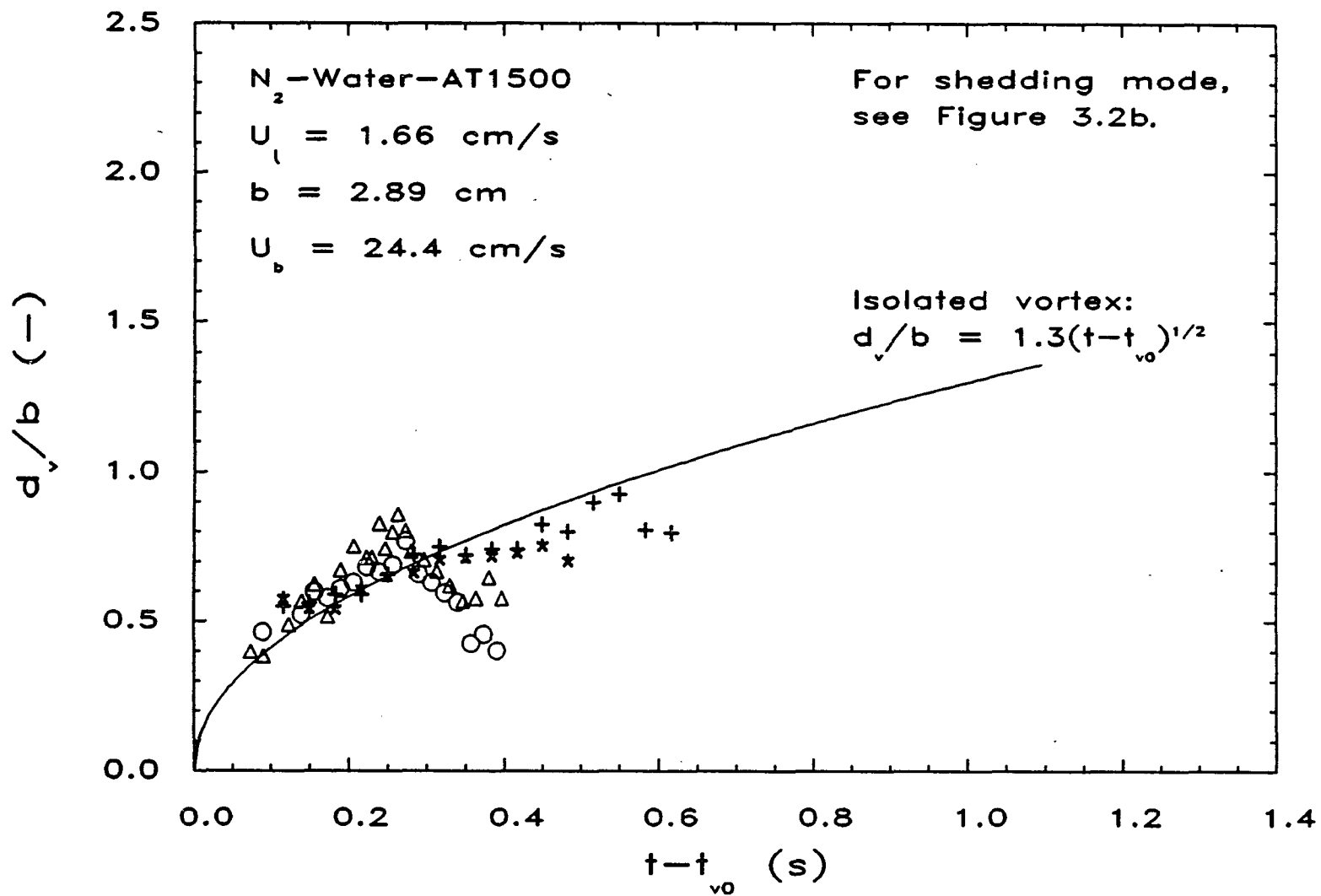


Figure 3.4b Time variation of equivalent circular diameter of vortices in a water-1.5 mm acetate particle fluidized medium.

which $x/b = 0$ for each vortex in Figs 3.3(a) and 3.3(b). The vortex diameter was evaluated from the actually measured vortex area, which was defined, in the present study, as an enclosure bounded by the outermost recognizable streamwise flow about the vortex center. Although thus evaluated vortex core size may not be accurate due to the experimental difficulties involved in the measurement - "the size of the vortex core is imponderable (Basset, 1888)" - it should reflect at least qualitative behavior of the vortex core size variation to be discussed in the following.

A theoretical curve for an isolated vortex core based on eq. (3.4) which fits the present data during the initial period is given by the solid line in each figure. Here only the qualitative relationship that $d_v \propto \sqrt{\tau}$ with τ being equivalent to $t-t_{v0}$ was employed: direct substitution of water kinematic viscosity $\nu = 0.01 \text{ cm}^2/\text{s}$ into eq. (3.4) gives $d_v = 0.45 \text{ cm}$ at $\tau = 1 \text{ s}$, which is one order of magnitude smaller than the present value. The present results in both systems followed a similar trend to this curve provided the vortex was in the primary wake, the corresponding $(t-t_{v0}) < 0.3-0.5 \text{ s}$ depending upon the type of vortex descending mode, and any strong vortex-vortex interaction was absent. When there was appreciable vortex-vortex interaction (Vortex pair 1-2 in the liquid system), the vortex size variation exhibited different trends. The dominant vortex increased its size faster than an isolated vortex outside the primary wake. The weaker vortex, on the other hand, actually decreased the size. The decrease in vortex size was observed eventually for all the vortices,

as shown in Figures 3.4(a) and 3.4(b), once the vortex interacts with the external, essentially irrotational flow of viscous nature for a sufficient period. This was particularly true in the liquid-solid system (see Vortices 3, 4 and 5 in Fig. 3.4(b)). The size decrease of the weaker vortex with strong vortex-vortex interaction, however, may be caused by an additional effect, destruction of vorticity due to the opposite-signed stronger vortical field. In some instances, vortices appeared to be completely annihilated (Vortex 1 in the liquid system).

The vortex-vortex interaction (this time, non-viscous, inertial effect) also induces the vortex shape deformation. Figures 3.5(a) and 5(b) show the vortex eccentricity (major axis length (d_{v1})/minor axis length (d_{v2}), also defined schematically in Fig. 3.5(a)) as a function of the vertical position (x/b). If the eccentricity is about unity, there is no vortex-vortex interaction. Some weak interactions are expected to exist if the eccentricity is in a range not so far from 1. This was the case when vortices were in the very near wake or descending alternately. Strong interactions occurred when two vortices descended in parallel: the eccentricity was as high as 3. It was observed that such a highly deformed vortex was sometimes torn into two small ones.

The variation of vortex eccentricity with respect to x/b in the course of vortex descent was also different between the two descending modes. The vortices in the alternate descending mode (with weak interactions) exhibited relatively constant eccentricity, for the distance between successive vortices was maintained above a limited

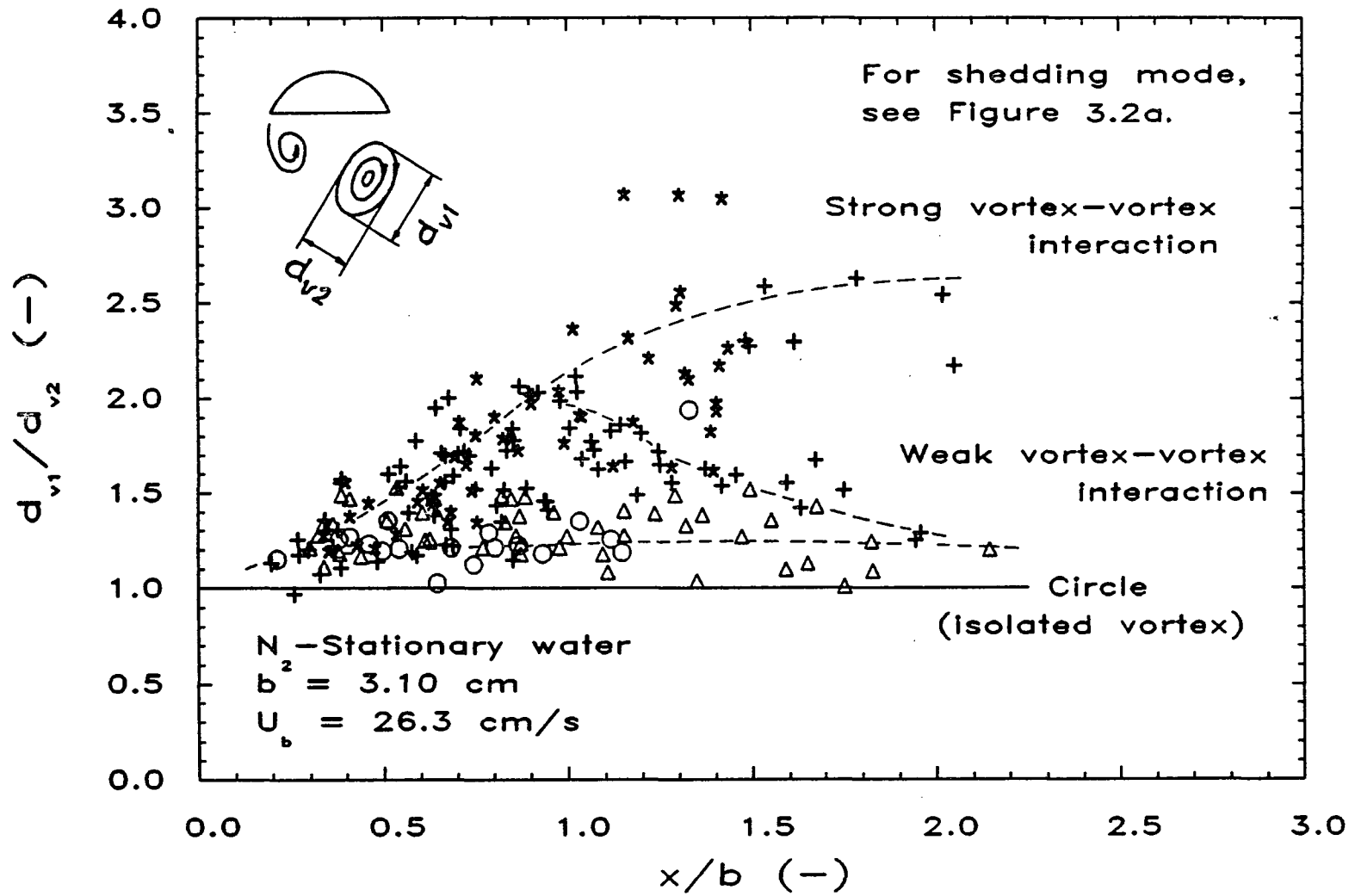


Figure 3.5a Positional variation of vortex eccentricity in stationary water.

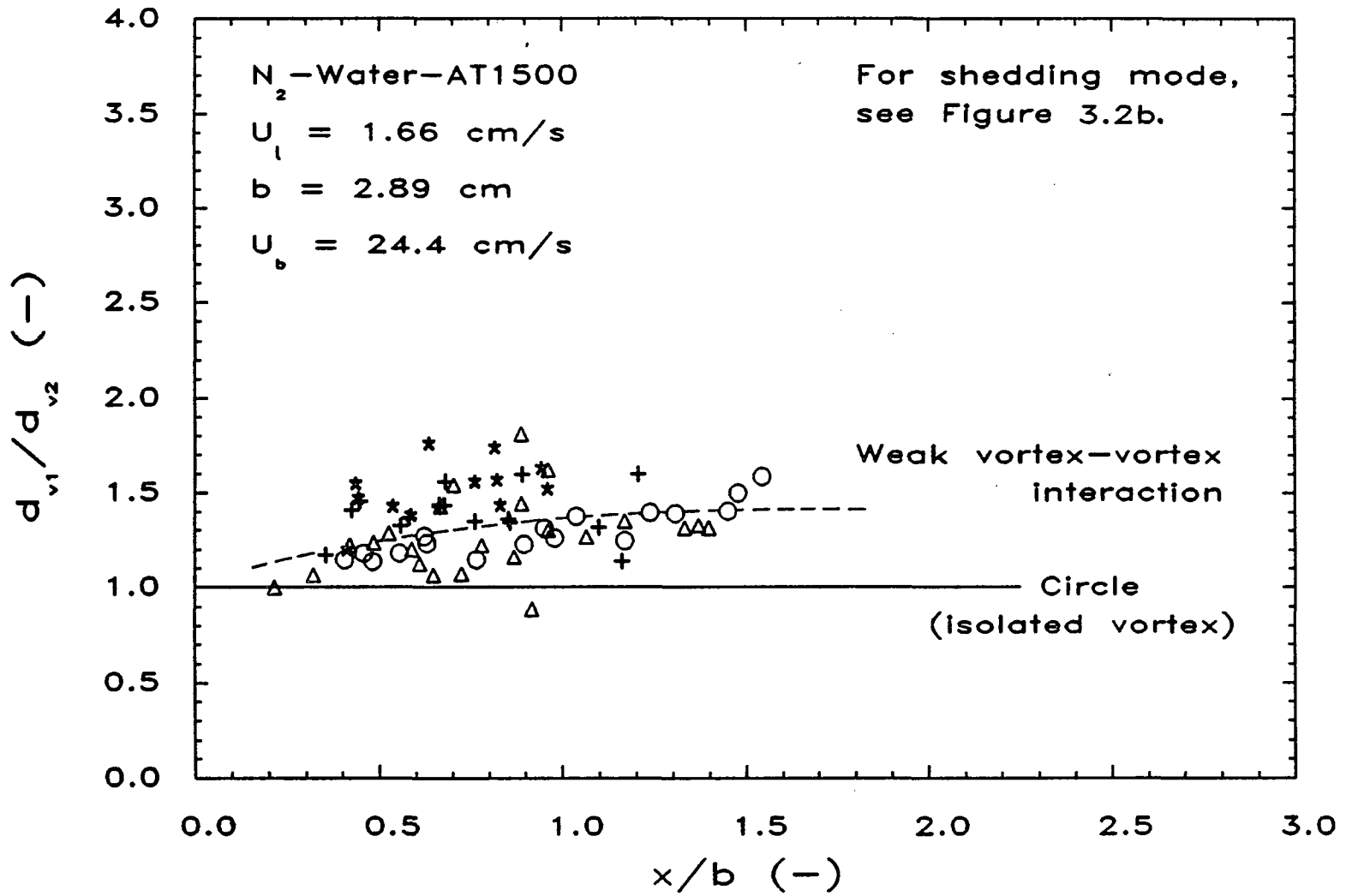


Figure 3.5b Positional variation of vortex eccentricity in a water-1.5 mm acetate particle fluidized medium.

value throughout their descent. The eccentricity of the vortices descending in parallel increased with x/b in general; however, the dominant vortex, when it lost its counterpart and took the same path followed by the alternate descending vortices (see Fig. 3.2(a)), gradually decreased its eccentricity to a value within the weak interaction range (Vortex 2 in the liquid system).

C. Liquid and Solid Particle Trajectories

The discussion, thus far, has been centered on the motion and geometric properties of the vortex core. In the following the large-scale vortical motion is described in terms of the motion of individual liquid elements in a liquid system or solid particles in a liquid-solid system around the near wake.

Figure 3.6 gives typical trajectories followed by liquid elements, traced by hydrogen bubbles, viewed from the bubble base center. Experimental conditions are identical to those in Fig. 3.2(a). Three different liquid elements were traced from the moment before they encounter the bubble roof till their leaving the near wake. Element 1 followed the stream just outside a free shear layer; thus, it actually never was trapped inside the near wake. Elements 2 and 3, on the other hand, flowed within a free shear layer and were trapped in the near wake. The paths taken by these liquid elements were extremely complex, influenced by successively descending vortices.

Nevertheless, a comprehensive analysis of these element trajectories can be made by decomposing the trajectory into $x/b-t$ and

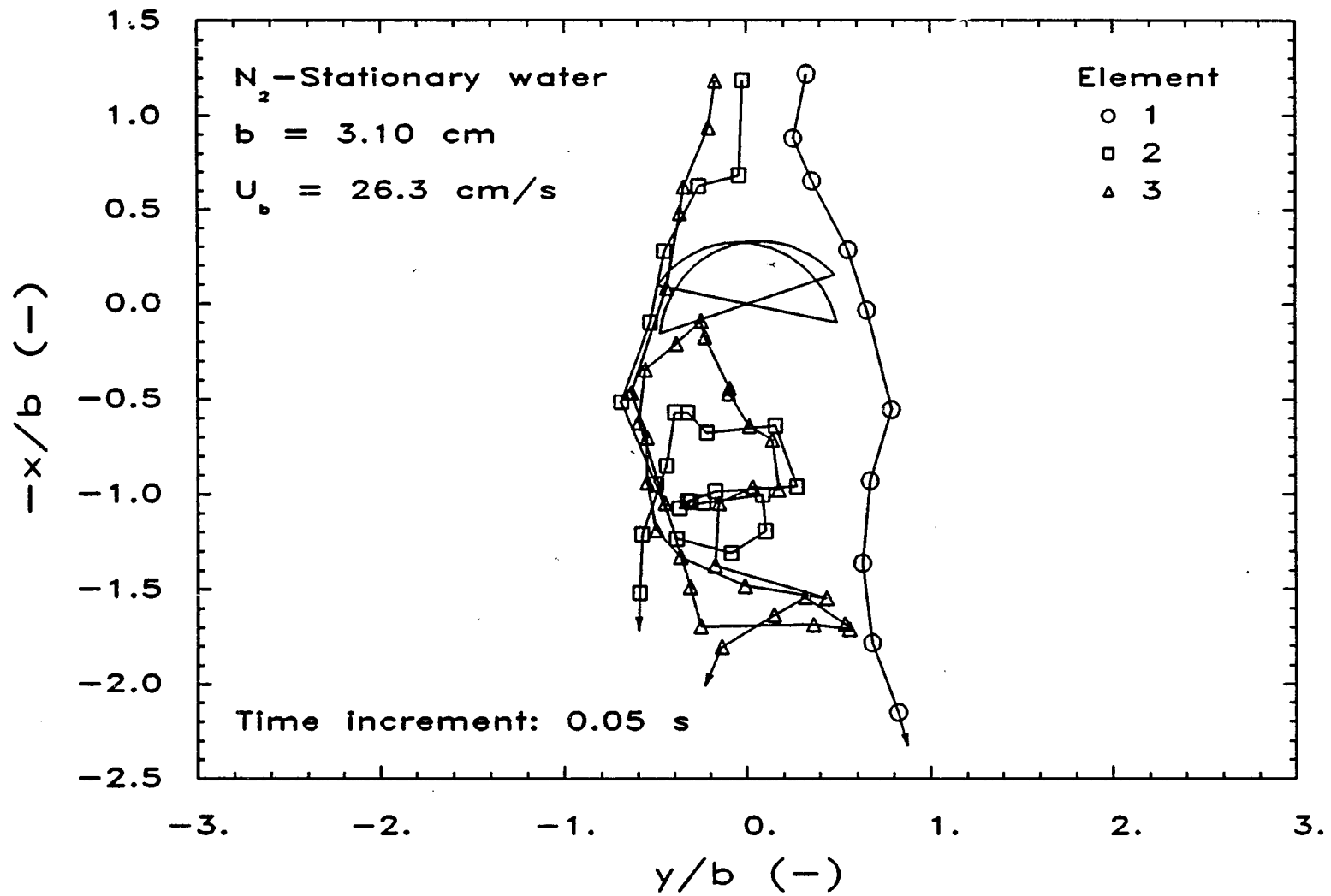


Figure 3.6 Liquid element trajectories viewed from bubble base center.

$y/b-t$ relationships. Figure 3.7 gives the former relationship. For Element 1, x/b increased nearly linearly with a slope very close to the average velocity of the external streams indicating no trapping into the wake. Elements 2 and 3, although initially followed the same trend, exhibited almost zero velocity periods. During these periods, the liquid elements had repeated the process of circling around a vortex center, escaping from it, and again circling about another vortex center until they completely left the near wake. Element 2 interacted with two successive vortices and Element 3 three vortices. Sometimes liquid elements were spouted very close to the bubble base by the vortical "thrust" (Element 3). The residence time of a liquid element in the primary wake thus can be roughly estimated from how many vortices the liquid element has interacted with and from the vortex shedding frequency.

The relationship between the lateral displacement (y/b) and t is shown in Fig. 3.8. When a liquid element is trapped in the wake, y/b varies on the positive and negative sides alternately as an approximately sinusoidal function of t . This is because the liquid element is influenced by a series of alternate vortices. If a liquid element is not trapped in the wake, on the other hand, the lateral displacement of the liquid element is similar to that caused by the drift effect, i.e., pushed away from the central axis and going back (although not completely to the original lateral location due to the presence of the far wake, or secondary wake).

As demonstrated above, the liquid elements within the primary wake undergo rapid changes in flow direction. In a liquid-solid

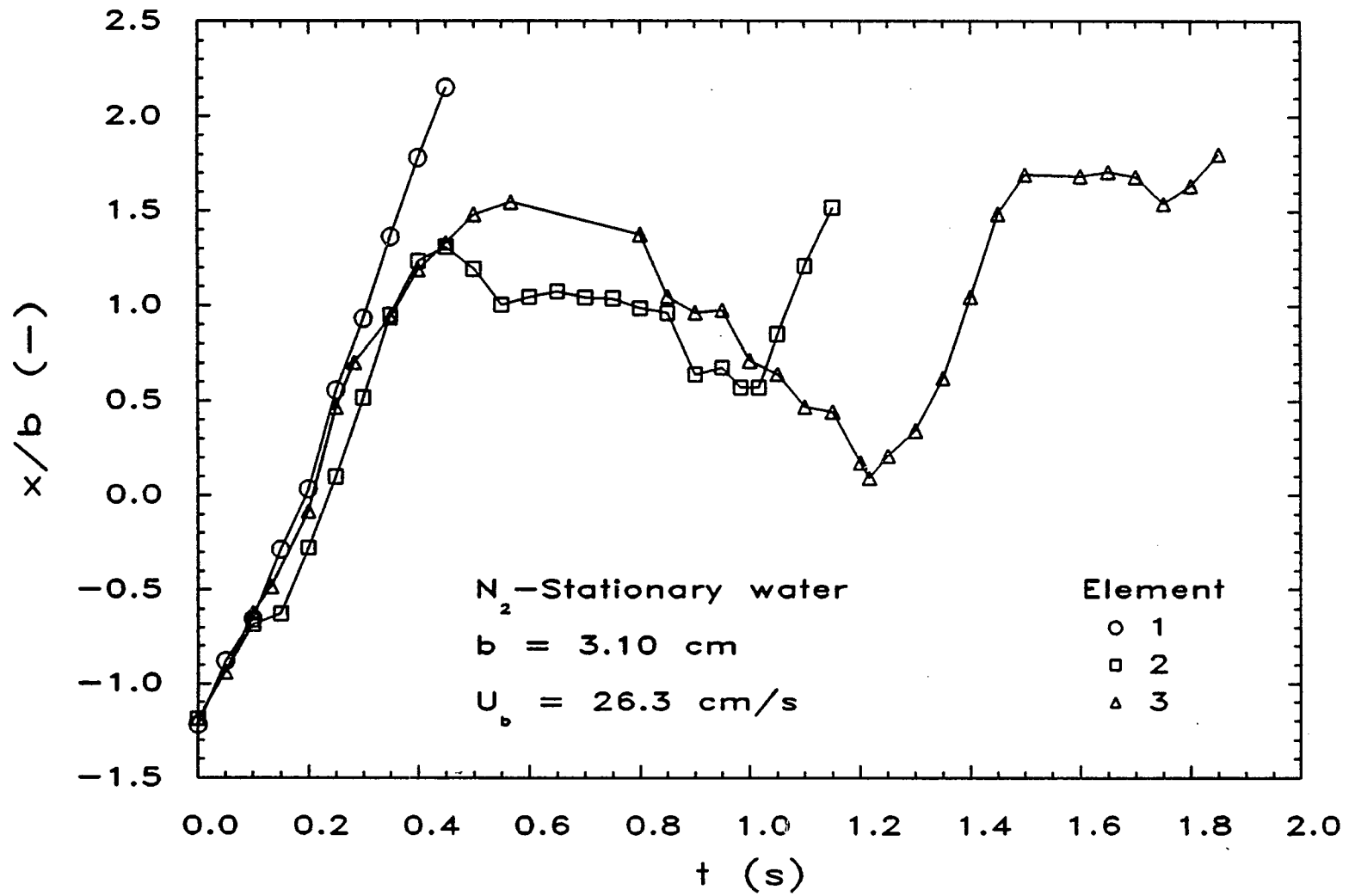


Figure 3.7 Time variation of vertical downward displacement of liquid elements.

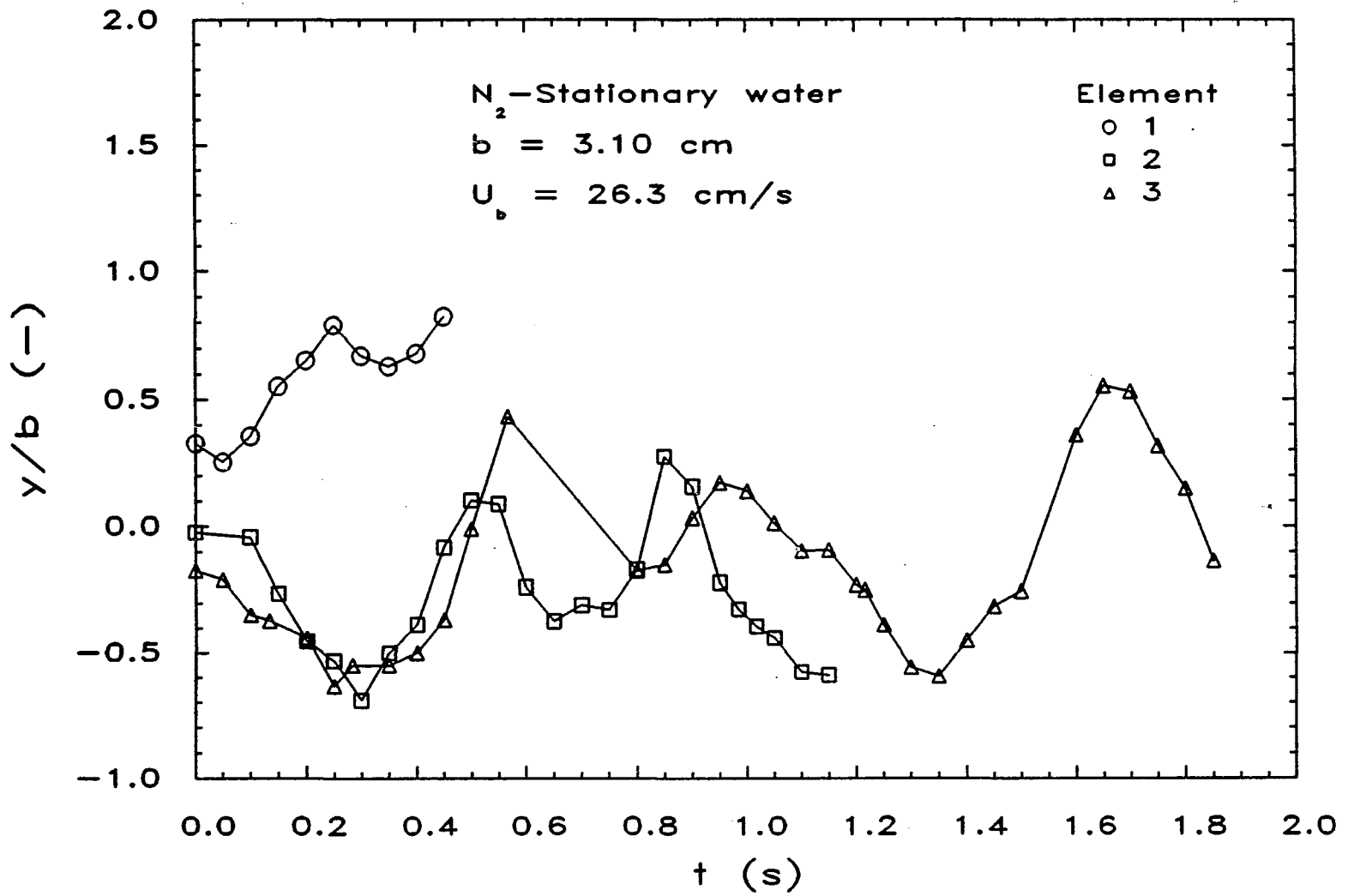


Figure 3.8 Time variation of lateral displacement of liquid elements.

system the vortical flow patterns also affects the solid particle motion, which is expected to deviate from the liquid flow path due to the larger inertia of solid particles. Figure 3.9 gives an example of a set of solid particle trajectories in a water-778 μm activated carbon particle (AC778, wet density of 1.509 g/cm^3) fluidized bed. Three types of trajectories were viewed from the bubble base center, as shown in Fig. 3.9(a). The bubble ($b = 4.04 \text{ cm}$) was of circular-cap shape and rose in a rectilinear path with slight rocking. Since vortices play an influential role in the particle flow patterns, the trajectory of the subject vortex center is also shown (crosses). Particles 1a and 1b were originally located in the external flow region and kept descending almost vertically without any appreciable influence from the vortex. Particle 2, however, was greatly affected by the presence of the vortex. This particle was trapped by the vortex and stayed momentarily stationary with respect to the bubble motion. It then moved down with the vortex. Particles 3a and 3b, originally located on the opposite side, continued descending until it was influenced by the induced circular flow due to the vortex which has already left the near wake and another vortex still in the near wake (left-hand side, not shown in the figure). Details of the particle flow patterns in the very near wake could not be clearly seen in this system due to the presence of particles flowing between the front wall of the two-dimensional bed and the bubble.

Figure 3.9(b) shows the trajectories of the same particles as those in Fig. 3.9(a) seen by an observer moving with the subject vortex center. The vortex center, represented by a cross, is fixed at

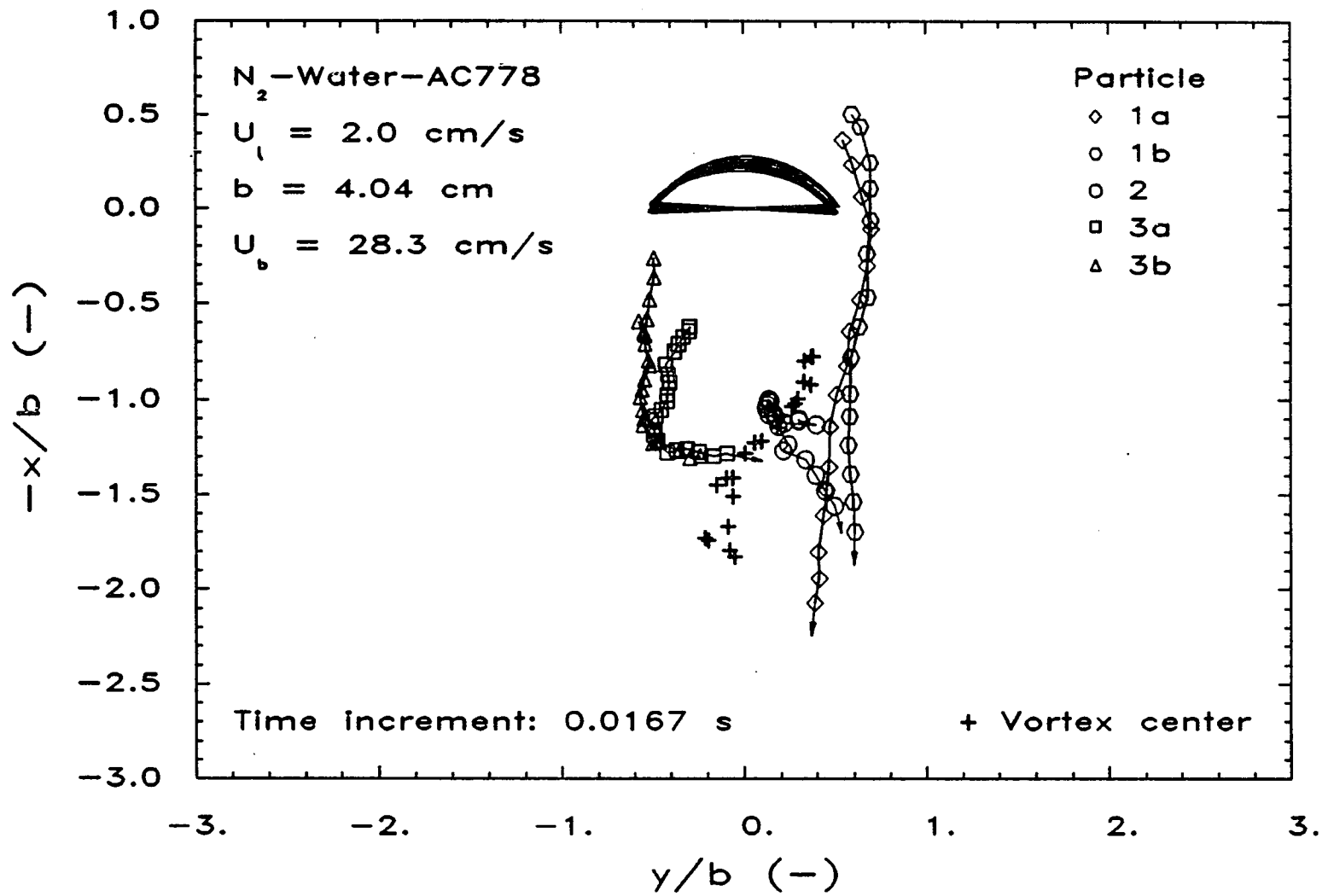


Figure 3.9a Solid particle trajectories: observer moving with bubble base center.

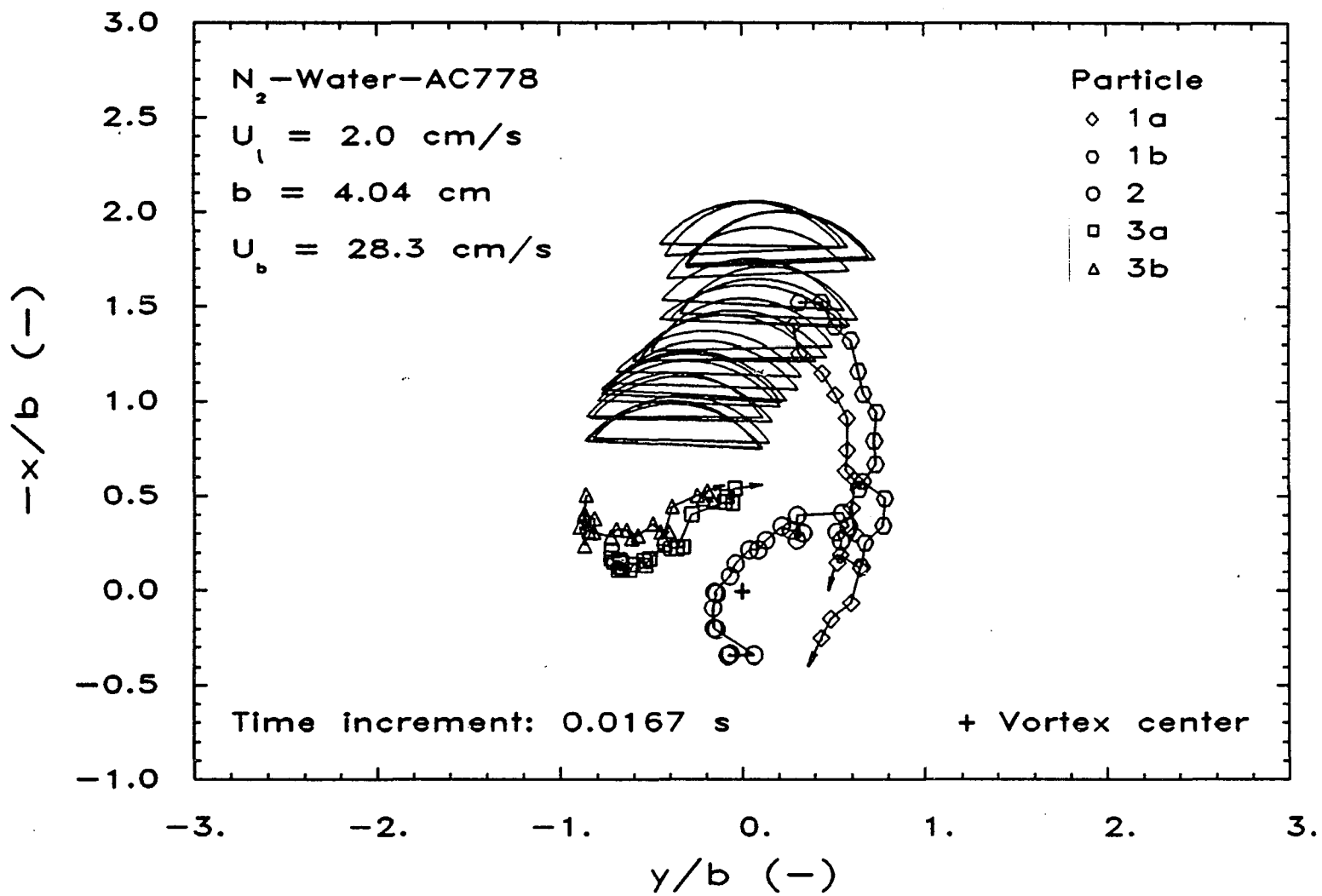


Figure 3.9b Solid particle trajectories: observer moving with vortex center.

the origin of the coordinates. In this frame of reference, the bubble appears to ascend relative to the vortex center. Note the circulating pattern of Particle 2 around the vortex center. It is also seen that this particle is being expelled from the vortical region partly due to the centrifugal force and partly due to the expanding nature of the vortex core by viscous action.

Because of their relatively small size and low density (terminal velocity less than 6 cm/s), activated carbon particles in Fig. 3.9(a) did not show distinct differences in trajectory from the liquid elements shown in Fig. 3.6. The deviation of the particle flow pattern from that of the liquid elements, however, was indirectly detected in particle concentration profiles when higher density particles were used. Figure 3.10 depicts regions of low particle concentration under a bubble rising in a water-774 μm glass bead (GB774, $\rho_g = 2.50 \text{ g/cm}^3$) fluidized bed. Immediately beneath the bubble base, a particle-free region (stable liquid layer) existed whose size and shape were almost invariant with respect to time for this large bubble ($b \approx 3.5 \text{ cm}$). Low solids concentration regions were also observed along the vortex sheets generated at the bubble edges. Note that this part of particle-free region seemed to stay near the vortex centers and continue descending. During the descent the size of the low concentration region kept expanding since the vortex core size increased with time and the solids concentration in this region kept increasing since the centrifugal force field weakened; eventually this region becomes indistinguishable from the liquid-solid fluidized region. The increasing core size and the weakening centrifugal force

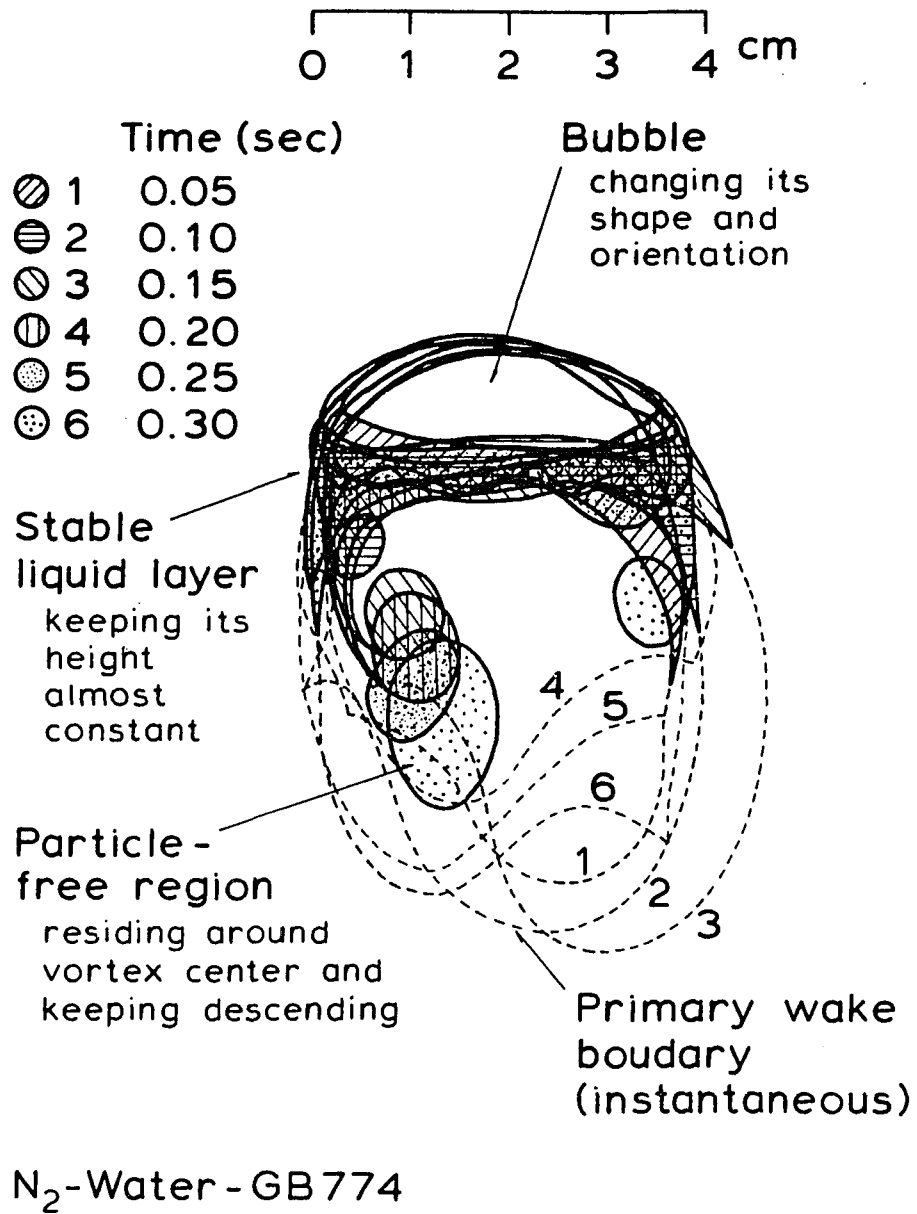


Figure 3.10 Sequential development of particle-free region.

are both due to viscous action as demonstrated by eqs (3.3) and (3.4).

D. Particle Velocity Profiles

Unlike the case of steady wakes, the velocity field in the unsteady wake flow is constantly subject to the transient variation due to wake shedding behavior. Thus, the particle velocity can only be represented at each instant during the course of its variation. In this study, instantaneous flow fields of solid particles around single bubbles were obtained using colored particle tracers for 778 μm activated carbon particles. Figure 3.11 shows a typical flow field represented by particle streaks which are the resultant of 1/60 s of exposure time in the video system. Experimental conditions are the same as those in Fig. 3.9. Since it takes 1/60 s to scan the whole screen in each field, there is a slight time lag between the top and bottom of the screen. Nevertheless, this is not significant as for the following analysis. A typical circulation pattern around Vortex 2 and a right-to-left cross flow of the external streams between Vortices 1 and 2 are noted in the figure. The cross flow divides the near/primary wake region from the far/secondary wake region. The regions of horizontal bands, designated by A and B, are specified to obtain the instantaneous velocity distributions of particles along the lateral coordinate. Region A covers the vortex center while Region B covers the cross flow region.

Figure 3.12(a) shows a plot of the vertical components of the instantaneous velocities versus the horizontal distance. The constant velocity region far from the bubble corresponds to the external flow

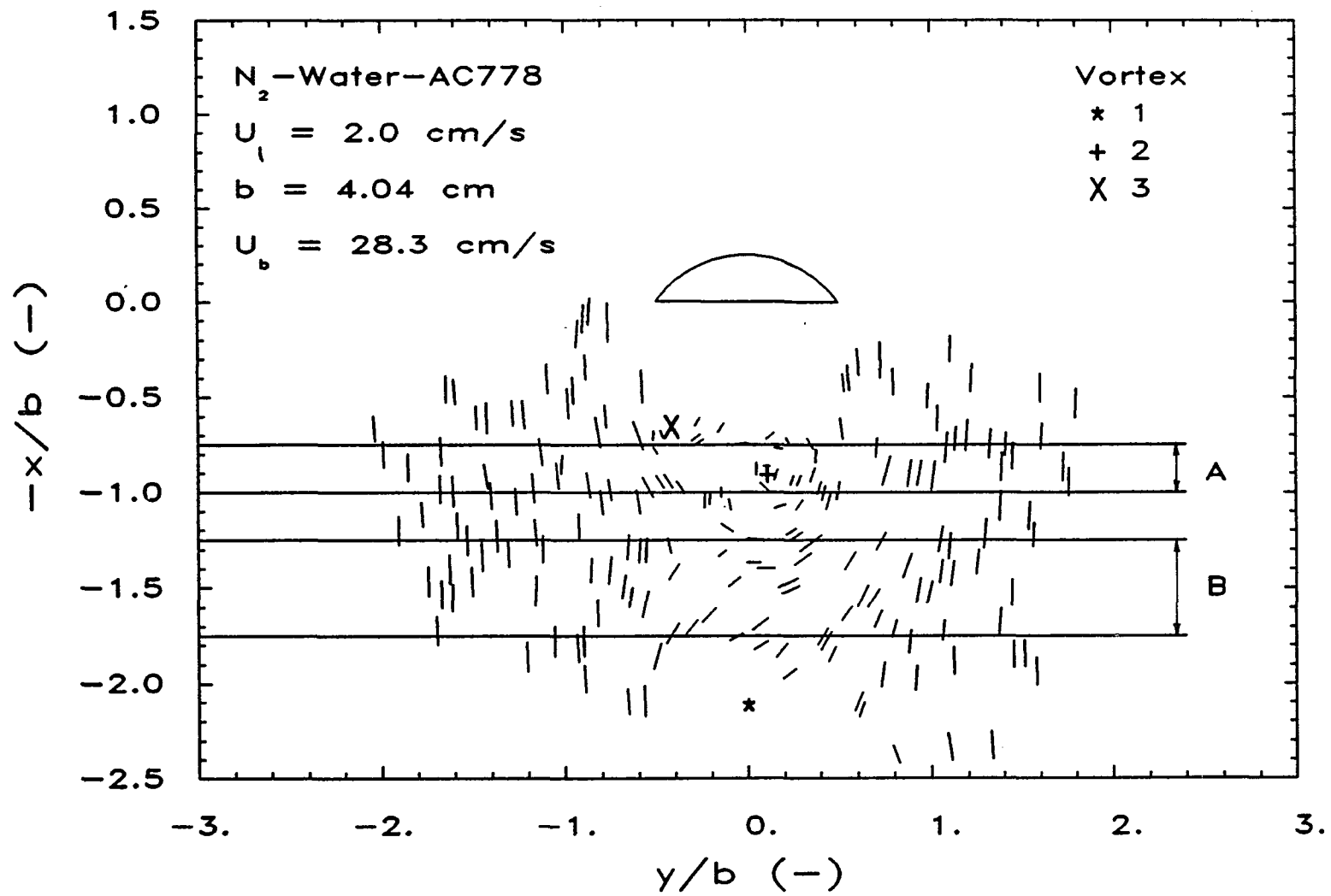


Figure 3.11 Instantaneous solids flow field expressed by particle streaks.

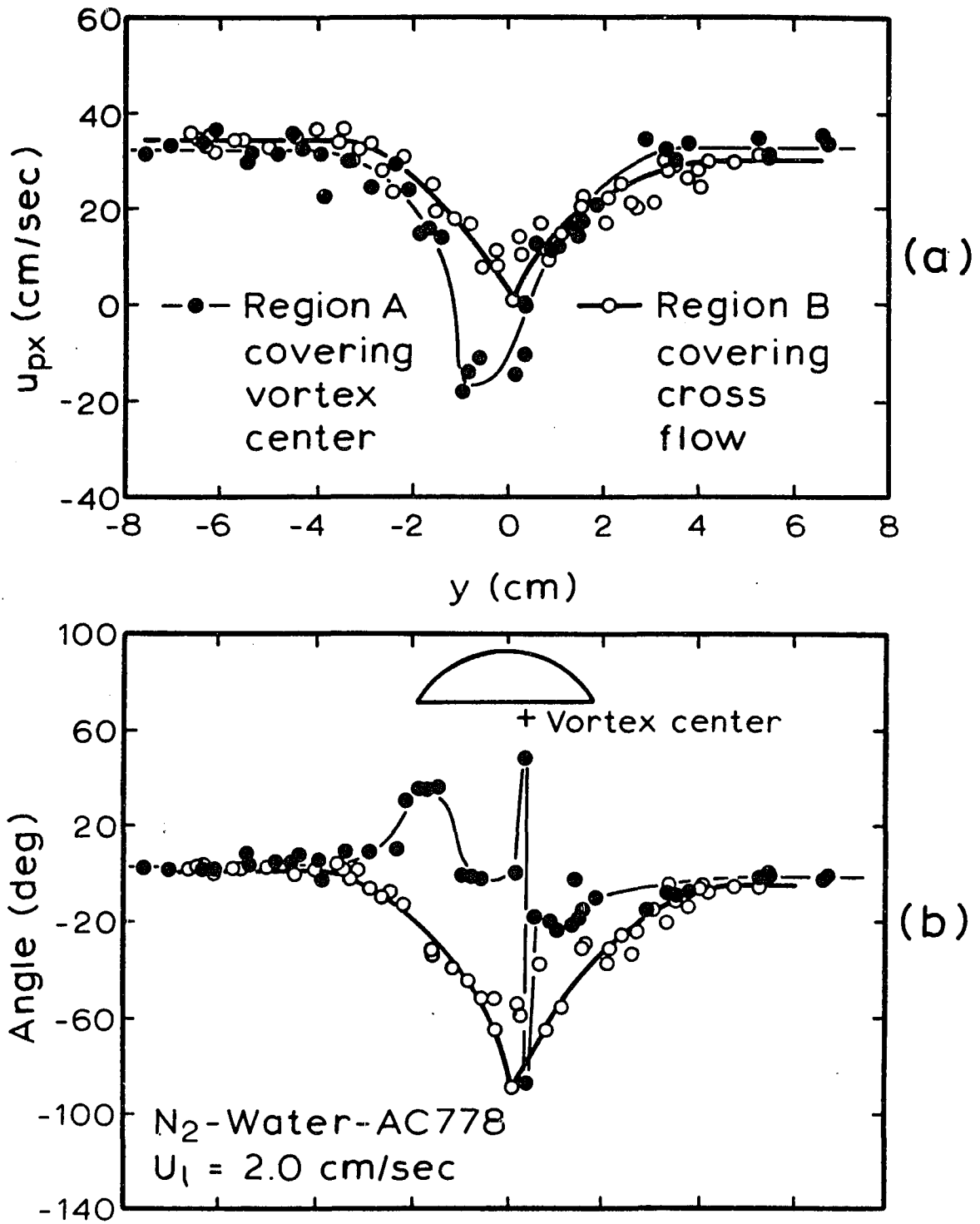


Figure 3.12 Instantaneous particle velocity profiles in the regions across the wake in terms of (a) vertical velocity component and (b) direction of velocity vector.

field, having about the same value as the absolute rise velocity of the bubble. The distinct feature in the distribution occurs between Regions A and B. The velocity distribution in Region A characterizes the rotational vortical motion, which is a typical distribution expected around the vortex center. On the other hand, the distribution in Region B is symmetric along the bubble center line, which characterizes the cross flow.

Figure 3.12(b) gives the angles of the velocity vectors whose tangent is defined as the ratio of the horizontal to vertical velocity component. For the flow field without a bubble, the angle is about zero degree. The disturbance caused by the rising bubble changes the direction of the local velocity vectors leading to the angle profiles shown in the figure. Note the symmetric angle distribution in Region B again showing the characteristic feature of the cross flow.

CONCLUDING REMARKS

The motion and geometric properties of vortices formed at the edges of relatively large, two-dimensional single gas bubbles have been found qualitatively similar in both stationary water and a water-solid fluidized medium when low-density solid particles are employed, although the vortex life was shorter in the liquid-solid fluidized medium than that in the liquid. Specifically, the vortices, descending relative to the bubble, followed a general trajectory in the near wake which can be characterized by an inverted isosceles triangle shape. The vortex descent velocity was found to be almost position invariant within the primary wake; however, once interacting with the

external flow, it gradually increased and eventually reached the external stream velocity relative to the bubble.

The vortex size, monotonically increasing with time in the absence of the vortex-vortex and/or external-to-vortex interactions, may decrease in the presence of these interactions outside the primary wake. The extent of size reduction was promoted by an opposite-signed stronger vortical field; the weaker vortex was sometimes totally annihilated. It was also severely promoted by the inertia of solid particles. The vortex-vortex interactions also caused the vortex shape deformation. In some instances, the interactions were strong enough to tear a very elongated weakening vortex into two small ones.

The motion of individual liquid or solid particles within the near wake was influenced by the successive vortices in such a manner that the particles would repeat the process of circling around and escaping from a vortex until they leave the near wake. The number of vortices with which a particle interacts is a key to determine the particle residence time in the primary wake.

CHAPTER 4

WAKE SIZE PREDICTION

ABSTRACT

A mechanistic model which interrelates the frequency of vortex shedding and the size of the bubble wake has been developed based on secondary motion of a single gas bubble rising in liquids and/or liquid-solid suspensions. In the model, the bubble and its primary wake were regarded as a single semi-rigid body steadily rocking at the vortex shedding frequency. All the necessary parameters appearing in the model equation, including bubble geometric parameters, the bubble rise velocity and the vortex shedding frequency, were expressed in terms of the bubble size to permit a priori prediction of the wake size. The predicted wake sizes were compared to the experimental values reported in the literature. Agreement was favorable over a wide range of the bubble Reynolds number considering the crude nature of the model against the complexity of the actual bubble-wake phenomena.

INTRODUCTION

In Chapter 2 it has been demonstrated that the wake flow behind a single gas bubble rising through a two-dimensional liquid-solid fluidized bed is a dynamic/cyclic phenomenon governed by vortex formation-shedding process. The primary wake, or near wake, was identified as an "effective" wake region which is responsible for various hydrodynamic phenomena such as bed contraction and solids mixing taking place in three-phase fluidized beds. Furthermore, it was inferred from the visual observations that such wake flow is dynamically steady and can be reasonably represented by the mean properties.

It is therefore extremely important to obtain quantitative information on the average wake properties such as the size of and solids holdup in the primary wake, which dictate wake "capacity," and the wake/vortex shedding frequency, which is a measure of wake instability. The wake size and/or solids holdup, however, is very difficult to directly measure under usual operating conditions due to unsteadiness of turbulent wakes (Henriksen and Ostergaard, 1974; Kojima et al., 1975; Kitano and Fan, 1987). The vortex shedding frequency, on the other hand, is relatively easy to determine if one is able to relate wake shedding to bubble behavior.

Theoretical evaluations of the vortex shedding frequency behind bluff objects in liquid streams have been attempted to some extent based on the observed motion of the wake behind a fixed circular cylinder (Birkhoff, 1953), far-wake configurations (vortex spacing)

together with wake (under)pressure (Birkhoff, 1953; Roshko, 1955), and the acoustic radiation of pressure pulses emitted from the cylinder (Torobin and Gauvin, 1959).

Birkhoff (1953) utilized the characteristic swinging of the wake to predict the order of magnitude of the observed Strouhal number. He adopted the theoretical lift force for a flat plate as an approximated cross-force acting on the wake. Based on Newton's second law applied to the transverse acceleration of the wake fluid, he obtained the expression:

$$Sr' = \frac{f_v' d}{U_o} = \frac{d}{2\sqrt{\pi} d_w h_w} \quad (4.1)$$

where f_v' is the shedding frequency of vortex pairs, U_o the mean stream velocity, d the cylinder diameter, and d_w and h_w the width and average length of the flapping portion of the wake, respectively. Using this relationship, one can roughly estimate the dimensions of the wake beneath a fixed object. Although the basic approach sounds promising, the direct application of Birkhoff's treatment to the bubble-wake motion does not seem feasible because the bubble itself moves transversely (see the following Physical Description section) contrary to the fixed cylinder.

In this regard, it is interesting to note a phenomenological theory, developed by Viets and Lee (1971), on the wandering motion of freely falling spheres. They claimed that a basic mechanism for the wandering is coupling between rocking of the spheres, which results from small displacements of their centers of gravity from their

geometric centers, and their motion perpendicular to the free fall direction. In the model, Viets and Lee approximated the lateral force acting on a sphere rocking in a uniform flow by that on a spinning sphere, the so-called Magnus effect, and regarded rocking as a gravity-driven pendulum motion.

The second approach based on the far-wake configurations has been most widely used, but is not directly relevant to the present study. The shedding frequency of vortex pairs expressed by

$$f_v' = \frac{U_o - U_v}{a} \quad (4.2)$$

requires the knowledge of the vortex velocity relative to the stream (U_v) and the distance between consecutive vortices on the same side of the body (a), or vice versa. These quantities, however, are in general specified when the wake is regarded as a pair of staggered parallel rows of periodic vortices, the so-called Karman vortex street, which recedes with a uniform speed away from the body, and thus are far-wake properties. Therefore, detailed information on the near wake cannot be incorporated in the theory.

In the third theory, vortex shedding is claimed to be caused by the resonant interaction between two acoustic vibrations, one of which is emitted from a separation point - a strong disturbance center - and the other from a shed vortex (Torobin and Gauvin, 1959). The frequency of acoustic pressure pulses traveling between the disturbance centers can be estimated from the distance along the cylinder surface and the speed of sound. The shed vortex, which continues to oscillate

at this frequency, will send back acoustic pulses to the still attached boundary layer at a frequency reduced, due to the Doppler effect, from the original frequency. The resulting resonant frequency leads to the expression:

$$Sr' = \frac{3}{4\pi} \left(1 - \frac{U_v}{U_o}\right) \quad (4.3)$$

for vortex pairs shed from the cylinder. When applying this theory to the case of a rising bubble, difficulties arise. The velocity fluctuations occurring about the disturbance centers, two strong ones at the separation points and a weak one at the front stagnation point, cause bubble shape oscillations, which introduce further complications. Besides, the vortex velocity U_v is again relevant to its definition: U_v varies with the downward distance from the bubble base and eventually approaches to zero far downstream (see Chapter 3).

In this chapter, the ideas presented by Birkhoff (1953) and Viets and Lee (1971) will be extended to secondary motion of a rising gas bubble and a mechanistic model to interrelate the vortex shedding frequency and the wake size is proposed. The model is based on the visual observation that the bubble, together with its primary wake, apparently experiences steady pendular motion, which in turn dictates the vortex shedding frequency. Experimentally obtained shedding frequencies, correlated in terms of the Strouhal number, in various systems (Lindt, 1971; Miyahara and Fan, 1987; Chapter 2) are employed to predict the size of the effective wake.

PHYSICAL DESCRIPTION AND MODELING

A. Motion of Single Bubble

A bubble rises vertically at a nearly constant velocity (terminal rise velocity) - primary motion. During its rise the bubble generates energy at a rate equal to its rise velocity times the buoyancy force acting on it. In a very viscous medium, this energy is completely balanced by energy dissipation due to viscosity (Bessler, 1984). In a low viscosity medium, however, the energy generated by the rising bubble may not be consumed by the viscous dissipation alone: some energy is utilized to generate an additional movement, bubble oscillations - secondary motion. This secondary motion is claimed to be attributed to the periodic shedding of vortices behind the bubble. Bubble oscillations are known to start with the onset of vortex shedding from the wake (Edge and Grant, 1971).

Secondary motion of the bubble, which has been observed over a wide range of bubble Reynolds number, is very complex. It can be any superimposition of two types of motion: (1) "rigid body" type vibration characterized by zig-zag or spiral trajectories and/or rocking and (2) "non-rigid body" deformation characterized by shape dilations or base oscillations (Clift et al., 1978; Bhaga and Weber, 1981). In the present analysis, however, it is assumed that the rigid body vibration is the major contribution to the determination of the vortex shedding frequency and thus, bubble shape oscillations can be neglected.

B. Rigid Body Vibration of a Bubble and Bubble-Wake

1. Physical description: Secondary motion of the first kind can be reasonably represented by a two-degrees-of-freedom oscillation consisting of lateral displacement and rotation of the bubble. Relative magnitudes of two distortions may depend on the size of bubble and the surrounding properties. For instance, small ellipsoidal bubbles in low viscosity liquids, showing helical or zig-zag motion, have both magnitudes being large: large spherical-cap bubbles have negligible lateral displacement but non-negligible rotation resulting in rocking motion. If the bubble is extremely large, however, both magnitudes are very small and only bubble base wobbling becomes important.

Careful observations in Chapters 2 and 3, however, revealed that not only the bubble but also its primary wake tends to oscillate at the same frequency as that of the bubble. This suggests that a region enclosing both a rising bubble and its primary, or "effective," wake can be treated as a single rigid body, or more loosely, "semi-rigid body," which shall be referred to as a "bubble-wake" in the present context. Despite their periodic variations at vortex shedding frequency (Chapter 2), the size and shape of the bubble-wake are assumed almost invariant with respect to time provided the time scale under consideration is relatively large (large enough to include several cycles of vortex formation-shedding process). The shape of the bubble-wake is prolate in general and may be characterized by a symmetrical Joukowski aerofoil shape (Batchelor, 1956; Bessler, 1984; Chapter 2) in an average sense. This leads to an important analogy

between the bubble-wake and an aerofoil in aerodynamics: an aerofoil placed in a uniform flow of air will move up and down and at the same time rotate about its own horizontal axis once the air speed exceeds a certain value (van Santen, 1953; Bishop, 1965). This type of vibration caused by self-excitation is known as a "coupled flutter."

The mechanism of flutter is more complicated than it appears to be. It originates from near-coincidence of the vortex shedding frequency with the natural frequency of a body. Periodic shedding of vortices alternately from each side of the body causes pressure fluctuations on the sides, and hence the rocking/rotational motion. In this sense, the rocking motion is apparently a resonant forced oscillation, at least initially; nevertheless, the motion is self-excited in that, once it has started, the motion in turn dictates the vortex shedding frequency (Bishop, 1965). It is known that by oscillating a bluff body transverse to the flow direction, the vortex shedding frequency can synchronize with a range of the frequency of the body oscillation (Williamson and Roshko, 1986). The rotation of the body generates an aerodynamic force, known as lift, which tends to displace the body laterally. This force exerted by the flowing fluid is in the same direction as the velocity of the body in its lateral movement, and if the velocity were to reverse, then the force would also reverse: the alternating force works as negative damping. That is, the fluid dynamic force in effect nullifies the damping of the vibrating system. Overall, flutter is regarded as a free vibration occurring at the natural frequency defined by the effective mass and stiffness of the system. Furthermore, the coupling of rotation and

lateral displacement is generally a one-way coupling, i.e., the rotation tends to change the displacement while a change of displacement will not affect the rotation.

Self-excitation is characterized by the extraction/dissipation of energy from an energy source which in this case is the flowing stream. The ratio of the energy input per cycle to the energy dissipated per cycle controls the damping mode. When this ratio is unity, it is possible for a steady oscillation to take place, neither growing nor diminishing. It has been observed that the bubble (thus bubble-wake) indeed exhibits this steady oscillation throughout its steady rise period. In particular, were the cause of self-excitation not dependent upon the amplitude of oscillation, the oscillation can be described mathematically by a set of linear differential equations with constant coefficients.

2. Bubble-wake pendulum model: When the bubble-wake is regarded as a compound pendulum of distributed mass, the zig-zag and/or rocking motion of the bubble can be simulated by a free vibration of the bubble-wake without damping based on the above physical argument. The following assumptions will be made towards a mathematical formulation:

(1) The bubble-wake has an axisymmetric shape about its central axis and consists of two parts: a gas bubble and an effective wake of a liquid and/or a liquid-solid mixture. The bubble may change its shape from a sphere to a spheroid to a spherical cap with increasing the bubble size, and its mass is negligible. The effective wake has

an arbitrary shape which can not be uniquely defined, but its specific gravity is assumed uniformly distributed.

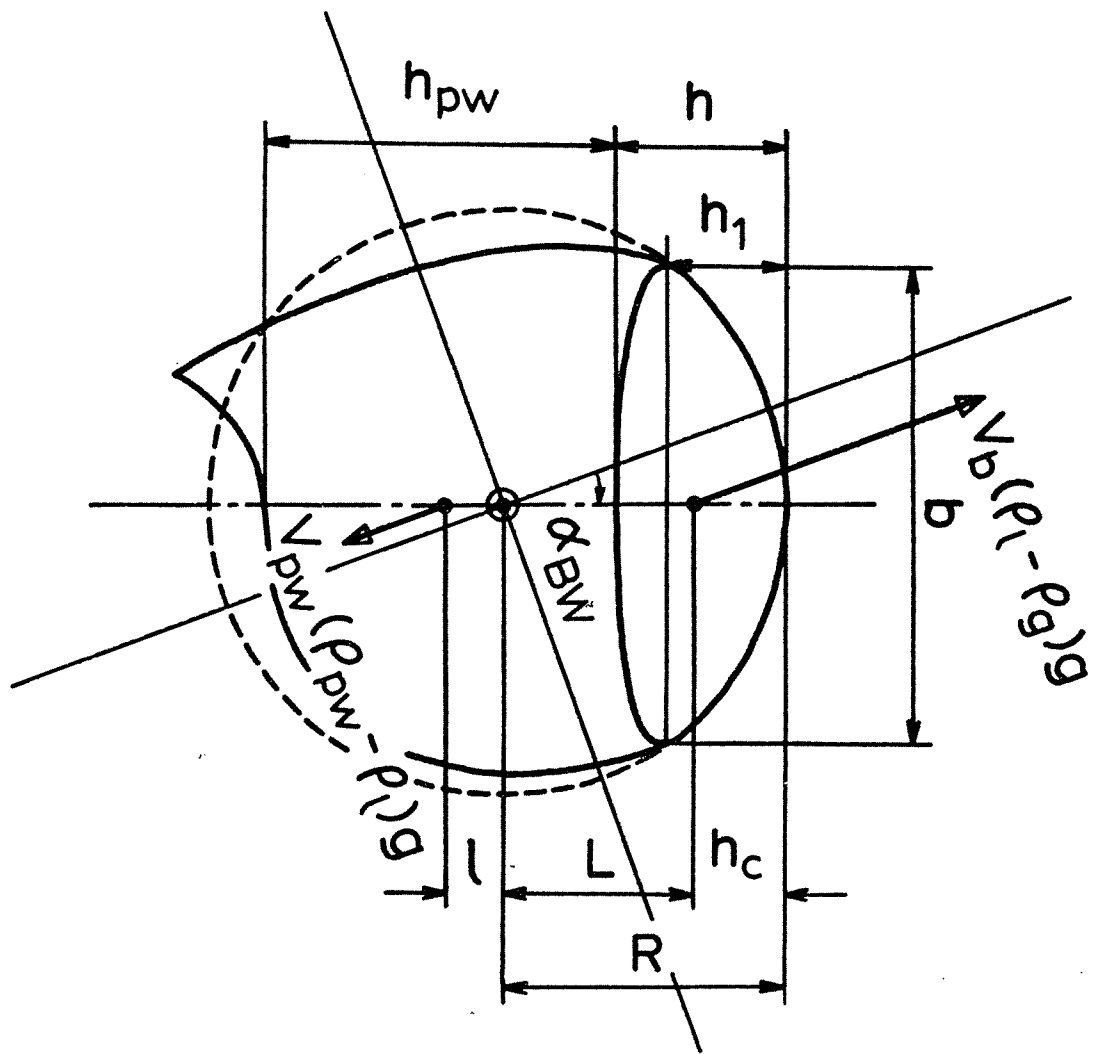
(2) The rocking motion is not affected by the disturbances caused by the bubble-wake motion, in particular, by the lateral displacement (refer to the one-way coupling discussed previously). Thus, the natural frequency of this vibrating system can be determined solely by the rocking of the bubble-wake.

(3) Based on the assumption (2), the center of rotation, or pivot, can be uniquely defined and fixed in space when the frame of reference is moving vertically with the bubble-wake. This was confirmed to be reasonable based on the visual observations made in a two-dimensional system in Chapter 2. The visual observations also suggested that the center of rotation locates around the center of an imaginary circle/sphere whose segments coincide with the frontal surface of the bubble at various phases of its rotation. Based on this finding, the location of the pivot is estimated from the average radius of curvature of the bubble roof.

(4) The bubble-wake motion, although it can be either a plane pendulum motion (corresponding to a zig-zag path of the bubble) or a gyration motion (corresponding to a spiral path), is effectively simulated by the former motion, i.e., a projected motion onto a two-dimensional field.

Figure 4.1 shows a schematic representation of the vibrating system. Since the mass is distributed over the body (two-part body), the system is a torsional vibrating system. Once the body has been deflected through an angle α_{BW} from the position of equilibrium,

Figure 4.1 Schematic representation of vibrating bubble-wake.



Newton's second law of motion can be applied to this torsional system to yield

$$I \frac{d^2 \alpha_{BW}}{dt^2} = T \quad (4.4)$$

where I and T are the mass moment of inertia and the restoring torque respectively about a horizontal axis passing through the pivot.

The restoring torque T can be evaluated through the collection of all the restoring forces acting on the bubble-wake. Doing this task, however, is extremely difficult since most fluid mechanic forces, such as the the force caused by the pressure difference between the primary wake and the external flow field, the pressure fluctuations due to shed vortices and the drag forces due to the external flow and/or the circulating flow around the shed vortices, are far from their quantitative evaluations. Fortunately, one can avoid this complication making use of the fact that the vibration is steady: that is, some forces, which excite the oscillation, work as negative damping, others act as positive damping, and thus both contributions, in effect, counterbalance each other. This leaves the buoyancy force as only the effective restoring force to maintain the steady vibration.

The effective buoyancy acting on the bubble-wake consists of two parts: one acting on the bubble and the other on the primary wake. The latter, however, is negligible because the density difference between the wake and the surrounding medium is in effect zero. Therefore, the restoring torque is approximated by

$$T \approx -V_b (\rho_l - \rho_g) g L \sin \alpha_{BW} \quad (4.5)$$

When the inclined angle α_{BW} (thus the oscillation) is small, $\sin \alpha_{BW} \approx \alpha_{BW}$ (error within $\pm 2\%$ if $|\alpha_{BW}| < 20^\circ$), which results in the differential equation (eq. (4.4)) becoming linear. For large α_{BW} , however, the equation is subject to an elliptic integration of the first kind. Physically speaking, it is more advantageous to expand $\sin \alpha_{BW}$ into an infinite series and to express T as

$$T = -V_b \rho_l g L \left(1 - \frac{\alpha_{BW}^2}{6}\right) \alpha_{BW} \quad (4.6)$$

retaining only the first two terms (note α_{BW} scarcely exceeds 45°). The form given by eq. (4.6) leads to what is known as a "soft" vibrating system which is characterized by a decrease in stiffness of the system with increasing the oscillation amplitude.

The total mass moment of inertia of the bubble-wake is the sum of that of the bubble and that of the primary wake, i.e.,

$$I = I_b + I_{pw} \quad (4.7)$$

where

$$I_b = V_b (\rho_g + C_A \rho_l) (\bar{r}_b^2 + L^2) \quad (4.7a)$$

$$I_{pw} = V_{pw} \rho_{pw} (\bar{r}_{pw}^2 + l^2) \quad (4.7b)$$

Since the bubble periodically accelerates and decelerates as its center of mass oscillates along a segment of a circle about the pivot, it is necessary to take into account the effect of an added mass of the surrounding medium on the bubble. C_A is the added mass coefficient and approximated (Clift et al., 1978) by

$$C_A = \frac{\sqrt{1-E^2} + \ln E - \ln(1+\sqrt{1-E^2})}{E^{-2}\sqrt{1-E^2} + \ln E - \ln(1+\sqrt{1-E^2})} \quad (4.8)$$

for a prolate spheroid moving along the circle segment where $E = h/b$, the bubble aspect ratio. No account is taken, on the other hand, of an added mass on the primary wake because of its negligible linear acceleration/deceleration. \bar{r}_b and \bar{r}_{pw} are the radii of gyration about horizontal axes passing through the centers of mass of the bubble and the primary wake, respectively. By assuming the geometry of each body, one can estimate the radius of gyration, which can be reasonably approximated, in the present study, by

$$\bar{r}_b = C_b (b^2 + h^2) \quad (4.9a)$$

$$\bar{r}_{pw} = C_{pw} (b^2 + h_{pw}^2) \quad (4.9b)$$

The coefficients C_b and C_{pw} depend on the geometry of the bubble and the primary wake, respectively. The distances from the pivot to the centers of gravity of the bubble and the primary wake, L and l , are given by

$$L = R - h_c \quad (4.10a)$$

$$l = |R - h - h_{pw}/2| \quad (4.10b)$$

Defining the volume ratio of the primary wake to the bubble and the density ratio of the primary wake to the surrounding medium as $k_{pw} = V_{pw}/V_b$ and $\gamma_{pw} = \rho_{pw}/\rho_f$, respectively, the moment of inertia of the vibrating system becomes

$$I = V_b \rho_f b^2 \left\{ C_A \left[C_b \left(1 + \left(\frac{h}{b} \right)^2 \right) + \left(\frac{R}{b} - \frac{h_c}{b} \right)^2 \right] \right.$$

$$+ k_{pw} \gamma_{pw} [C_{pw} (1 + (\frac{h_{pw}}{b})^2) + (\frac{R}{b} - \frac{h}{b} - \frac{h_{pw}}{2b})^2] \} \quad (4.11)$$

Replacing $(1 - \alpha_{BW}^2/6)$ in eq. (4.6) by $(1 - \bar{\alpha}_{BW}^2/6)$ with $\bar{\alpha}_{BW}$ being an average inclined angle, the oscillating system (eq. (4.4)) becomes linear as described by

$$\frac{d^2 \alpha_{BW}}{dt^2} + (2\pi f_{BW})^2 \alpha_{BW} = 0 \quad (4.12)$$

where f_{BW} is the natural frequency of the bubble-wake and given by

$$f_{BW} = \frac{1}{2\pi} \frac{\sqrt{-T/\alpha_{BW}}}{I} \quad (4.13)$$

where T and I are given by eqs (4.6) and (4.11), respectively. Assuming the frequency of the bubble-wake oscillation to be identical to the vortex shedding frequency (f_v'), the size of the primary wake can be estimated as a function of f_v' by solving the following equation for h_{pw}/b :

$$A_3 (h_{pw}/b)^3 + A_2 (h_{pw}/b)^2 + A_1 (h_{pw}/b) + A_0 = 0 \quad (4.14)$$

where

$$A_3 = K_{pw} \gamma_{pw} (1 + 4C_{pw}) \quad (4.14a)$$

$$A_2 = 4K_{pw} \gamma_{pw} (h/b - R/b) \quad (4.14b)$$

$$A_1 = 4K_{pw} \gamma_{pw} [C_{pw} + (h/b - R/b)^2] \quad (4.14c)$$

$$A_0 = (\frac{h}{b}) \{ 4C_A [C_b (1 + (\frac{h}{b})^2) + (\frac{h_c}{b} - \frac{R}{b})^2] + (\frac{1}{\pi f_v'})^2 (\frac{g}{b}) (\frac{h_c}{b} - \frac{R}{b}) (1 - \frac{\bar{\alpha}_{BW}^2}{6}) \} \quad (4.14d)$$

In the derivation the volume ratio of the primary wake to the bubble was related to h_{pw}/b as

$$k_{pw} = K_{pw} \frac{h_{pw}/b}{h/b} \quad (4.15)$$

with an appropriate assumption on the geometries of two bodies. For instance, K_{pw} becomes 1.5 for an ellipsoidal bubble and a cylindrical primary wake. The shedding frequency term in eq. (4.14d) can be replaced by the dimensionless groups, i.e.,

$$\frac{bf_v^2}{g} = Fr_b^2 Sr_b'^2 \quad (4.16)$$

where the Froude number and Strouhal number are defined as $Fr_b = U_b^2/gb$ and $Sr_b' = f_v'b/U_b$, respectively.

RESULTS AND DISCUSSION

A. Simulation Parameters

In order to predict the vortex shedding frequency or the primary wake size using eq. (4.13) or (4.14), it is necessary to evaluate, a priori, all the other parameters appearing in these equations. These parameters were expressed as a function of the bubble size, b , and are summarized in Table 4.1. The performance of these equations are demonstrated in Appendix B.

Bubble shape parameters such as aspect ratio (h/b), upper semi-height-to-breadth ratio (h_1/b) and equivalent diameter-to-breadth ratio (d_e/b) were correlated based on the data for nitrogen bubbles in two-dimensional water-solid mixtures ($d_p = 0.46-1.5$ mm, $\rho_g = 1.25-2.50$ g/cm³) employed in Chapters 2 and 3 and in three-dimensional water/water-solid media (Miyahara and Fan, 1987). In the correlations

Table 4.1. Relationships for Parameters Necessary to Evaluate Effective Wake Size (unit: cgs)

Bubble shape parameters

Aspect ratio (2D, 3D)

$$\frac{h}{b} = \begin{cases} 1 & 0 < b < b_c \\ 1 - 0.70[1 - \exp(-\frac{1-b/b_c}{2.7})] & b_c < b \end{cases} \quad (T4.1)$$

$$\frac{h_1}{b} = \begin{cases} 0.5 & 0 < b < b_c \\ 0.5 - 0.22[1 - \exp(-\frac{1-b/b_c}{2.3})] & b_c < b \end{cases} \quad (T4.2)$$

Equivalent diameter

$$\frac{d_e}{b} = \begin{cases} (h/b)^{1/2} & (2D) \\ (h/b)^{1/3} & (3D) \end{cases} \quad (T4.3)$$

Radius of rotation (2D, 3D)

$$\frac{R}{b} = \frac{0.125}{h_1/b} + \frac{h_1/b}{2} \quad (T4.4)$$

Center of gravity (2D, 3D)

$$\frac{h_c}{b} = \left(\frac{h_c}{h}\right)\left(\frac{h}{b}\right) \approx 0.5\left(\frac{h}{b}\right) \quad (T4.5)$$

Bubble rise velocity

$$U_b = \left(\frac{1}{U_1} + \frac{1}{U_2}\right)^{-1}$$

$$U_1 = d_e^2 \begin{cases} 544 & (2D) \\ 1560 & (3D) \end{cases} \quad U_2 = \frac{\sqrt{0.294}}{d_e} + d_e \begin{cases} 19.0 & (2D) \\ 20.9 & (3D) \end{cases} \quad (T4.6)$$

Coefficients for mass moment of inertia (3D)

$$C_b = 0.05 \quad (\text{Ellipsoid})$$

$$C_{pw} = 0.051 \quad (\text{Ellipsoid, cylinder, or paraboloid})$$

the critical bubble diameter (b_c), which is the maximum diameter for the bubble to be spherical, was fixed at 2 mm (Levich, 1962).

The radius of rotation (R) was approximated by the average frontal radius of curvature of the bubble and geometrically related to h_1/b . Since this parameter is a very critical one, the R estimated from this approximation was compared to the experimental values directly obtained from the visual observations made in the two-dimensional system in Chapter 2 and in the three-dimensional system (Miyahara and Fan, 1987). The comparison is shown in Fig. 4.2. Fair agreement was obtained indicating the validity of the assumption.

The coefficients for the mass moment of inertia (C_b , C_{pw}) were evaluated by assuming the geometries of the bubble and the primary wake. Based on the arguments presented by Kojima et al. (1975) and in Chapter 2, the bubble shape is reasonably approximated by either an ellipsoidal shape (3D) or elliptical shape (2D). The geometry of the primary wake is very difficult to define since no physical boundary actually exists and because of its unsteadiness in shape and size. An average value over three different geometries, i.e., cylinder, ellipsoid and paraboloid (3D), was employed as a representative value in the calculations.

The average inclined angle of the bubble-wake ($\bar{\alpha}_{BW}$) was set equal to zero in the simulation since it was less than 20° over the entire bubble size range studied (see Fig. A.5 noting that $\bar{\alpha}_{BW}$ is about half the maximum inclined angle).

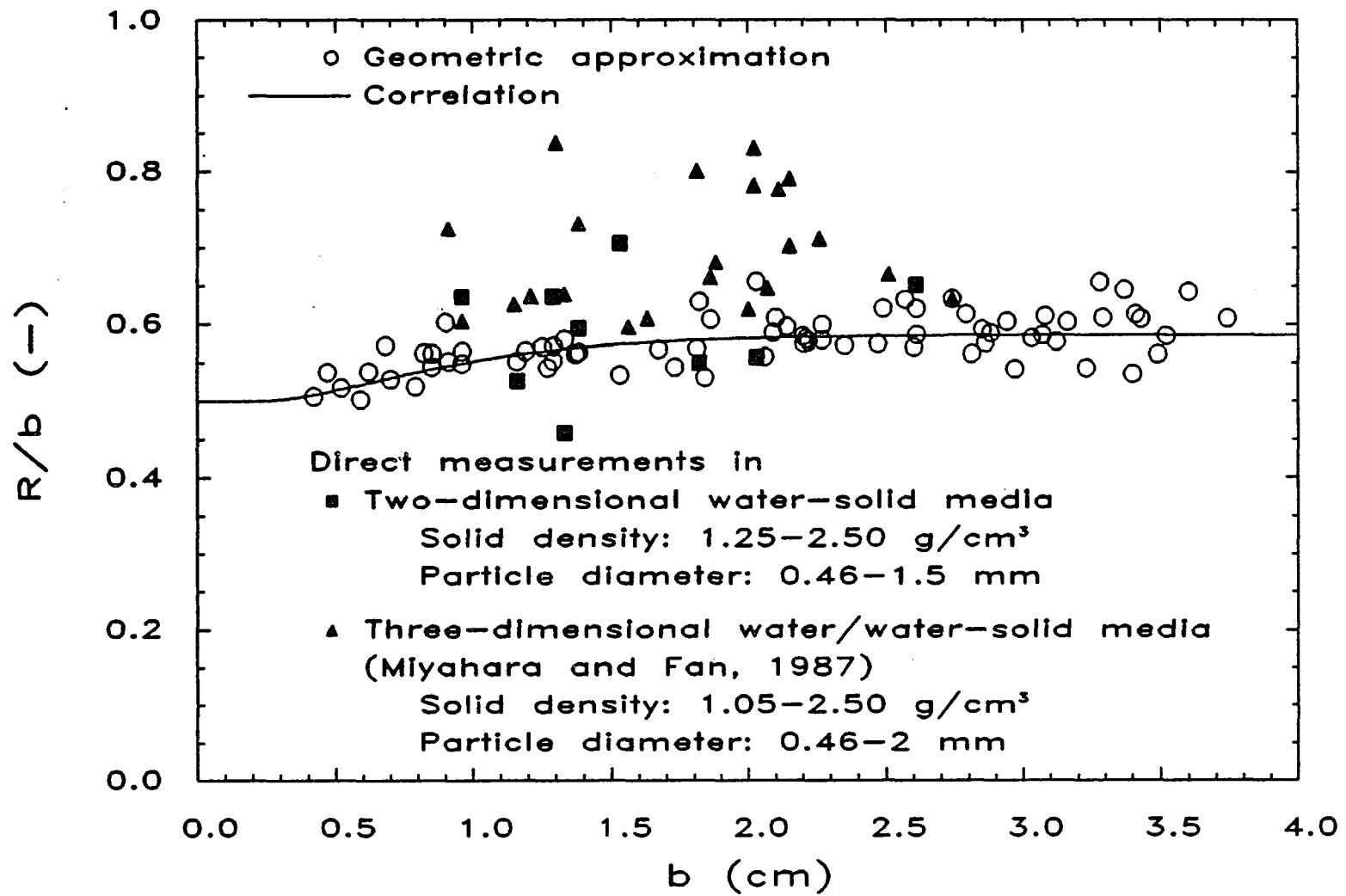


Figure 4.2 Radius of rotation of bubble-wake rocking correlated in terms of bubble size.

B. Effect of Wake Size on Vortex Shedding Frequency

Based on eq. (4.13) the frequency of alternate vortex shedding (f_v') can be estimated once the dimensions of the bubble and its primary wake are known. A comprehensive analysis revealed that, among the parameters, the size of the primary wake strongly affects f_v' . The primary wake size has been measured visually for unsteady wakes (Henriksen and Ostergaard, 1974; Kojima et al., 1975; Kitano and Fan, 1987; Miyahara and Fan, 1987; Chapter 2); however, it was found very difficult to determine due to its unsteadiness. The order of magnitude of the primary wake volume relative to the bubble volume (k_{pw}) ranged from 3 to 6 (corresponding $h_{pw}/b \approx 0.6-1.2$ based on eq. (4.15) with $K_{pw} = 1.5$) as an average. Although k_{pw} periodically fluctuated around the average value due to vortex shedding (see Chapter 2, Figs 9, 10 and 11), k_{pw} was almost constant with respect to or a moderate function of the bubble Reynolds number.

Determining the vortex shedding frequency, on the other hand, is less laborious provided the bubble rocking motion is distinct. This is because of the synchronization between the alternate vortex shedding frequency and the bubble rocking frequency as mentioned earlier. The alternate vortex shedding frequency is plotted against the bubble size in Figs 4.3(a) and 4.3(b) under various conditions, including both in the absence and presence of solid particles, in two- and three-dimensional systems, respectively. Figures 4.3(a) and 4.3(b) also show the predicted values based on eq. (4.13) with h_{pw}/b as a parameter (solid lines). The predicted f_v' falls in the same range as the experimental values using the experimentally obtained

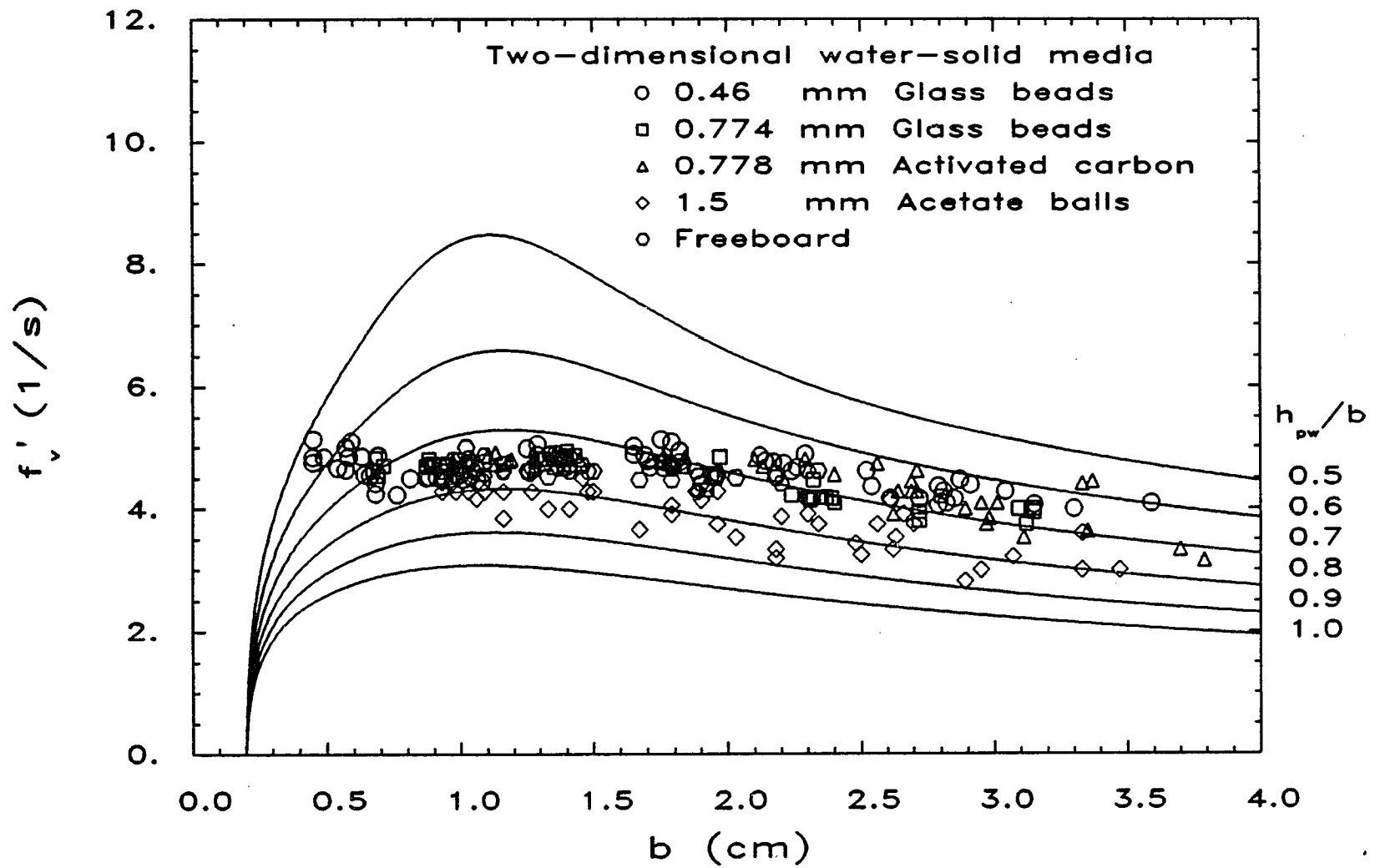


Figure 4.3a Effect of wake size on alternate vortex shedding frequency in two-dimensional water-solid fluidized media.

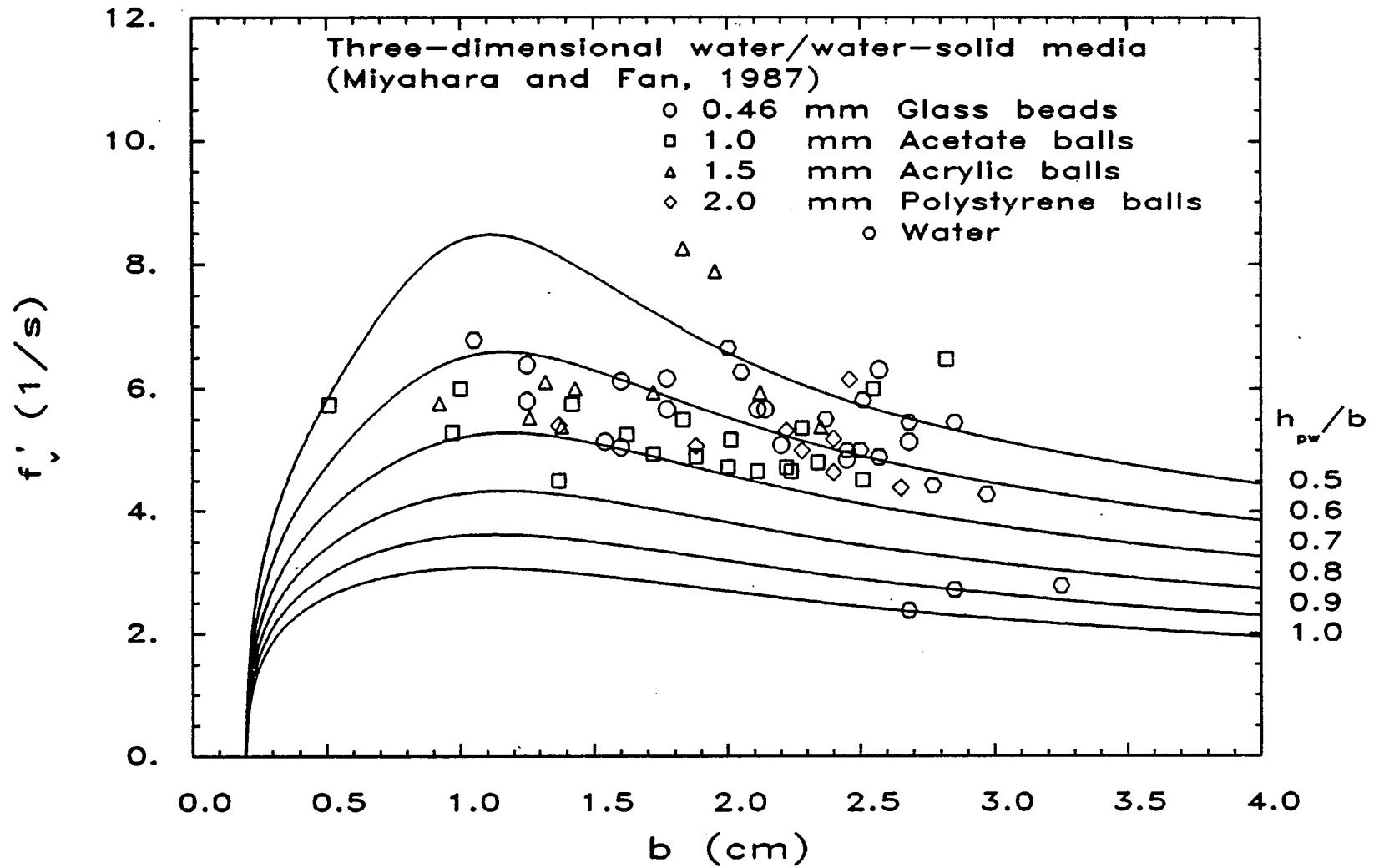


Figure 4.3b Effect of wake size on alternate vortex shedding frequency in three-dimensional water and water-solid media.

order of magnitude of h_{pw}/b . Furthermore, the model demonstrates the trend that f_v' increases with decreasing h_{pw}/b : the same trend was physically argued by Gerrard (1966).

C. Prediction of Wake Size from Vortex Shedding Frequency

As demonstrated in the previous section, f_v' is very sensitive to the wake dimensions which are usually very difficult to determine. Therefore, it is more reasonable to predict the wake size (h_{pw}/b or k_{pw}) from f_v' in order to test the performance of the model equation (eq. (4.13) or (4.14)). Figure 4.4 shows both the experimental k_{pw} obtained in Chapter 2 and the predicted k_{pw} from eq. (4.14). The figure also includes the experimental values reported by Miyahara and Fan (1987). In the calculation, eq. (4.14), a cubic equation, gave only one real, positive root for each bubble. The vortex shedding frequency was correlated in terms of the Strouhal number (Sr_b') with the bubble Reynolds number (Re_b) based on the experimental data obtained in two-dimensional systems. The correlations are given in the form:

$$Sr_b' = \frac{1}{A Re_b^{-B} + C} \quad (4.17)$$

where $A = 4840$, $B = 1.02$, $C = 1.55$ for stationary water (Lindt, 1971) and $A = 3200$, $B = 0.934$, $C = 2.22$ for water-solid fluidized media (Chapter 2), and resulted in two predicted curves (solid lines), Curve 1 and Curve 2 respectively, in the figure. Curve 2 predicted slightly lower values than Curve 1 due to probably greater wake instability

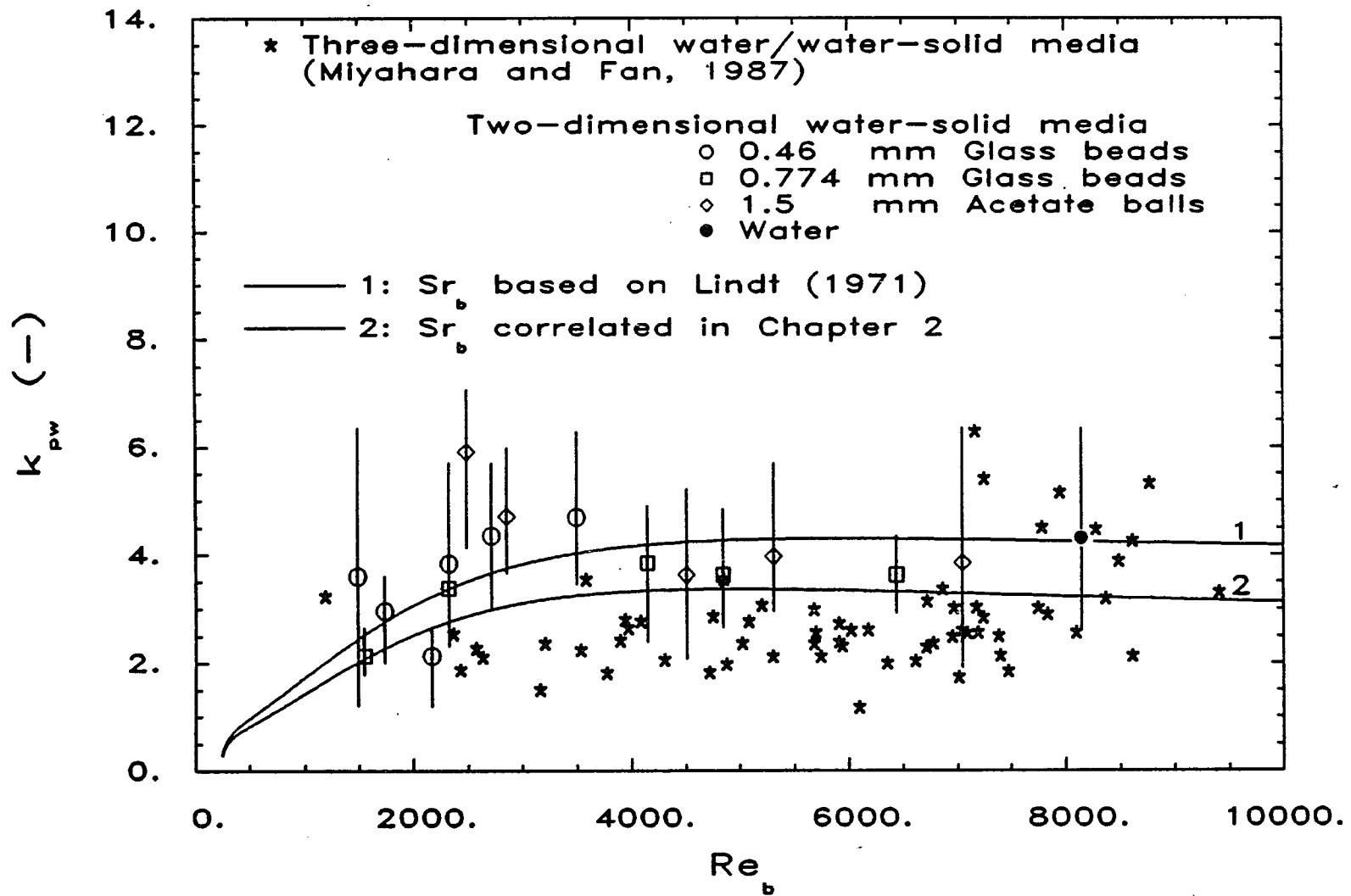


Figure 4.4 Prediction of wake size under various conditions.

induced by the external flow in the fluidized media. Most importantly, however, the two curves reasonably agreed with the experimental results indicating that the model equation (eq. (4.14)) can give a fair estimate of the order of magnitude of the primary wake size once the vortex shedding frequency is given.

A sensitivity analysis revealed that h_{pw}/b is most sensitive to the value of C_{pw} besides f_v' . As indicated earlier, the actual primary wake periodically changes its shape, especially its "waving tail" portion, as well as its size; nevertheless, a perfect stiffness of the bubble-wake was assumed in the calculation. This "rigid body" assumption thus may lead to some error in the prediction. If an elastic nature of the primary wake is introduced into the evaluation of C_{pw} , C_{pw} for the actual flexible primary wake should become somewhat lower than that for a rigid primary wake. Taking this into account, predicted h_{pw}/b is now plotted with C_{pw} as a parameter in Fig. 4.5. As can be seen in the figure, the introduction of primary wake elasticity (i.e., the reduction of effective moment of inertia of the primary wake) improved the model prediction performance.

The bubble size considered in the above analyses ranged from intermediate ($b = 0.4$ cm) to moderately large ($b = 4$ cm) size. It is known that if the bubble size becomes extremely large, however, zig-zag or rocking motion becomes less distinct and the vortex shedding frequency may not be determined uniquely for each bubble size (see Chapter 2). This could be a limitation of the present rigid-body pendulum model.

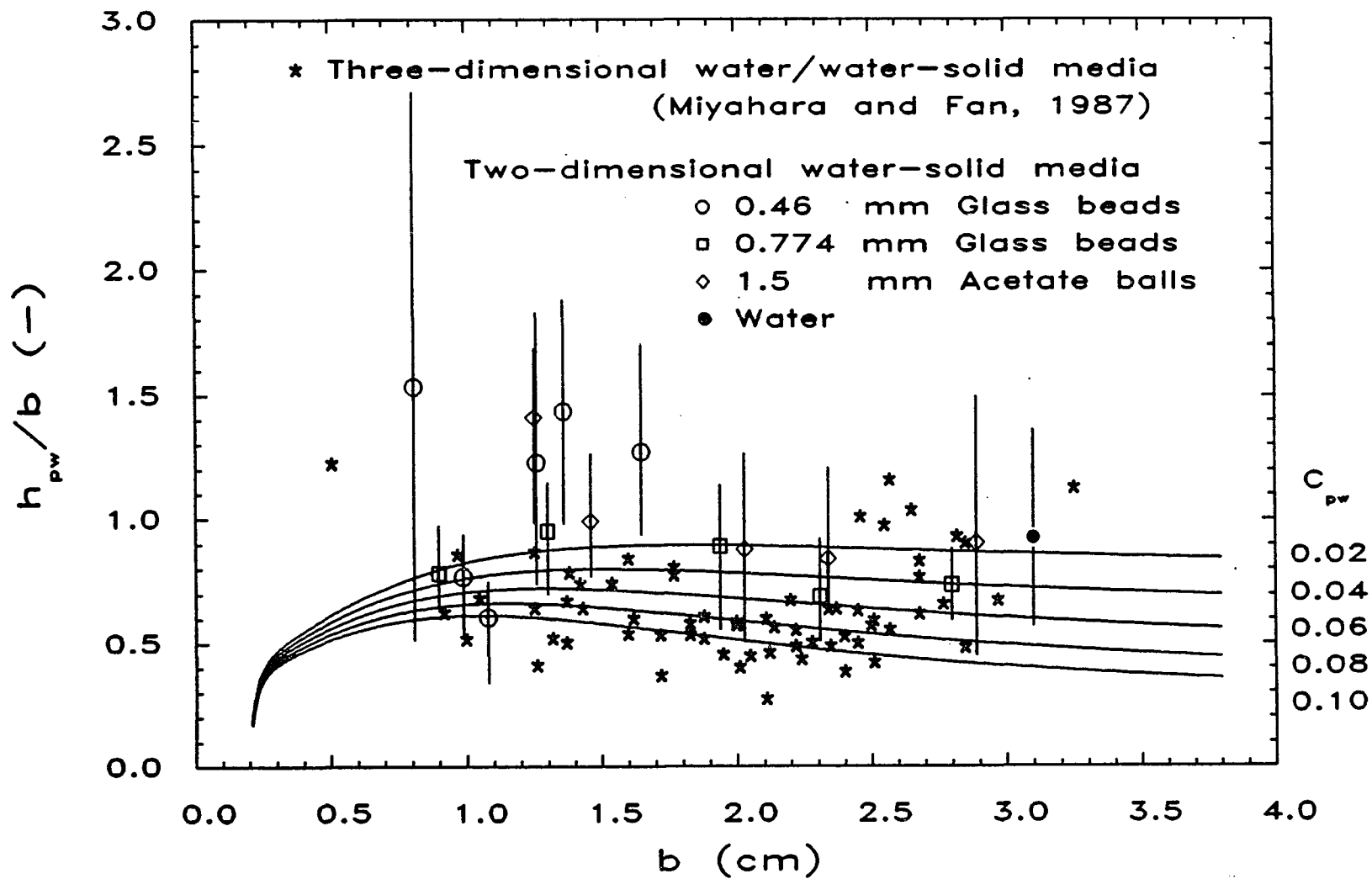


Figure 4.5 Effect of moment of inertia of the primary wake on wake size.

CONCLUDING REMARKS

The size of an effective wake and the frequency of vortex shedding from the wake have been interrelated based on a simple mechanistic model which accounts for the rigid body type bubble-wake motion. In the model, the shedding frequency was assumed to be the same order of magnitude as the natural frequency of the bubble-wake defined by the effective mass and stiffness of the bubble-wake. The stiffness of the effective wake was found to be most influential on the estimation of the wake size besides the shedding frequency.

The model demonstrates qualitatively the trend that the vortex shedding frequency tends to decrease with increasing the effective wake size for a fixed bubble size. The model also provides a fair quantitative prediction of the wake size provided the vortex shedding frequency is known. The use of the present model, however, should be limited to intermediate-to-moderately large bubble size ($b = 0.4$ - 4 cm).

CHAPTER 5

CONCLUSIONS AND RECOMMENDATIONS

As the commercialization of gas-liquid-solid fluidization has grown in recent years in various fields such as chemical, petrochemical and biochemical processing, the understanding of fundamental fluidized bed behavior has been recognized as the key to reactor design. In this study bubble-wake dynamics, one of the most fundamental bed characteristics, was found to be controlled by the local fluid mechanics of the bubble and its surrounding medium. The specific conclusions of this study are given in the following:

1. The wake of a relatively large gas bubble, including elliptical and circular-cap shapes, in a liquid-solid fluidized bed consists of two regions: the primary and secondary wakes. The primary wake, or near-wake, is characterized by large-scale vortical motion and is responsible for bed contraction, solids mixing and particle entrainment.

2. The most critical fluid dynamic characteristic of the wake is its instability. Periodic wake shedding can take place either asymmetrically or symmetrically. The dynamics of vortical motion is the key to vortex formation and shedding.

3. The asymmetric vortex formation-shedding mechanism consists of the roll-up of a vortex sheet, growth of a circular vortex, and entrainment of external flow by the growing vortex on one side and the cut-off stream from the other side which intercepts the vorticity supply and isolates the vortex. The vortex sheet instability occurring independently on each side of a large bubble is responsible for the symmetric shedding. Vortex shedding frequency, expressed in terms of the Strouhal number, is a function of the Reynolds number for each shedding mode and appears independent of particle properties.

4. The primary wake size varies periodically in the form of a saw-tooth wave function, while the liquid wake exhibits no appreciable cyclic variation in size. The mean primary wake size is a weak function of the Reynolds number and may depend on the bubble-shape and motion regime. The mean value for the ratio of the primary wake area to the bubble area was estimated to be 3.3 ± 1.2 for the range $1500 < Re_b < 8150$, which is less than one half of the value for a circle-completing wake, i.e., 7.27.

5. The motion and geometric properties of vortices formed at the edges of relatively large, two-dimensional single gas bubbles have been found qualitatively similar in both stationary water and a water-solid fluidized medium when low-density solid particles are employed, although the vortex life was shorter in the liquid-solid fluidized medium than that in the liquid.

6. The vortices, descending relative to the bubble, followed a general trajectory in the near wake which can be characterized by an inverted isosceles triangle shape. The vortex descent velocity was

found to be almost position invariant within the primary wake; however, once interacting with the external flow, it gradually increased and eventually reached the external stream velocity relative to the bubble.

7. The vortex size, monotonically increasing with time in the absence of the vortex-vortex and/or external-to-vortex interactions, may decrease in the presence of these interactions outside the primary wake. The extent of size reduction was promoted by an opposite-signed stronger vortical field; the weaker vortex was sometimes totally annihilated. It was also severely promoted by the inertia of solid particles. The vortex-vortex interactions also caused the vortex shape deformation. In some instances, the interactions were strong enough to tear a very elongated weakening vortex into two small ones.

8. The motion of individual liquid or solid particles within the near wake was influenced by the successive vortices in such a manner that the particles would repeat the process of circling around and escaping from a vortex until they leave the near wake. The number of vortices with which a particle interacts is a key to determine the particle residence time in the primary wake.

9. The size of an effective wake and the frequency of vortex shedding from the wake have been interrelated based on a simple mechanistic model which accounts for the rigid body type bubble-wake motion. In the model, the shedding frequency was assumed to be the same order of magnitude as the natural frequency of the bubble-wake defined by the effective mass and stiffness of the bubble-wake. The

stiffness of the effective wake was found to be most influential on the estimation of the wake size besides the shedding frequency.

10. The model demonstrates qualitatively the trend that the vortex shedding frequency tends to decrease with increasing the effective wake size for a fixed bubble size. The model also provides a reasonable prediction of the wake size provided the vortex shedding frequency is known. The use of the present model, however, should be limited to intermediate-to-moderately large bubble size ($b = 0.4-4$ cm).

The basic behavior of the bubble wake investigated in the present study is believed to represent the inherent characteristics of the bubble wake dynamics prevailing in the most of the practical multi-phase systems. The system studied in this dissertation, however, is not complicated enough to apply the present findings directly to the actual situations: bubbles exist in a swarm with various bubble size distributions, the system is three-dimensional, and the liquid properties such as viscosity and surface tension and the particle properties such as size and density are more diverse than the ranges examined in the present study. Some recommendations for future study are described in the following:

1. The wake structure in a chain of bubbles in a two-dimensional bed should be investigated to evaluate the effect of nearby bubbles on the bubble wake of interest. Bubble-bubble interaction is known to be

much stronger in the vertical direction than in the horizontal direction.

2. The study of single and successive bubbles regarding the wake structure is to be continued in a three-dimensional system.

3. Bubble coalescence and breakup phenomena can be studied in a chain of bubbles in terms of the effect of wake on the bubble-bubble interaction.

4. The freeboard phenomena such as solids entrainment can also be studied based on the wake concept. The maximum height of solid particles carried into the freeboard region is an important parameter for the design of three-phase fluidized bed reactors.

5. The bubble wake phenomena should eventually be investigated in free bubbling situations. This can be done by injecting a bubble into a gas-liquid-solid fluidized bed with free bubbling. The bubble of interest is followed in the same technique used in the present study to visualize the wake structure, bubble-bubble interaction, and bubble-wake interaction.

6. A wide range of the physical properties of liquid and solid particles should be examined so that they can simulate more closely the practical three-phase fluidized bed reactors.

BIBLIOGRAPHY

- Baker, C.G.J., Kim, S.D. and Bergougnou, M.A., 1977, Wake characteristics of three-phase fluidized beds. Powder Technol. **18**, 201.
- Barker, S.J. and Crow, S.C., 1977, The motion of two-dimensional vortex pairs in a ground effect. J. Fluid Mech. **82**, 659.
- Basset, A.B., 1888, Treatise on Hydrodynamics. Vol. *II*, Cambridge Univ. Press, London.
- Batchelor, G.K., 1956, A proposal concerning laminar wakes behind bluff bodies at large Reynolds number. J. Fluid Mech. **1**, 388.
- Batchelor, G.K., 1967, An Introduction to Fluid Dynamics. Cambridge Univ. Press, London.
- Bessler, W.F., 1984, Analytical and experimental studies of wakes behind circularly capped bubbles. Ph.D. Dissertation, R.P.I., New York.
- Beveridge, G.S.G. and Schechter, R.S., 1970, Optimization: Theory and Practice. McGraw-Hill, New York.
- Bhaga, D. and Weber, M.E., 1981, Bubbles in viscous liquids: shapes, wakes and velocities. J. Fluid Mech. **105**, 61.
- Bhatia, V.K. and Epstein, N., 1974, Three phase fluidization: a generalized wake model. Fluidization and Its Applications (Edited by Angelino, H. et al.), p.380. Cepadues-Editions, Toulouse.
- Birkhoff, G., 1953, Formation of vortex streets. J. Appl. Phys. **24**, 98.
- Bishop, R.E.D., 1965, Vibration. Cambridge Univ. Press, London.
- Brignell, A.S., 1974, Mass transfer from a spherical cap bubble in laminar flow. Chem. Engng Sci. **29**, 135.
- Calderbank, P.H., 1967, Review series No. 3 gas absorption from bubbles. Trans. Inst. Chem. Engrs **45**, CE209.

- Calderbank, P.H., Johnson, D.S.L. and Loudon, J., 1970, Mechanics and mass transfer of single bubbles in free rise through some Newtonian and non-Newtonian liquids. Chem. Engng Sci. **25**, 235.
- Christiansen, J.P. and Zabusky, N.J., 1973, Instability, coalescence and fission of finite-area vortex structures. J. Fluid Mech. **61**, 219.
- Chiba, T. and Kobayashi, H., 1977, Solid exchange between the bubble wake and the emulsion phase in a gas-fluidised bed. J. Chem. Engng Japan **10**, 206.
- Clift, R., Grace, J.R. and Weber, M.E., 1978, Bubbles, Drops, and Particles. Academic Press, New York.
- Collins, R., 1965a, A simple model of the plane gas bubble in a finite liquid. J. Fluid Mech. **22**, 763.
- Collins, R., 1965b, Structure and behaviour of wakes behind two-dimensional air bubbles in water. Chem. Engng Sci. **20**, 851.
- Coppus, J.H.C., Rietema, K. and Ottengraf, S.P.P., 1977, Wake phenomena behind spherical-cap bubbles and solid spherical-cap bodies. Trans. Inst. Chem. Engrs **55**, 122.
- Crabtree, J.R. and Bridgwater, J., 1967, The wakes behind two-dimensional air bubbles. Chem. Engng Sci. **22**, 1517.
- Currie, I.G., 1974, Fundamental Mechanics of Fluids. McGraw-Hill, New York.
- Darton, R.C. and Harrison, D., 1975, Gas and liquid hold-up in three-phase fluidisation. Chem. Engng Sci. **30**, 581.
- Darton, R.C. and Harrison, D., 1976, Bubble wake structure in three-phase fluidization. Fluidization Technology (Edited by Keairns, D.L.) **I**, p.399. Hemisphere.
- Davies, R.M. and Taylor, G.I., 1950, The mechanics of large bubbles rising through extended liquids and through liquids in tubes. Proc. Roy. Soc. London **A200**, 375.
- Dayan, A. and Zalmanovich, S., 1982, Axial dispersion and entrainment of particles in wakes of bubbles. Chem. Engng Sci. **37**, 1253.
- Edge, R.M. and Grant, C.D., 1971, The terminal velocity and frequency of oscillation of drops in pure systems. Chem. Engng Sci. **26**, 1001.
- Efremov, G.I. and Vakhrushev, I.A., 1970, A study of the hydrodynamics of three-phase fluidized beds. Int. Chem. Engng **10**, 37.
- El-Temtamy, S.A. and Epstein, N., 1978, Bubble wake solids content in three-phase fluidized beds. Int. J. Multiphase Flow. **4**, 19.

- Fage, A. and Johansen, F.C., 1927, On the flow of air behind an inclined flat plate of infinite span. Proc. Roy. Soc. London A116, 170.
- Gerrard, J.H., 1966, The mechanics of the formation region of vortices behind bluff bodies. J. Fluid Mech. **25**, 401.
- Gibilaro, L.G. and Rowe, P.N., 1974, A model for a segregating gas fluidised bed. Chem. Engng Sci., **29**, 1403.
- Grace, J.R. and Harrison, D., 1967, The influence of bubble shape on the rising velocities of large bubbles. Chem. Engng Sci. **22**, 1337.
- Harper, J.F. and Moore, D.W., 1968, The motion of a spherical liquid drop at high Reynolds number. J. Fluid Mech. **32**, 367.
- Henriksen, H.K. and Ostergaard, K., 1974, Characteristics of large two-dimensional air bubbles in liquids and in three-phase fluidized beds. Chem. Engng J. **7**, 141.
- Hill, M.J.M., 1894, On a spherical vortex. Phil. Trans. Roy. Soc. **185**, 213.
- Hills, J.H., 1975, The two-dimensional elliptical cap bubble. J. Fluid Mech. **68**, 503.
- Karamcheti, K., 1966, Principles of Ideal-Fluid Aerodynamics. John Wiley and Sons, New York.
- Kitano, K. and Fan, L.-S., 1987, Near-wake structure of a single gas bubble in a two-dimensional liquid-solid fluidized bed: solids holdup. Chem. Engng Sci. (in review).
- Kiya, M. and Arie, M., 1977, A contribution to an inviscid vortex-shedding model for an inclined flat plate in uniform flow. J. Fluid Mech. **82**, 223.
- Kojima, E., Akehata, T. and Shirai, T., 1975, Behavior of single air bubbles held stationary in downward flow. J. Chem. Engng Japan **8**, 108.
- Kubota, M., Akehata, T. and Shirai, T., 1967, Behavior of single air bubbles in low-viscosity liquids. Kagaku Kogaku **31**, 1074.
- Lazarek, G.M. and Littman, H., 1974, The pressure field due to a large circular capped air bubble rising in water. J. Fluid Mech. **66**, 673.
- Leonard, A., 1980, Review: vortex methods for flow simulation. J. Comput. Phys. **37**, 289.
- Levich, V.G., 1962, Physicochemical Hydrodynamics. Prentice-Hall, Englewood Cliffs, New Jersey.

- Lindt, J.T., 1971, Note on the wake behind a two-dimensional bubble. Chem. Engng Sci. **26**, 1776.
- Maneri, C.C. and Mendelson, H.D., 1968, The rise velocity of bubbles in tubes and rectangular channels as predicted by wave theory. AIChE J. **14**, 295.
- Maxworthy, T., 1967, A note on the existence of wakes behind large, rising bubbles. J. Fluid Mech. **27**, 367.
- Mendelson, H.D., 1967, The prediction of bubble terminal velocities from wave theory. AIChE J. **13**, 250.
- Miyahara, T. and Fan, L.-S., 1987, Wake properties of a single gas bubble in a three-dimensional liquid-solid fluidized bed. to be submitted to Chem. Engng Sci. (in preparation).
- Muroyama, K. and Fan, L.-S., 1985, Fundamentals of gas-liquid-solid fluidization. AIChE J. **31**, 1.
- Naimer, N.S., Chiba, T. and Nienow, A.W., 1982, Parameter estimation for a solids mixing/segregation model for gas fluidised beds. Chem. Engng Sci. **37**, 1047.
- Oseen, C.W., 1911, Über Wirbelbewegung in einer reibenden Flüssigkeit. Arkiv for Matematik, Astronimi och Fysik. **7**, 14.
- Ostergaard, K., 1965, On bed porosity in gas-liquid fluidization. Chem. Engng Sci. **20**, 165.
- Ostergaard, K., 1973, Flow phenomena of three-phase (gas-liquid-solid) fluidized beds. AIChE Symp. Ser. No. 128 **69**, 28.
- Page, R.E. and Harrison, D., 1974, Particle entrainment from a three-phase fluidized bed. Fluidization and Its Applications (Edited by Angelino, H. et al.), p.393. Cepadues-Editions, Toulouse.
- Parlange, J.-Y., 1969, Spherical cap bubbles with laminar wakes, J. Fluid Mech. **37**, 257.
- Perry, A.E., Chong, M.S. and Lim, T.T., 1982, The vortex-shedding process behind two-dimensional bluff bodies. J. Fluid Mech. **116**, 77.
- Powell, M.J.D., 1964, An efficient method for finding the minimum of a function of several variables without calculating derivatives. Comput. J. **7**, 155.
- Rigby, G.R. and Capes, C.E., 1970, Bed expansion and bubble wakes in three-phase fluidization. Can. J. Chem. Engng **48**, 343.
- Rosenberg, B., 1950, David W. Taylor Model Basin, Rept. 727, Navy Dept., Washington D.C.

- Roshko, A., 1955, On the wake and drag of bluff bodies. J. Aero. Sci. **22**, 124.
- Rowe, P.N. and Partridge, B.A., 1962, An X-ray study of bubbles in fluidised beds. Trans. Inst. Chem. Engrs **43**, T157.
- Rowe, P.N., Partridge, B.A., Cheney, A.G., Henwood, G.A. and Lyall, E., 1965, The mechanisms of solids mixing in fluidised beds. Trans. Inst. Chem. Engrs **43**, T271.
- Saffman, P.G. and Baker, G.R., 1979, Vortex interactions. Ann. Rev. Fluid Mech. **11**, 95.
- Sarpkaya, T., 1975, An inviscid model of two-dimensional vortex shedding for transient and asymptotically steady separated flow over an inclined plate. J. Fluid Mech. **68**, 109.
- Schlichting, H., 1960, Boundary Layer Theory. 4th ed., McGraw-Hill, New York.
- Slaughter, I. and Wraith, A.E., 1968, The wake of a large gas bubble. Chem. Engng Sci. **23**, 932.
- Sommerfeld, A., 1950, Mechanics of Deformable Bodies. Academic Press, New York.
- Stewart, P.S.B. and Davidson, J.F., 1964, Three-phase fluidization: water, particles and air. Chem. Engng Sci. **19**, 319.
- Sutherland, K.S., 1961, Solids mixing studies in gas fluidised beds Part I a preliminary comparison of tapered and non-tapered beds. Trans. Inst. Chem. Engrs **39**, 188.
- Tadaki, T. and Maeda, S., 1961, On the shape and velocity of single air bubbles rising in various liquids. Kagaku Kogaku **25**, 254.
- Ting, L. and Tung, C., 1965, Motion and decay of a vortex in a non-uniform stream. Phys. Fluids **8**, 1039.
- Torobin, L.B. and Gauvin, W.H., 1959, Fundamental aspects of solids-gas flow Part II. The sphere wake in steady laminar fluids. Can. J. Chem. Engng **37**, 167.
- Uno, S. and Kintner, R.C., 1956, Effect of wall proximity on the rate of rise of single air bubbles in a quiescent liquid. AIChE J. **2**, 420.
- van Santen, G.W., 1953, Introduction to a Study of Mechanical Vibration. Philips Technical Library, Eindhoven, Netherlands.
- Viets, H. and Lee, D.A., 1971, Motion of freely falling spheres at moderate Reynolds numbers. AIAA J. **9**, 2038.

Wegener, P.P. and Parlange, J.-Y., 1973, Spherical-cap bubbles. Ann. Rev. Fluid Mech. 5, 79.

Wellek, R.M., Agrawal, A.K. and Skelland, A.H.P., 1966, Shape of liquid drops moving in liquid media. AIChE J. 12, 854.

Williamson, C.H.K. and Roshko, A., 1986, Vortex dynamics in the wake of an oscillating cylinder. Paper (BF4) presented at the 39th Ann. Mtg. APS, Fluid Dynamics Div., Columbus, OH, Nov. 23-25.

Woollard, N.M. and Potter, E., 1968, Solids mixing in fluidized beds. AIChE J. 14, 388.

Yabe, K. and Kunii, D., 1978, Dispersion of molecules diffusing from a gas bubble into a liquid. Int. Chem. Engng 18, 666.

APPENDIX A

Raw Data - Average Bubble Properties

Table A.1. Average Bubble Properties

Type of Particle	b [cm]	Re _b	Alternate	f _v [1/s] Parallel	Average
GB460	0.46±0.02	0.76±0.05	9.79±0.40		
	0.62±0.08	1.05±0.19	9.43±0.86		
	0.90±0.16	1.69±0.35	9.00±0.33		
	1.34±0.08	2.55±0.28	9.69±0.45		
	1.75±0.09	3.83±0.33	9.72±0.49		
	2.22±0.11	5.16±0.45	9.51±0.27	11.0 ±1.1	10.2 ±1.6
	2.52±0.09	6.02±0.27	8.77±0.45	10.3 ±0.6	9.53±1.34
	2.82±0.10	7.18±0.43	8.47±0.42	10.5 ±1.0	9.10±1.80
	3.15±0.08	8.20±0.40	8.24±0.20	10.9	8.91±1.46
	3.64±0.06	10.2 ±0.01	8.18	10.0	9.09±0.91
GB774	0.69±0.02	1.05±0.08	9.34±0.28		
	0.90±0.04	1.53±0.11	9.45±0.11		
	1.37±0.07	2.54±0.13	9.64±0.26		
	1.95±0.03	4.13±0.20	9.10±0.54	10.6 ±0.04	9.48±1.05
	2.34±0.08	5.12±0.41	8.41±0.38	10.2	8.61±1.01
	2.74±0.05	6.35±0.22	7.97±0.40	10.5 ±0.3	9.41±1.60
	3.10±0.11	7.62±0.46	7.85±0.25	10.4 ±0.6	9.36±1.66
AC778	1.02±0.05	1.93±0.13	9.40±0.23		
	1.20±0.09	2.33±0.20	9.56±0.22		
	1.39±0.07	2.86±0.18	9.54±0.22		
	1.79±0.07	3.85±0.10	9.56±0.18		
	2.17±0.10	4.95±0.28	9.53±0.11	12.5 ±1.1	10.7 ±2.1
	2.55±0.11	6.05±0.31	8.80±0.82	13.3	9.93±2.74
	2.72±0.13	6.51±0.30	8.64±0.62		
	3.00±0.08	7.46±0.31	7.85±0.56	12.6	8.54±2.77
	3.35±0.02	8.81±0.13	8.33±0.81		
	3.75±0.05	10.0 ±0.05	6.50±0.18		
AT1500	1.00±0.07	1.80±0.14	8.93±0.57		
	1.13±0.04	2.10±0.08	8.63±0.77		
	1.39±0.13	2.72±0.31	8.56±0.62		
	1.82±0.12	3.81±0.37	8.11±0.63		
	1.98±0.04	4.25±0.25	7.71±0.76		
	2.24±0.08	4.99±0.30	7.22±0.73		
	2.61±0.11	6.08±0.30	7.27±0.90		
	2.97±0.09	7.28±0.24	6.02±0.40		
	3.38±0.07	8.32±0.30	6.40±0.60		

* Alternate wake shedding in freeboard region (gas-liquid).

APPENDIX B

**Raw Data and Correlations for
Bubble Shape Parameters and Bubble Rise Velocity**

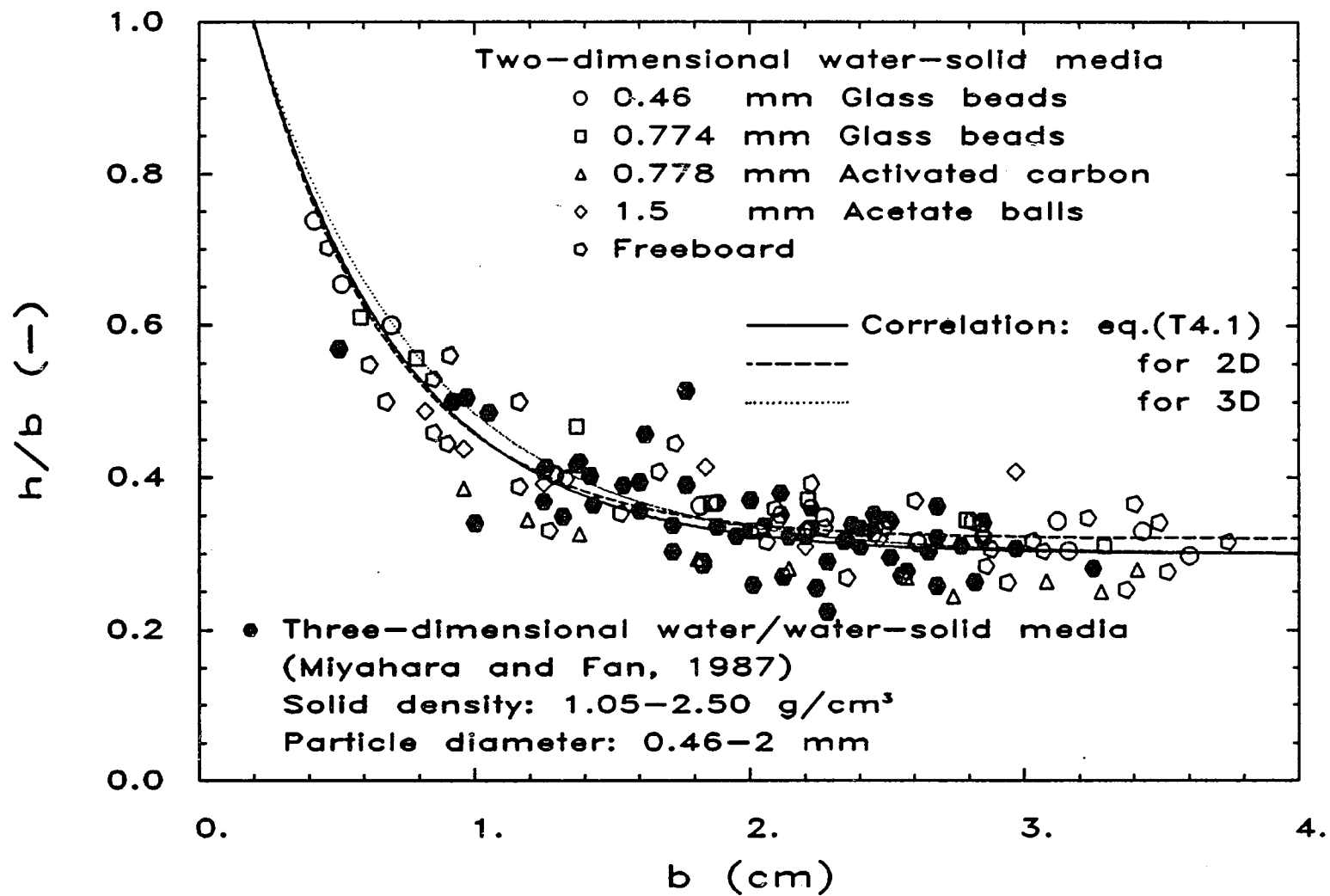


Figure A.1 Aspect ratio of single bubbles correlated in terms of bubble size.

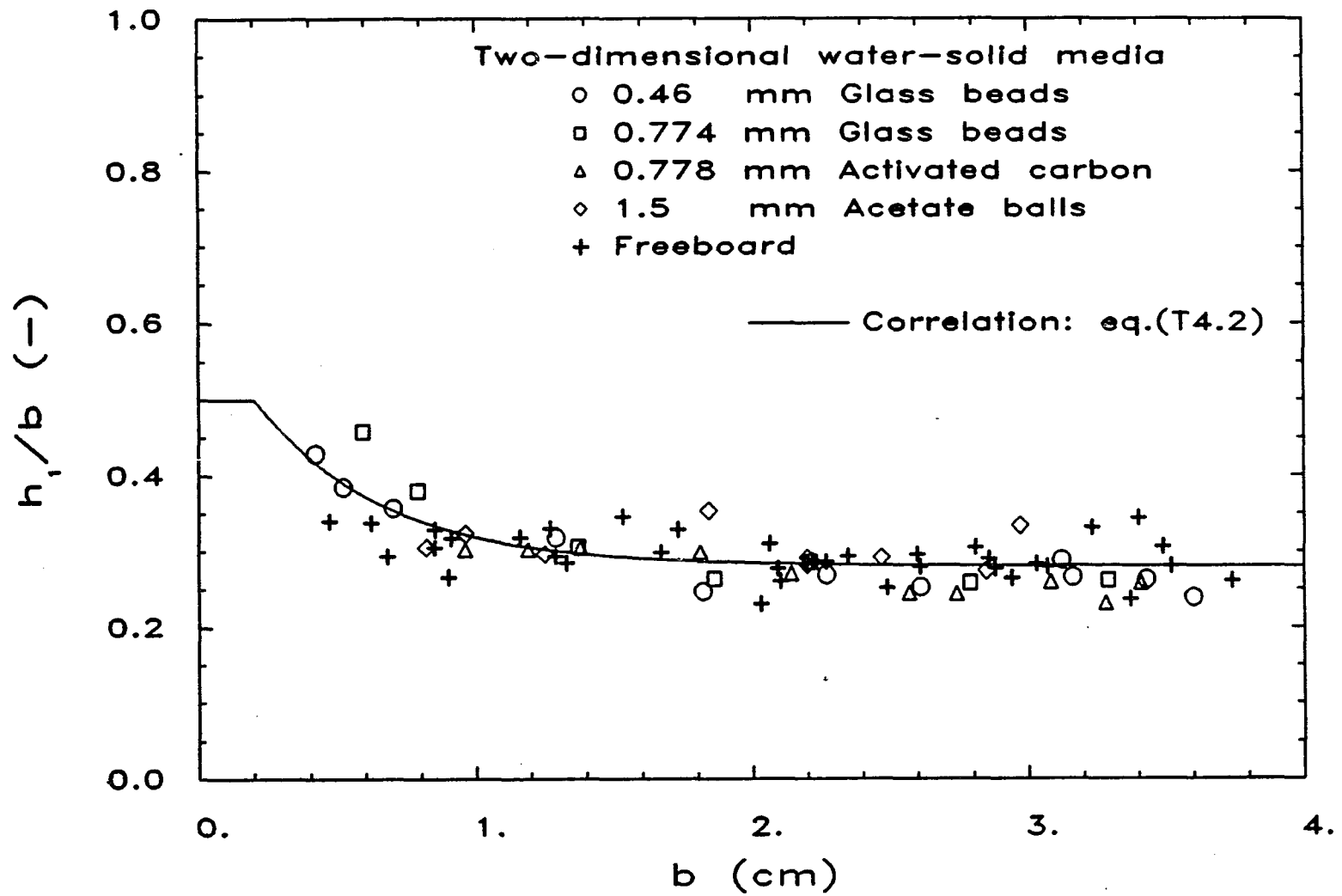


Figure A.2 Upper semi-height-to-breadth ratio of single bubbles correlated in terms of bubble size.

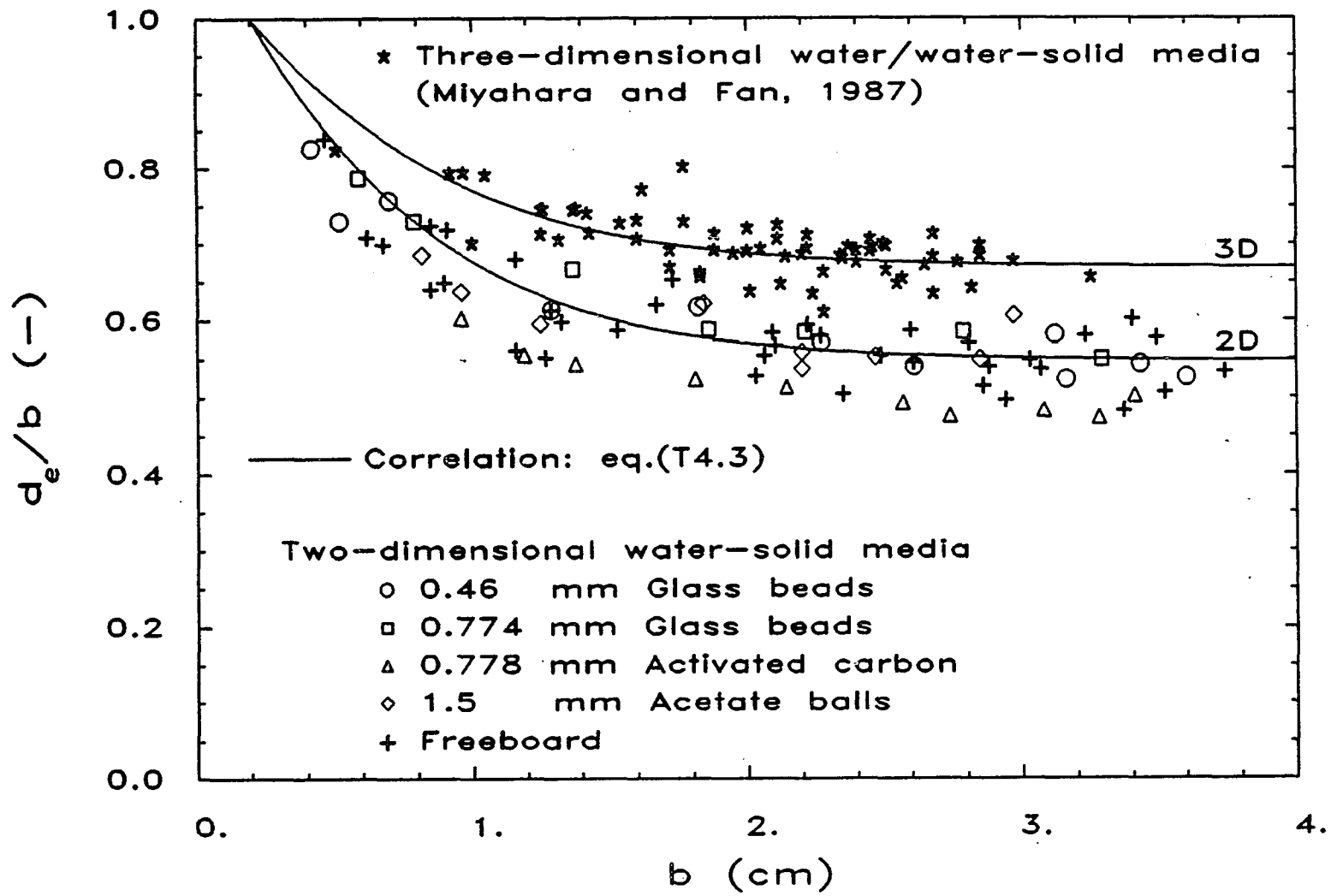


Figure A.3 Equivalent bubble diameter of single bubbles correlated in terms of bubble size.

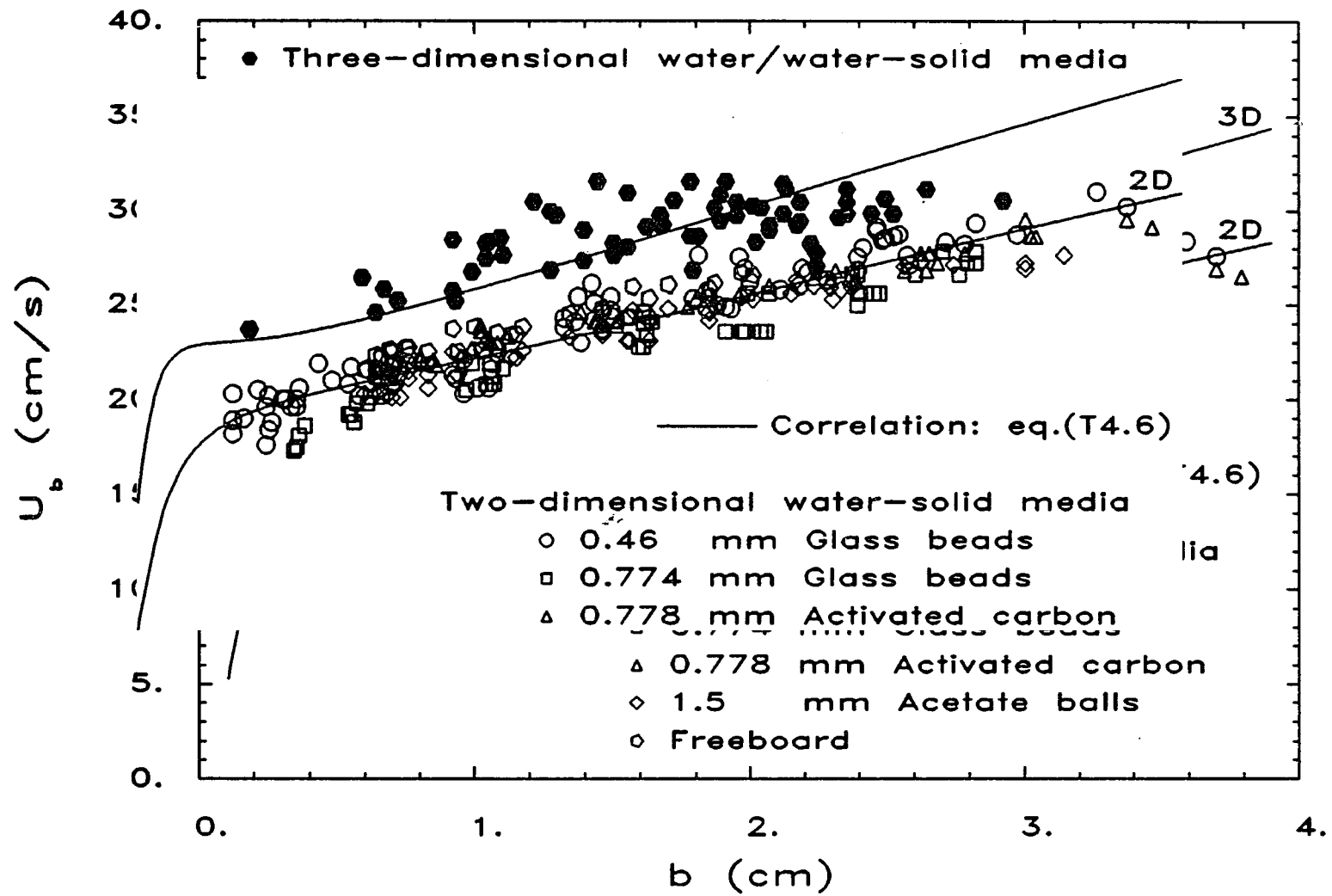


Figure A.4 Rise velocity of single bubbles correlated in terms of bubble size.

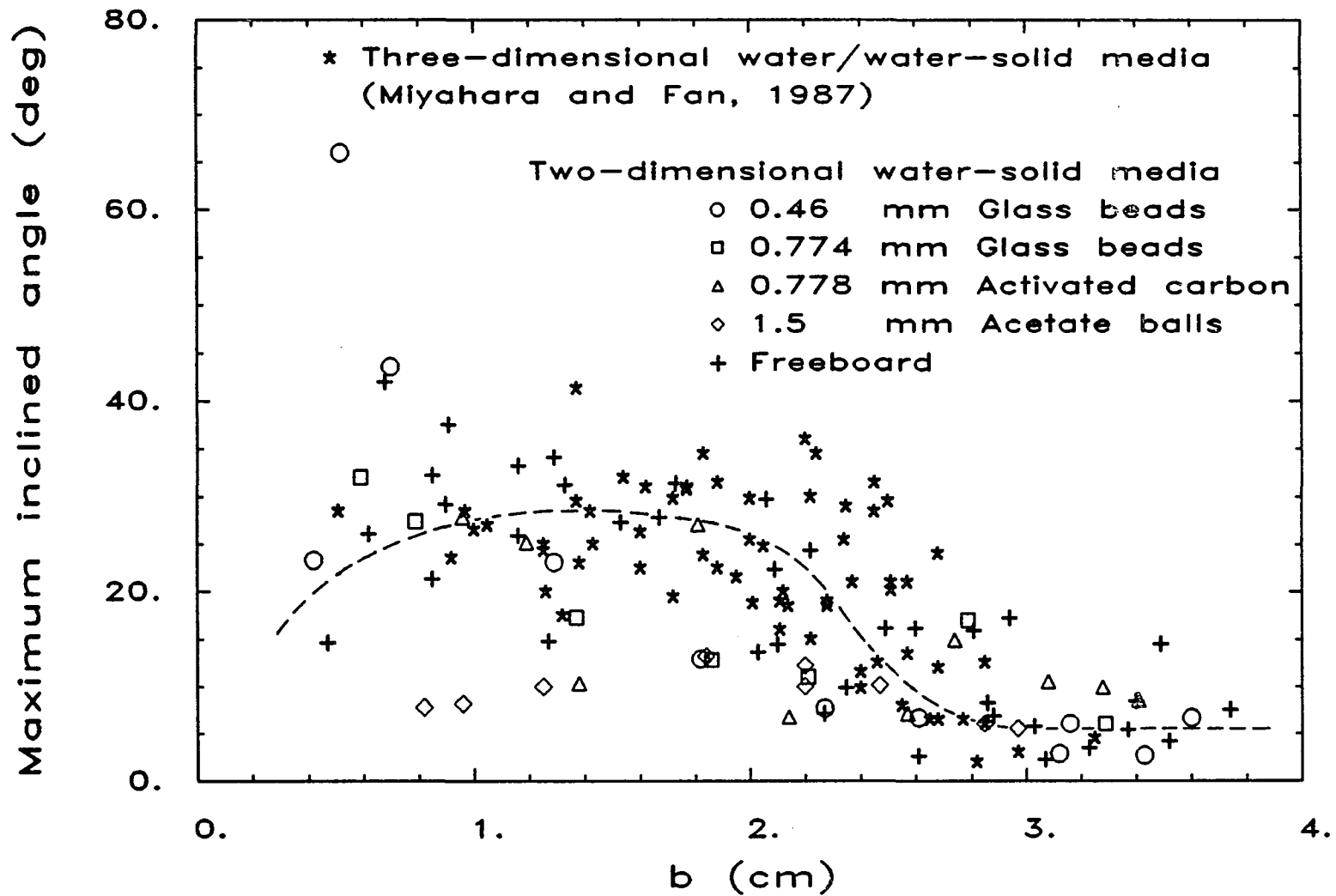


Figure A.5 Variation of maximum inclined angle of bubble-wake with respect to bubble size.